MINERALOGICAL MAGAZINE

JOURNAL OF THE MINERALOGICAL SOCIETY

Vol. 32 June 1959 No. 245

Nepheline solid solutions

By GABRIELLE DONNAY, Ph.D., and J. F. SCHAIRER, Ph.D.

Geophysical Laboratory, Carnegie Institution of Washington,

Washington, D.C., U.S.A.

and J. D. H. DONNAY, E.M., Ph.D.

The Johns Hopkins University, Baltimore, Maryland, U.S.A.

[Taken as read 2 April 1959.]

Summary. Published chemical analyses demonstrate that the nepheline formula should be written $K_xNa_yCa_z\square_{8-(x+y+z)}Al_{x+y+2z}Si_{16-(x+y+2z)}O_{32}$, where $\square$ stands for vacant sites. X-ray data are presented for the nepheline phase in four binary systems: Ne–$CaAl_2O_4$, Ne–An, Ne–Ab, Ne–Kp. Only in two of these systems do the cell-dimensions change with composition. In the first one, the cell-volume V increases linearly with increasing calcium content; in the last one, two singularities in the curve of V against x divide the phase $Na_{8-x}K_xAl_8Si_8O_{32}$ into three subphases: subpotassic ($0 < x < 0{\cdot}25$), mediopotassic ($0{\cdot}25 < x < 2{\cdot}00$), and perpotassic ($2{\cdot}00 < x < 4{\cdot}73$). Only in the subpotassic range are both high- and low-temperature forms found. Twenty-eight natural nephelines, for which chemical analyses and X-ray data are available in the literature, show that only the potassium content affects cell-dimensions. Although all analysed natural nephelines fall outside the subpotassic range, the re-examination of a Monte Somma specimen studied by Bannister (1931) reveals a few euhedral crystals of subpotassic nepheline in a mediopotassic phase.

NEPHELINE is an interesting example of a mineral that forms more than one type of solid solution, a fact which the formula as it is usually written, (Na,K)$AlSiO_4$, does not bring out. Even before the crystal structure of nepheline had been determined, Bannister (1931) pointed out that the number of oxygen atoms per cell is 32, and that the number of silicon and aluminium atoms must equal 16 if nepheline is a framework structure. The formula obtained from chemical analysis can be written essentially[1] as $K_xNa_yCa_zAl_nSi_mO_{32}$, with $x = K + \Delta K$, $y = Na + \Delta Na$, ..., &c., where K, Na, ..., are the exact numbers of potassium, sodium, ..., atoms per cell and ΔK, ΔNa, ..., are the corresponding errors of the analysis.

[1] Neglecting small amounts of other cations whose role is discussed below.

TABLE I. Cell contents and X-ray data of natural nephelines

$(K, Na, Ca, Mg, Fe^{2+}, Mn, Ti, \square)_8(Si, Al, Fe^{3+})_{16}O_{32}$.

For each specimen the following data are listed: numbers of cations per cell (as obtained from the chemical analysis, i.e., K+ stands for $x = K+\Delta K$, Na+ for $y = Na+\Delta Na$, Ca+ for $z = Ca+\Delta Ca$, &c.); number of vacant sites □ (taken as the difference between 8 and the observed total number of cations per cell); numbers of tetrahedrally co-ordinated atoms per cell (as for cations, Al+ stands for Al+ΔAl, &c.); $\Sigma = (Al+Fe^{3+}+Si)+(\Delta Al+\Delta Fe^{3+}+\Delta Si)$, i.e. observed total number of tetrahedral atoms; $\Delta = \Delta Al+\Delta Fe^{3+}+\Delta Si$; cell edges a and c (Å. units), $a \pm 0{\cdot}05\%$, $c \pm 0{\cdot}1\%$; $V_{obs.}$, cell-volume (Å.^{3}) found by X-rays; $K_{pr.}$ = K predicted from cell-volume (fig. 3); $\partial K = K_{obs.} - K_{pr.}$; $V_{pr.}$, cell-volume predicted from K content (fig. 3); $\partial V = V_{obs.} - V_{pr.}$; $D_{calc.}$ and $D_{obs.}$, calculated and observed densities (g./cm.^{3}).

Nos. 1, 4, 7, 9, 13 are M. Hey's nos. I, II, V, VI, VII, respectively (Bannister, 1931). No. 15 is N. Saito's Shinjozan (Miyashiro and Miyashiro, 1954). The remaining analyses (Smith and Sahama, 1954) are identified as follows: Nos. 2, 3, 5, 11, 14, 16, 18 are J. H. Scoon's nos. 63197, 34475, 34480, 238, 273, 276, E2, respectively. Nos. 6, 10, 19, 20, 21, 23, 24, 25, 27, 28 are P. Ojanperä's FEAE nos. 198, 170, 90, 49, 89, 88, 87, 86, 92, 93, respectively. Nos. 8 and 26 are H. B. Wiik's FEAE-134 and C9956. No. 12 is E. G. Zies' Gooderham. No. 17 is M. Lehijärvi's Ivoara. No. 22 is R. B. Ellestad's R-118.

No.	1.	2.	3.	4.	5.	6.	7.	8.	9.
K+	0·76	0·90	0·94	0·97	1·15	1·24	1·25	1·28	1·29
Na+	6·00	6·43	6·31	5·59	6·28	5·96	5·97	5·84	5·53
Ca+	0·51	0·15	0·28	0·38	0·16	0·07	0·25	0·00	0·44
Mg+	—	0·00	0·02	—	0·01	0·00	—	0·02	—
Fe^{2+}+	—	—	—	—	—	0·05	—	0·04	—
Mn+	—	—	0·00	—	0·00	0·00	—	0·00	—
Ti+	—	0·00	0·00	—	0·00	0·01	—	0·00	—
□	0·73	0·52	0·45	1·06	0·40	0·67	0·53	0·82	0·74
Al+	7·69	7·26	7·64	7·70	7·60	7·33	7·58	7·44	7·89
Fe^{3+}+	—	0·08	0·02	—	0·07	0·14	—	0·08	—
Si+	8·29	8·59	8·29	8·39	8·30	8·53	8·38	8·55	8·16
Σ	15·98	15·93	15·95	16·09	15·97	16·00	15·96	16·07	16·05
Δ	−0·02	−0·07	−0·05	+0·09	−0·03	0·00	−0·04	+0·07	+0·05
a	9·997	9·981	9·987	9·972	9·988	9·990	9·982	9·990	9·982
c	8·348	8·361	8·368	8·378	8·374	8·373	8·378	8·381	8·363
$V_{obs.}$	722·5	721·4	722·8	721·5	723·5	723·7	723·0	724·4	721·7
$K_{pr.}$	1·00	0·82	1·05	0·83	1·17	1·20	1·08	1·32	0·87
∂K	−0·24	+0·18	−0·11	+0·14	−0·02	+0·04	+0·17	−0·04	+0·42
$V_{pr.}$	721·3	722·1	722·4	722·5	723·6	724·1	724·2	724·3	724·4
∂V	+1·2	−0·7	+0·4	−1·0	−0·1	−0·4	−1·2	+0·1	−2·7
$D_{calc.}$	2·621	—	—	2·617	—	—	2·637	—	2·644
$D_{obs.}$	2·614	—	—	2·620	—	—	2·629	—	2·608

No.	10.	11.	12.	13.	14.	15.	16.	17.	18.
K+	1·29	1·31	1·34	1·40	1·43	1·49	1·49	1·50	1·76
Na+	5·81	5·65	5·87	5·47	6·09	5·95	6·14	6·10	6·03
Ca+	0·10	0·36	0·15	0·30	0·10	0·06	0·05	0·00	0·03
Mg+	0·01	0·04	0·01	—	0·00	0·09	0·00	0·04	0·00
Fe^{2+}+	0·03	—	—	—	—	—	—	0·05	—
Mn+	0·00	—	0·00	—	—	—	—	0·00	—
Ti+	0·01	0·00	0·00	—	—	—	0·00	0·00	—
□	0·75	0·64	0·63	0·83	0·38	0·41	0·32	0·31	0·13
Al+	7·30	7·96	7·68	7·47	7·71	7·83	7·67	7·81	7·78
Fe^{3+}+	0·14	0·02	0·01	—	0·02	0·08	0·03	0·18	0·02
Si+	8·58	8·08	8·35	8·53	8·27	8·13	8·29	8·06	8·18
Σ	16·02	16·06	16·04	16·00	16·00	16·04	15·99	16·05	15·98
Δ	+0·02	+0·06	+0·04	0·00	0·00	+0·04	−0·01	+0·05	−0·02
a	9·992	9·999	10·003	9·992	9·994	10·014	9·997	9·999	10·001
c	8·374	8·387	8·382	8·388	8·372	8·392	8·381	8·385	8·388
$V_{obs.}$	724·1	726·2	726·3	725·3	724·2	728·8	725·5	726·0	726·6
$K_{pr.}$	1·27	1·62	1·63	1·47	1·28	2·05	1·50	1·58	1·68
∂K	+0·02	−0·31	−0·29	−0·07	+0·15	−0·56	−0·01	−0·08	+0·08
$V_{pr.}$	724·4	724·5	724·7	725·0	725·2	725·5	725·5	725·6	727·1
∂V	−0·3	+1·7	+1·6	+0·3	−1·0	+3·3	0·0	+0·4	−0·5
$D_{calc.}$	—	—	—	2·623	—	—	—	—	—
$D_{obs.}$	—	—	—	2·597	—	—	—	—	—

TABLE I. (*cont.*)

No.	19.	20.	21.	22.	23.	24.	25.	26.	27.	28.
K+	1·95	2·35	2·78	2·80	2·81	2·84	3·01	3·11	3·11	3·19
Na+	5·39	4·68	4·63	4·79	4·65	4·62	4·42	4·20	4·36	4·20
Ca+	0·19	0·11	0·19	0·19	0·19	0·17	0·19	0·31	0·19	0·19
Mg+	0·02	0·09	0·07	0·07	0·07	0·05	0·05	0·03	0·05	0·05
Fe^{2+}+	0·08	0·05	0·03	—	0·03	0·03	0·05	0·10	0·04	0·03
Mn+	0·00	0·00	0·03	—	0·00	0·00	0·00	—	0·00	—
Ti+	0·01	0·02	0·01	0·02	0·01	0·01	0·01	0·01	0·01	0·01
□	0·36	0·70	0·26	0·13	0·24	0·28	0·27	0·24	0·24	0·33
Al+	7·60	7·68	7·77	7·76	7·78	7·80	7·76	7·64	7·68	7·76
Fe^{3+}+	0·12	0·26	0·16	0·12	0·15	0·13	0·16	0·27	0·15	0·13
Si+	8·24	8·14	8·07	8·04	8·05	8·09	8·05	8·02	8·16	8·12
Σ	15·96	16·08	16·00	15·92	15·98	16·02	15·97	15·93	15·99	16·01
Δ	−0·04	+0·08	0·00	−0·08	−0·02	+0·02	−0·03	−0·07	−0·01	+0·01
a	10·009	10·042	10·064	10·079	10·069	10·064	10·084	10·101	10·068	10·092
c	8·390	8·412	8·427	8·432	8·415	8·422	8·439	8·447	8·429	8·441
$V_{obs.}$	728·0	734·7	739·1	741·8	738·9	738·7	743·2	746·4	739·9	744·5
$K_{pr.}$	1·92	2·53	2·90	3·13	2·88	2·86	3·25	3·52	2·97	3·36
∂K	+0·03	−0·18	−0·12	−0·33	−0·07	−0·02	−0·24	−0·41	+0·14	−0·17
$V_{pr.}$	728·2	732·6	737·7	738·0	738·1	738·5	740·5	741·7	741·7	742·6
∂V	−0·2	+2·1	+1·4	+3·8	+0·8	+0·2	+2·7	+4·7	−1·8	+1·9
$D_{calc.}$	—	—	—	—	—	—	—	—	—	—
$D_{obs.}$	—	—	—	—	—	—	—	—	—	—

By the framework criterion we must have Al+Si = 16 (i), and, to balance the charges, K+Na+2Ca = Al (ii). By definition we have $n+m-16 = (\mathrm{Al}+\Delta\mathrm{Al})+(\mathrm{Si}+\Delta\mathrm{Si})-16$, and, in view of (i), $n+m-16 = \Delta\mathrm{Al}+\Delta\mathrm{Si}$ (iii). (The analytical error in the determination of aluminium +silicon equals the number of aluminium and silicon atoms reported in excess of 16 when the analysis is referred to 32 oxygens.) Likewise by definition we write $x+y+2z-n = (\mathrm{K}+\Delta\mathrm{K})+(\mathrm{Na}+\Delta\mathrm{Na})+(2\mathrm{Ca}+2\Delta\mathrm{Ca})-(\mathrm{Al}+\Delta\mathrm{Al})$ and, in view of (ii), $x+y+2z-n = \Delta\mathrm{K}+\Delta\mathrm{Na}+2\Delta\mathrm{Ca}-\Delta\mathrm{Al}$ (iv).

The expressions (iii) and (iv) are the two quantities, considered by Bannister and Hey, which in a good analysis should be as small as possible. Because a chemical analysis is reported in the form of oxides, we have (sum of positive charges) $x+y+2z+3n+4m = 64$, equivalent to Bannister's identity[1] $x+y+2z-n = 4[16-(n+m)]$. In order to write the idealized formula of nepheline, we assume an error-free chemical analysis and therefore set (iv) and (iii) equal to zero. This gives $x+y+2z = n$ and $n+m = 16$.

In addition we now know, from the crystal structure determination of nepheline (Buerger, Klein, and Donnay, 1954; Hahn and Buerger, 1955), that the alkali and alkaline earth ions occupy eight sites, namely those of positions 2:*b* and 6:*c* in space-group $P6_3$. But all the available chemical analyses of natural nephelines (table I) show a deficiency of

[1] Bannister (1931, p. 576) writes $[(n+m)-16]$ when he means $[16-(n+m)]$.

cations of such an order of magnitude that it cannot be ascribed to analytical errors. The idealized formula must therefore take into account the possibility of some cation sites being vacant; it is written as

$$K_xNa_yCa_z\square_{8-(x+y+z)}Al_{x+y+2z}Si_{16-(x+y+2z)}O_{32},$$

where $\square$ stands for vacant cation sites.

Additional elements reported present in small amounts are Mg, Fe, Mn, and Ti. Adding the experimentally determined number of ferric ions to the sum $(n+m)$ of silicon and aluminium atoms reduces the analytical error $|16-(n+m)|$ for all but three of the twenty-eight analyses given in table I. As might be predicted from ionic size considerations, ferric ions appear to substitute for silicon and aluminium in tetrahedral co-ordination, whereas all other cations substitute for Na, K, or Ca.

To study the effect of substitutions on the cell-dimensions of nepheline in the laboratory, it is convenient to consider the one-phase synthetic-nepheline region in each of four binary systems. Natural nephelines, on the other hand, may lie in the quinary system $NaAlSiO_4$(Ne)–$KAlSiO_4$(Kp)–$NaAlSi_3O_8$(Ab)–$CaAl_2Si_2O_8$(An)–$CaAl_2O_4$. X-ray results obtained on synthetic samples will be given for pure-sodium nepheline and for each binary system. They will be compared with X-ray data for analysed natural nephelines, taken from Bannister (1931), Smith and Sahama (1954), and Miyashiro and Miyashiro (1954). Of the thirty-four available analyses, we are using (table I) the twenty-eight that obey Hey's reliability criterion (in Bannister, 1931)

$$|\Delta Al+\Delta Fe^{3+}+\Delta Si| \leqslant 0{\cdot}10.$$

X-ray procedure.

The sample is powdered to 200-mesh size and a smear mount is prepared on a glass slide for use with the Norelco diffractometer. Silicon, with its 111 peak at $2\theta = 28{\cdot}465°$, is used as an internal standard. The samples are run under the following conditions: scanning speed, usually $\frac{1}{2}°$ per minute ($\frac{1}{4}°$ for some repeat runs); chart scale 1 inch per degree; receiving slit 0·003 inch; Cu-$K\alpha$ radiation ($\lambda = 1{\cdot}5418$ Å.). Two charts are taken for each run (see table II), one (I) with the Geiger counter moving in the direction of decreasing 2θ values, the other (II) with the motion reversed (Parrish and Wilson).[1] Six peaks, in the range $2\theta = 19°$ to $2\theta = 32°$,

[1] W. Parrish and A. J. C. Wilson, Precision measurement of lattice parameters of polycrystalline specimens, Philips Lab., Irvington-on-Hudson, New York, Techn. Report, 1954, no. 85, p. 16; Internat. Tables X-ray Cryst., vol. 2 (in press).

TABLE II. Calculation of cell-dimensions from powder data by method of least squares
Synthetic high temperature $NaAlSiO_4$. $s = h^2 + hk + k^2$

		Chart I.		Chart II.											
	hkil.	$2\theta_{obs.}$	$2\theta_{corr.}$	$2\theta_{obs.}$	$2\theta_{corr.}$	$2\theta_{ave.}$	$Q_{obs.}$	*s.*	l^2.	s^2.	sl^2.	l^4.	*s*Q	l^2Q.	$Q_{calc.}$
Si	111	28·431	28·465	28·538	28·465	—	—	—	—	—	—	—	—	—	—
	corr.	+0·034		−0·073											
	$20\bar{2}0$	20·540	20·574	20·638	20·565	20·570	0·05364	4	0	16	0	0	0·21456	0	0·05365
	0002	21·205	21·239	21·333	21·260	21·250	0·05721	0	4	0	0	16	0	0·22884	0·05720
	$20\bar{2}1$	23·158	23·192	23·260	23·187	23·190	0·06798	4	1	16	4	1	0·27192	0·06798	0·06795
	$21\bar{3}0$	27·289	27·323	27·400	27·327	27·325	0·09388	7	0	49	0	0	0·65716	0	0·09388
	$20\bar{2}2$	29·705	29·739	29·816	29·743	29·741	0·11083	4	4	16	16	16	0·44332	0·44332	0·11085
	$30\bar{3}0$	31·038	31·072	31·143	31·070	31·071	0·12071	9	0	81	0	0	1·08639	0	0·12071
										178	20	33	2·67335	0·74014	
										A	B	C	D	E	

$$a^{*2} = \frac{\begin{vmatrix} DB \\ EC \end{vmatrix}}{\begin{vmatrix} AB \\ BC \end{vmatrix}} = 0{\cdot}013412 \text{ Å.}^{-2} \qquad c^{*2} = \frac{\begin{vmatrix} AD \\ BE \end{vmatrix}}{\begin{vmatrix} AB \\ BC \end{vmatrix}} = 0{\cdot}014300 \text{ Å.}^{-2}$$

$$a^* = 0{\cdot}115810 \text{ Å.}^{-1} \qquad c^* = 0{\cdot}119583 \text{ Å.}^{-1}$$

$$a = 9{\cdot}971 \text{ Å.} \pm 0{\cdot}05\% \qquad c = 8{\cdot}362 \text{ Å.} \pm 0{\cdot}05\%$$

$$V = 2\sqrt{3}/3 a^{*2} c^* = 720{\cdot}0 \text{ Å.}^3$$

Remark: Sums A, B, C, and therefore the determinants in the denominators of a^{*2} and c^{*2} are the same for all charts, as long as all the reflections can be measured. $20\bar{2}0$ is occasionally too weak to give an accurate reading.

are used to obtain the cell-dimensions by the method of least squares (table II). The values of $Q(hkil)$ are obtained from the observed values of 2θ (Cu-$K\alpha$) by use of appropriate tables (Donnay and Donnay).[1]

Single crystals were studied on precession and Weissenberg cameras with Cu-$K\alpha$ and Mo-$K\alpha$ ($\lambda = 0{\cdot}7107$ Å.) radiations.

Pure-sodium nepheline.

A large number of pure-sodium nephelines with different thermal histories were examined (table III) to find out whether the cell-dimensions

TABLE III. X-ray data for pure-sodium nepheline; synthetic samples with different thermal histories. Synthesized by J. F. Schairer, except for the last specimen, prepared by F. R. Boyd.

Thermal history (° C.).	a (Å.).	c (Å.).	V (Å.^{3}).	c/a.
1100°, 6 hrs. quenched high-temp. form	9·971	8·362	720·0	0·8386*
900°, 20 days low-temp. form	9·984	8·333	719·3	0·8346
900°, 34 ,, ,,	9·988	8·333	719·9	0·8343
1000°, 6 ,, ,,	9·986	8·331	719·5	0·8343
1000°, 34 ,, ,,	9·986	8·328	719·2	0·8340
1050°, 6 ,, ,,	9·984	8·333	719·3	0·8346
1050°, 34 ,, ,,	9·991	8·331	720·2	0·8339
1200°, 2 ,, ,,	9·984	8·328	719·1	0·8341
1200°, 10 ,, ,,	9·984	8·328	719·1	0·8341
540°, 1 week, 2000 bars, hydrothermal low-temp. form	9·989	8·328	719·6	0·8337

* Calculated specific gravity is 2·621. Observed value is 2·619 at 21° C. (Bowen, 1912, p. 10).

vary continuously with the temperature of crystallization, as is the case for albite (MacKenzie, 1957). The data for the low-temperature form show that the cell-dimensions are independent of the thermal history of the specimen. They are (averaged values): $a = 9{\cdot}986$, $c = 8{\cdot}330$, both $\pm 0{\cdot}005$ Å., $c/a = 0{\cdot}8342 \pm 0{\cdot}005$. For the high-temperature form one sample gave $a = 9{\cdot}971$, $c = 8{\cdot}362$, both $\pm 0{\cdot}005$ Å., $c/a = 0{\cdot}8386 \pm 0{\cdot}005$. The X-ray patterns of the two forms are so similar that they cannot be told apart on inspection,[2] but measurements lead to a difference of 0·4% in the c-dimension, a difference well outside the limits of error of our determinations. Because the high-temperature form was

[1] G. Donnay and J. D. H. Donnay, Tables for the interpretation of X-ray diffraction data, giving the square, Q, of the reciprocal lattice vector. . . . Crystallographic Laboratory of the Johns Hopkins University, 1951. Reprinted 1955 (limited edition).

[2] We cannot confirm the lowering of symmetry from hexagonal to orthorhombic reported for the high-temperature form by Smith and Tuttle (1957).

obtained only accidentally on quenching, it appeared advisable to confirm the low-high transition. A low-temperature pure-sodium nepheline was heated on the diffractometer. The reflection $20\bar{2}2$ was recorded at the following temperatures: 240°, 410°, 610°, 810°, 1050°, and 1150°, all ±50° C. A plot of $2\theta(20\bar{2}2)$ against temperature (fig. 1) shows a

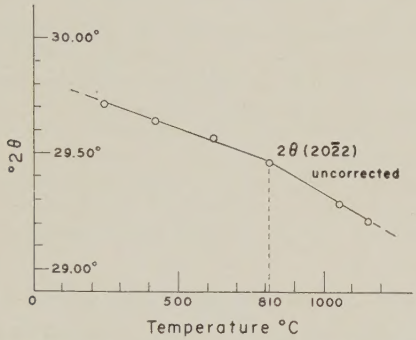

FIG. 1. Synthetic pure-sodium nepheline. Uncorrected angle $2\theta(20\bar{2}2)$ obtained with Cu-$K\alpha$ radiation at various temperatures (° C., ±50°). The transition between low-temperature and high-temperature forms is marked by a break in the curve in the neighbourhood of 810°.

break at 810±50° C. Smith and Tuttle (1957) place the transition at 900° C. We have studied the extent of solid solution range for the low- and high-temperature forms only in the binary system Ne–Kp.

To our knowledge, no natural occurrence of potassium-free nepheline has been reported in the literature. Evidence for such an occurrence at Monte Somma, Italy, will be presented below.

The four solid solutions.

Double substitution—calcium replacing sodium and aluminium replacing silicon, $Na_{8-Z}Ca_ZAl_{8+Z}Si_{8-Z}O_{32}$. *Solid solution A.* This is of the type encountered in the plagioclase series. It is represented by the one-phase nepheline region in the binary system $NaAlSiO_4$–$CaAl_2O_4$ (Goldsmith, 1949). Dr. Goldsmith kindly placed his powder samples at our disposal. Because single crystals were not available for study, the presence of superstructure reflections (as are observed on plagioclases) cannot be ruled out. The cell-volume increases linearly with increasing calcium content by an amount of 2·2 Å.^{3} per calcium ion (table IV A and fig. 2). Extrapolating the plot of cell-dimensions against calcium content to $Z = 0$ leads to cell-dimensions $a = 8{\cdot}362$, $c = 9{\cdot}970$ Å., equal to

those for high-temperature pure-sodium nepheline. The limit of solid solution falls beyond 60 wt.% $CaAl_2O_4$, corresponding to $Z > 4{\cdot}6$ in the above formula.

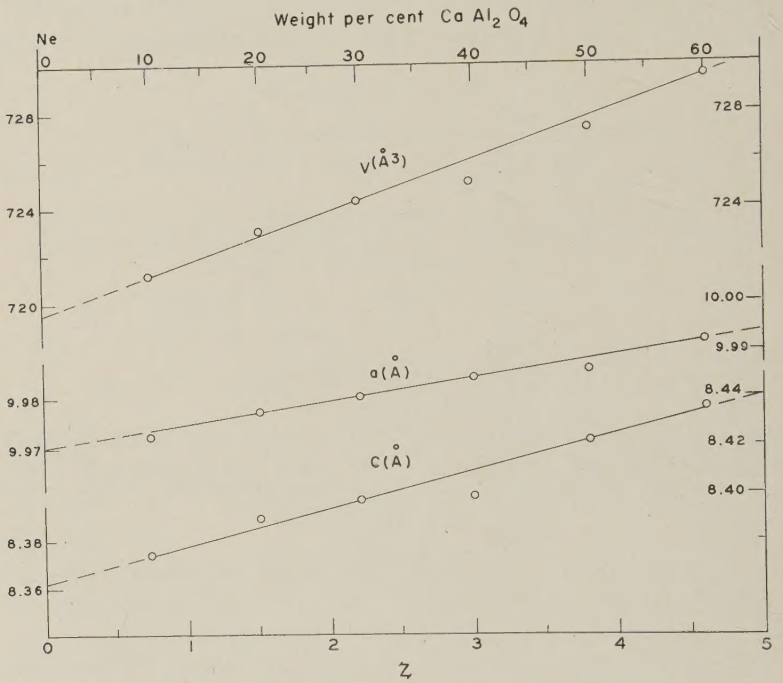

FIG. 2. Change of cell-dimensions (c and a in Å.; V in Å.^{3}) in synthetic $Na_{8-Z}Ca_ZAl_{8+Z}Si_{8-Z}O_{32}$.

The abscissa gives the number Z of calcium atoms per cell (lower scale) or the wt. % $CaAl_2O_4$ (upper scale).

Substitution plus omission—calcium and vacant sites in equal proportions replacing sodium, $Na_{8-2z}Ca_z\square_zAl_8Si_8O_{32}$. *Solid solution B.* This is represented by the one-phase nepheline region in the binary system $NaAlSiO_4$–$CaAl_2Si_2O_8$ (Bowen, 1912; Gummer, 1943). Two samples (Schairer's nos. 877 and 869, table IV B) of compositions 20 and 45 wt.% $CaAl_2Si_2O_8$, consist of a nepheline and a plagioclase phase when completely crystallized. Both sets of cell-dimensions therefore refer to the composition with maximum z value, which is less than 1·33. The cell-dimensions are the same, within experimental error, as those of the high-temperature pure-sodium nepheline.

Omission and substitution—vacant sites replacing sodium and silicon

replacing aluminium, $Na_{8-y}\square_y Al_{8-y}Si_{8+y}O_{32}$. *Solid solution C*. This is represented by the one-phase nepheline region in the binary system $NaAlSiO_4$–$NaAlSi_3O_8$ (Greig and Barth, 1938). Dr. W. S. MacKenzie, who studied this system with water as an additional component, kindly gave us a thick-tabular crystal, 0·2 mm. in its largest dimension, on the preparation of which he reports as follows:

A glass of composition 37½% $NaAlSiO_4$.62½% SiO_2 (wt. %) prepared by Dr. J. F. Schairer was held at 700° C. at a water vapour pressure of 2000 bars for a period of eleven days in a Tuttle hydrothermal quenching apparatus. The charge of glass was contained in a small platinum tube open at one end so that there was free access of water to the silicate glass. When the charge was quenched and examined, it was found that the upper surface was covered with euhedral nepheline crystals and below was a mass of very small albite crystals and some glass. The nepheline crystals are believed to be of composition 76 $NaAlSiO_4$.24 $NaAlSi_3O_8$ (wt. %) since this is the limit of omission solid solution in nepheline at this temperature. (MacKenzie, unpublished data.)

The cell-dimensions of the limiting composition, $y = 1{\cdot}0$, are given in table IV c; they are the same as those of high-temperature pure-sodium nepheline, within the limits of experimental accuracy. Thus, in neither of the solid solutions *B* and *C* does the introduction of vacant sites into the structure lead to a change in the cell-dimensions of the high-temperature form.

Substitution—potassium replacing sodium, $K_xNa_{8-x}Al_8Si_8O_{32}$. *Solid solution D*. This solid solution, the simplest and in nature the most important one of the four, is represented by the one-phase nepheline region in the binary system $NaAlSiO_4$–$KAlSiO_4$ (Bowen, 1917; Smith and Tuttle, 1957). Samples used in this study were prepared by Dr. Bowen in 1917, and by one of us (J. F. S.) in 1935 and 1956. Small amounts of beta-alumina and corundum can be detected under the microscope in all of the completely crystalline samples and the experimentally determined liquidus temperatures do not fall on a smooth curve. Thus all samples are slightly off composition because of alkali loss by volatilization during preparation, but the departure from composition by synthesis must be small, probably less than 1 wt.%, which is equivalent to $x = 0{\cdot}07$.

The sample of composition 62·50 wt.% $KAlSiO_4$, $x = 4{\cdot}796$, is the first one whose powder pattern shows non-nepheline lines. The cell-dimensions of its nepheline phase (table IV d) indicate that the limit of solid solution at 1200° C. occurs at $x = 4{\cdot}73$ or 61·7 wt.% $KAlSiO_4$ (fig. 3). Within the range $x = 0$ to $x = 4{\cdot}73$ the plot of cell-dimensions against potassium content x (fig. 3) consists of several straight-line

TABLE IV. X-ray data for synthetic nephelines.

A. System Ne–$CaAl_2O_4$, $Na_{8-Z}Ca_ZAl_{8+Z}Si_{8-Z}O_{32}$ (synthesized by Goldsmith).

Run.	$CaAl_2O_4$ wt. %.	Z.	Thermal history (° C.).	a ±0·2%	c ±0·2%	V.
—	0	0	—	*9·970 Å.	*8·362 Å.	*719·6 Å.^{3}
72	10	0·73	1000°, 3 days	9·972	8·374	721·2
169*a*	20	1·5	800°, 10 days	9·977	8·389	723·1
169*b*	30	2·2	800°, 10 days	9·980	8·397	724·3
165	40	3·0	1060°, 90 hours	9·984	8·398	725·1
170*c*	50	3·8	800°, 25 days and 900°, 11 days	9·986	8·421	727·3
170*d*	60	4·6	800°, 25 days	9·992	8·436	729·5

B. System Ne–An, $Na_{8-2Z}Ca_Z\square_ZAl_8Si_8O_{32}$ (synthesized by Schairer).

No.	$CaAl_2Si_2O_8$ wt. %	z.	Thermal history (° C.).	a ±0·05%.	c ±0·05%.	V.
877	20·00†	‡	1060°, 3 months	9·969 Å.	8·363 Å.	719·8 Å.^{3}
869	45·00†	‡	1100°, 18 days	9·968	8·364	719·7

C. System Ne–Ab, $Na_{8-y}\square_yAl_{8-y}Si_{8+y}O_{32}$ (synthesized by MacKenzie).

Run.	$NaAlSi_3O_8$ wt. %.	y.	Thermal history (° C.).	a ±0·3%.	c ±0·3%.	V.
A12	24†	1·0	700°, 2000 bars, 11 days, water	9·971 Å.	8·361 Å.	719·9 Å.^{3}

* Cell-dimensions obtained by extrapolation (cf. values for high-temperature form, table III).
† Composition of original glass.
‡ Limit of solid solution at given temperature ($z < 1·33$).

D. System Ne–Kp, $K_xNa_{8-x}Al_8Si_8O_{32}$.

Quenched high-temperature form

Synthesized by.	$KAlSiO_4$ wt. %.	x	Thermal history (° C.).	Present work a ±0·05%	Present work c ±0·05%.	Present work V.	Smith and Tuttle (1957) a ±0·05%.	Smith and Tuttle (1957) c ±0·05%.	Smith and Tuttle (1957) V.
Schairer	2·00	0·144	1200°, 8 days	9·971 Å.	8·356 Å.	719·4 Å.^{3}	—	—	—
,,	2·00	0·144	1200°, 8 days	9·973	8·358	719·9	—	—	—
,,	3·75	0·270	1050°, 12 days	9·971	8·358	719·6	—	—	—
,,	3·75	0·270	1100°, 10 days	9·975	8·360	720·4	—	—	—
,,	3·75	0·270	1200°, 12 days	9·975	8·358	720·2	—	—	—

TABLE IV. (*cont.*)

Low-temperature form

Synthesized by.	$KAlSiO_4$ wt. %.	x	Thermal history (° C.).	Present work a ±0·05%.	Present work c ±0·05%.	Present work V.	Smith and Tuttle (1957) a ±0·05%.	Smith and Tuttle (1957) c ±0·05%.	Smith and Tuttle (1957) V.
Schairer	2·00	0·144	1200°, 5 days	9·989	8·333	719·7 (*a*)	—	—	—
				9·980	8·333	719·2 (*b*)	—		
,,	2·50	0·180	1060°, 29 days	9·977	8·341	719·1	—	—	—
,,	2·50	0·180	1200°, 6 days	9·970	8·332	717·2	—	—	
				9·977	8·337	718·6	—	—	—
,,	2·50	0·180	1200°, 3 days	9·985	8·335	719·7	—	—	—
,,	3·00	$0·216_5$	1200°, 7 days	9·966	8·356	718·7	—	—	—
,,	4·00	0·289	1100°, 10 days	9·969	8·354	719·0	—	—	—
,,	4·00	0·289	1200°, 5 days	9·963	8·354	718·3	—	—	—
,,	4·00	0·289	1200°, 8 days	9·971	8·355	719·4	—		—
Bowen	5·00	0·361	1100°, 7 days	9·968	8·353	718·8	—	—	
Schairer	6·00	0·434	1200°, 5 days	9·963	8·347	717·2 (*a*)		—	—
				9·971	8·354	718·8 (*b*)	—	—	
,,	6·00	0·434	1200°, 8 days	9·976	8·361	720·6	—		
Bowen	10·00	0·726		—	—	—	9·981 Å.	8·360 Å.	721·2 Å.[3]
Schairer	20·00	1·467	1100°, 34 days	10·001	8·375	725·4	9·998	8·376	725·1
Bowen	25·00	1·843	1300°, 6 hours				10·011	8·387	727·9
Schairer	27·07	2·000	1100°, 33 days	10·015	8·387	728·5	—	—	
,,	29·00	2·147	cryst. at 1200°		—		10·018	8·396	729·7
,,	32·50	2·415	cryst. at 1200°	10·041	8·400	733·4	10·035	8·401	732·7
,,	37·50	2·802	cryst. *c*. 1300°	10·063	8·418	738·2	10·060	8·417	737·7
Bowen	40·00	2·996	cryst. at 1300°	—	—	—	*10·074	8·423	740·3
Schairer	42·50	3·192	—	—	—	—	10·087	8·428	742·6
,,	45·00	3·389	cryst. *c*. 1350°	10·099	8·439	745·5	—	—	
,,	47·50	3·587	cryst. at 1350°	—	—	—	10·110	8·440	747·1
Bowen	50·00	3·785	cryst. at 1300°		—	—	*10·122	8·445	749·3
Schairer	52·50	3·985	cryst. at 1200°	10·133	8·455	751·8	10·133	8·449	751·3
,,	55·00	4·186	cryst. at 1200°	10·145	8·464	754·4	—	—	
,,	57·50	4·389	cryst. at 1350° then at 1200°	—	—	—	10·163	8·461	756·8
,,	62·50	4·796	cryst. at 1350° then at 1200°	10·178	8·480	760·8	10·183	8·473	760·9

(*a*) ¼°/minute, (*b*) ½°/minute.

* Cell-dimensions calculated from 2θ values obtained by Smith (in Smith and Sahama, 1954).

portions. The low- and high-temperature forms are observed only near the sodium end of the series; the low-temperature form extends from $x = 0$ to $x = 0{\cdot}25$ whereas the high-temperature form is found to extend from

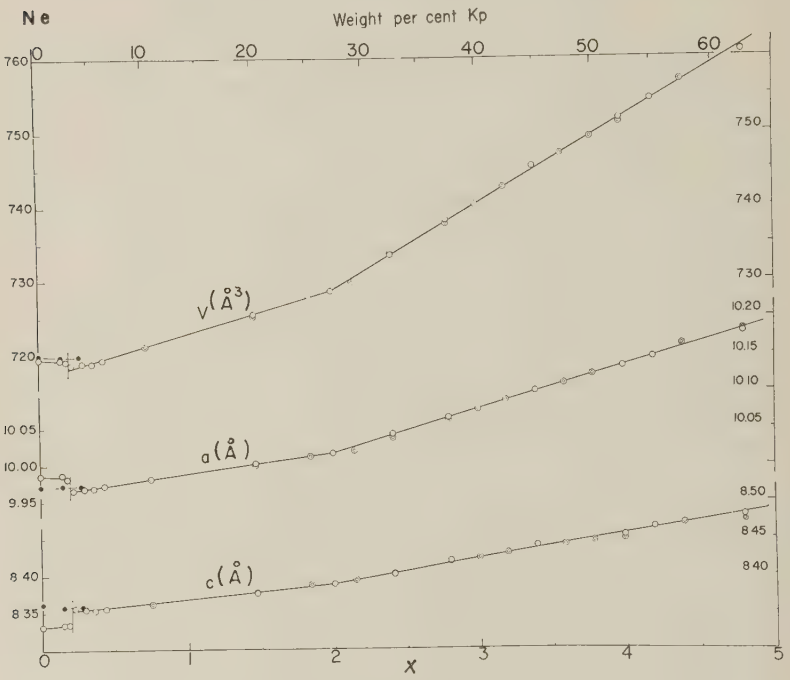

FIG. 3. Change of cell-dimensions (c and a in Å.; V in Å.^{3}) in synthetic $Na_{8-x}K_xAl_8Si_8O_{32}$.

The abscissa gives the number x of potassium atoms per cell (lower scale) or the wt. % Kp (upper scale). Black circles, quenched high-temperature form; white circles, low-temperature form; double rings, previous data (Smith and Tuttle, 1957).

$x = 0$ to $x = 0{\cdot}27$. Because of the uncertainty in composition, however, this difference in solid solution range cannot be considered a significant one. Beyond $x = 0{\cdot}25$ only one form is observed. Its cell-volume increases linearly by 5·82 Å.^{3} per potassium ion. At $x = 2{\cdot}00$ the volume curve shows a singularity; for $x > 2{\cdot}00$ the curve is again a straight line with a slope corresponding to 11·8 Å.^{3} per potassium ion.

The experimental uncertainty in cell-volume and composition makes it impossible to decide whether a singularity or discontinuity occurs in the cell-volume at $x = 0{\cdot}25$, whereas at $x = 2{\cdot}00$ all experimental data point towards a singularity. The fact that the 'one-phase' nepheline

region in this binary system can be subdivided into three 'subphases' has been discussed elsewhere (Donnay, 1957). We propose to use the adjectives 'subpotassic', 'mediopotassic', and 'perpotassic' to designate the nephelines with the following composition ranges: $0 < x < 0{\cdot}25$, $0{\cdot}25 < x < 2{\cdot}00$, and $2{\cdot}00 < x < 4{\cdot}73$, respectively.

Comparison of X-ray data for natural and synthetic nephelines.

Let us first investigate the effect of potassium content on the cell-volume of natural nephelines (fig. 4). Superposing the corresponding

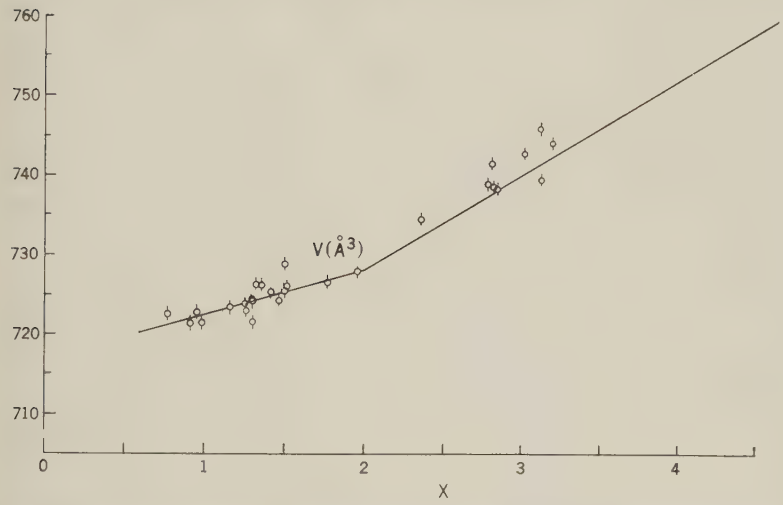

FIG. 4. Natural nephelines. Change of cell-volume V (in Å.^{3}) with number x of potassium atoms per cell. Length of line segment at each point indicates limits of error of X-ray determination. Superposed is the curve obtained for synthetic nephelines (from fig. 3).

curve obtained for the synthetic samples in the binary system Ne Kp shows that, on the basis of the literature data used here, the potassium content can be estimated with reasonable accuracy, as shown in row $\partial K = K_{obs.} - K_{pred.}$ (table I).

It is of historic interest to note that Bannister (1931, fig. 3) already suspected a simple relation of cell-volume to potassium content. But he was handicapped because the only X-ray data available to him were those he had determined himself (on nine samples). For all the other samples he calculated the cell-volume from the density and cell-content of the analysed material. As the density changes very little with composition

(table I), the points he plotted were widely scattered, and he concluded that '. . . the relation between cell-volume and the potassium content must be treated with reserve unless further evidence can be adduced'. The fact that this evidence is now at hand is due in large part to the availability of synthetic samples covering and even exceeding the range of nepheline compositions reported in natural specimens. Smith and Sahama (1954) already used the data from synthetic samples to try to predict the chemical composition of natural nephelines. Their treatment differs from ours in that it does not take vacant sites into consideration; their curves of $2\theta_{Cu}$ for $21\bar{2}0$ and $20\bar{2}2$, which take the place of cell-dimensions, are plotted against the atomic ratio K/(K+Na+Ca) rather than against the number of potassium atoms per cell.

We are now in a position to predict the cell-volume, $V_{pred.}$, on the basis of the analytical x value, $K_{obs.} = K + \Delta K$ (fig. 3), and to investigate the relation between $\partial V = V_{obs.} - V_{pred.}$ and the observed number of vacant sites. Inspection of the corresponding two rows in table I shows that no relationship exists. In natural nephelines as well as in the binary systems Ne An and Ne Ab, replacement of cations by vacant sites produces no noticeable change in cell-volume.

Finally let us inquire whether a relationship exists between ∂V and the number of calcium ions. A comparison of the corresponding rows in table I shows no correlation.

Because increasing calcium content leads to increasing cell-volume in the binary system Ne $CaAl_2O_4$, this type of solid solution cannot be responsible for the presence of calcium in natural nephelines. The solid solution in the system Ne–An, in which calcium content has no effect on cell-volume, should be effective in natural nephelines. This conclusion could not have been reached from the chemical analysis alone for the following reason:

Let us assume that all four types of solid solutions contribute to the composition of a natural nepheline. The formula can then be written $A_aB_bC_cD_d$, where a capital letter stands for the formula given for that type of solid solution and where $a + b + c - d = 1$. This relation, together with the numbers of various atoms per cell obtained from the analysis, yields seven equations in eight unknowns (a, b, c, d, x, y, z, and Z). The system cannot be solved.

Predicted structural differences for subphases.

Because a singularity or discontinuity in cell-volume at a given composition indicates a sudden change in crystal structure, it is of interest

to know for which of the subphases the crystal structure was actually determined. The cell-dimensions of the crystal from Monte Somma used by Hahn and Buerger (1955) are $a = 10{\cdot}01_0$, $c = 8{\cdot}40_5$ Å., $V = 729{\cdot}4$ Å.^{3}. Using the curve for synthetic samples $(Na,K)AlSiO_4$ (fig. 3), we predict a potassium content of $2{\cdot}00 \pm 0{\cdot}2$ ions per cell. The reported crystal structure shows striking evidence that the composition is near a transition point. The two framework oxygen atoms O_1, which would be expected to lie in a twofold position on the threefold axes, are found to be statistically distributed over a sixfold position, in the neighbourhood of the threefold axes. Another feature of the structure—six small holes occupied by sodium with seven nearest neighbours (at about 2·7 Å.) and two large holes filled by potassium with nine nearest neighbours (at about 2·9 Å.)—indicates that the composition falls on the mediopotassic side of the transition composition. The predicted perpotassic structure would have eight holes nearly equal in size, larger than the sodium holes in the determined structure. The predicted subpotassic structure would also have eight such holes, but their size would be nearly the same as that of the small sodium holes in the determined structure; the change from the low- to the high-temperature form would be due to a more or less uniform increase in the size of all eight holes. These hypotheses account for the existence of both low- and high-temperature phases in the subpotassic region and the absence of a second phase in the mediopotassic and perpotassic ranges of nepheline composition.

Evidence for subphases in other mineral systems.

The prediction of two nepheline crystal structures in addition to the one reported in the literature rests on the observation of three subphases on the nepheline phase diagram. The reverse situation holds in the case of tourmaline, where two structure determinations have been published, one on a rose-coloured lithium tourmaline from Brazil,[1] the other on a white magnesium tourmaline from de Kalb, New York.[2] These structures differ; the ring composed of six silicon tetrahedra has nearly hexagonal symmetry in the lithium tourmaline; it has ditrigonal symmetry in the magnesium crystal. An investigation of the tourmaline phase diagram should therefore show a transition in the magnesium–lithium field.

In general, the fine details of a mineral structure may be significant only in a limited range of composition. In other words, a mineral may

[1] T. Ito and R. Sadanaga, Acta Cryst., 1951, vol. 4, p. 385.
[2] G. Donnay and M. J. Buerger, Acta Cryst., 1950, vol. 3, p. 379.

turn out to have more than one crystal structure, if accurate work is done on specimens of different compositions.

Occurrence of subpotassic nepheline in nature.

Of all the nephelines described in the literature, one stands out because its cell-dimensions are quite out of line. It is a sample of nepheline from Monte Somma (B.M. 51495), described by Bannister (1931). The chemical analysis (by Hey) can be recast in the following formula

$$K_{1\cdot18}Na_{4\cdot46}Ca_{0\cdot91}\square_{1\cdot45}Al_{7\cdot78}Si_{8\cdot30}O_{32},$$

to represent the content of the cell. The cell-dimensions, determined by Bannister by the oscillating crystal method, are:

$$a = 9{\cdot}96_2,\ c = 8{\cdot}32_8 \text{ Å. (from kX)},\ c/a = 0{\cdot}8360,\ V = 715{\cdot}_8 \text{ Å.}^3,$$

which lead to a calculated density of 2·645. The reported observed density, $D_{15^\circ}^{15^\circ} = 2{\cdot}576$ g./cm.^{3}, is abnormally low. No other nepheline specimen has as small a cell-volume; the next smallest value is $721{\cdot}_4$ Å.^{3}; no other has as low a value of a (next lowest a is $9{\cdot}97_2$ Å.) or of c (next smallest c is $8{\cdot}34_8$ Å.).

Dr. M. Hey kindly sent us part of the sample that he had analysed and on which the cell-dimensions had been determined by Dr. Bannister in 1931.

The sample, when examined under the binocular microscope, was seen to consist of fragments; it yielded one small euhedral crystal suitable for X-ray study by single-crystal techniques. Its cell-dimensions were determined by the precession method: $a' = 9{\cdot}988$, $c' = 8{\cdot}328$ Å., $\pm 0{\cdot}3$ %; $c'/a' = 0{\cdot}8338$, $V = 719{\cdot}5$ Å.^{3}, in agreement with Bannister's result. Another portion of the sample was used to obtain a powder pattern on the diffractometer; it gave the following cell constants: $a'' = 9{\cdot}985$, $c'' = 8{\cdot}372$ Å., $\pm 0{\cdot}05$ %; $c''/a'' = 0{\cdot}8385$, $V = 722{\cdot}9$ Å.^{3}; comparison with the plot of V against x for synthetic $(Na,K)AlSiO_4$ (fig. 3) leads to a predicted potassium content of $1{\cdot}07 \pm 0{\cdot}20$ ions per cell in agreement with the analysed value of 1·18. The sample must therefore contain two phases, for even though $a' = a''$ within the limits of error, the difference between c' and c'' exceeds the uncertainty of the measurements. The phase detected as a single crystal must exist in the sample in very small quantity, as its effect on the powder pattern is not noticeable. Its cell-dimensions are those of subpotassic nepheline; because the cell-dimensions remain so nearly constant throughout this subphase, no better estimate of the potassium content can be made.

The occurrence of two nepheline subphases on one hand specimen emphasizes again the need for caution when chemical composition is to be determined from X-ray cell-dimensions. Bannister (1931) already showed, by means of optical measurements, that the chemical composition of the material occasionally changes from grain to grain in one hand specimen. Even within one crystal zoning may change the composition.

It is interesting to note that Cesàro (1920) made a careful goniometric study of small perfect crystals from Monte Somma, in which he was able to measure the angle $(10\bar{1}0):(10\bar{1}1)$ to 2 or 3 minutes of arc. The lowest c/a ratio he records is 0·8358. This value is lower than the c/a ratio 0·8381, which is the smallest value found by X-rays in the mediopotassic region. Cesàro too seems to have encountered a specimen of subpotassic nepheline in his Monte Somma material.

Acknowledgements. We wish to thank Professors N. V. Belov, M. J. Buerger, and C. E. Tilley for the interest they showed in our work.

References.

Bannister (F. A.), 1931. Min. Mag., vol. 22, p. 569.

Bowen (N. L.), 1912. The binary system: $Na_2Al_2Si_2O_8$-$CaAl_2Si_2O_8$. Abstract of Thesis, Mass. Inst. of Tech., pp. 1–14.

—— 1917. Amer Journ. Sci., ser. 4, vol. 43, p. 115 [M.A. **1**–167].

Buerger (M. J.), Klein (G. E.), and Donnay (G.), 1954. Amer. Min., vol. **39**, p. 805 [M.A. **12**–528].

Cesàro (G.), 1920. Mém. Acad. roy. Belgique (Cl. Sc.) Coll. in-8°. Ser. 2, vol. 4, p. 1.

Donnay (G.), 1957. Third International Meeting on Reactivity of Solids, Madrid, April 1956, Section I, p. 279.

Goldsmith (J. R.), 1949. Amer. Min., vol. 34, p. 471 [M.A. **11**–94].

Greig (J. W.) and Barth (T. F. W.), 1938. Amer. Journ. Sci., ser. 5, vol. 35 A, p. 93 [M.A. **7**–287].

Gummer (W. K.), 1943. Journ. Geol., Chicago, vol. 51, p. 503 [M.A. **9**–285].

Hahn (Th.) and Buerger (M. J.), 1955. Zeits. Krist., vol. 106, p. 308.

MacKenzie (W. S.), 1957. Amer. Journ. Sci., vol. 225, p. 481.

Miyashiro (A.) and Miyashiro (T.), 1954. Journ. Fac. Sci. Univ. Tokyo, Sect. II, vol. 9, p. 267 [M.A. **12**–528].

Smith (J. V.) and Sahama (Th. G.), 1954. Min. Mag., vol. 30, p. 439 [M.A. **12**–506].

—— and Tuttle (O. F.), 1957. Amer. Journ. Sci, vol. 255, p. 282.

The transformation of tobermorite into xonotlite.

By H. F. W. Taylor, D.Sc., Ph.D.

Department of Chemistry, University of Aberdeen.

[Read 6 November 1958.]

Summary. This hydrothermal process has been studied using single crystal X-ray methods. A crystal of tobermorite ($Ca_5Si_6O_{22}H_{10}$), treated with water at 380° C. and 250 atmospheres, gives a preferred orientation aggregate of xonotlite ($Ca_6Si_6O_{17}(OH)_2$), together probably with unoriented silica. The relationship of orientations of product and starting material was established. The change occurs without intermediate dehydration of the tobermorite to the 9·35 Å. state. The structural basis of the relationship is discussed, and it is compared with those already reported for the transformations of tobermorite into β-$CaSiO_3$ and of xonotlite into β-$CaSiO_3$. A simple experimental procedure for the single-crystal study of hydrothermal reactions is described.

XONOTLITE is a hydrated calcium silicate that occurs in contact zones, and its formation is easily reproduced in the laboratory under hydrothermal conditions between about 150° and 400° C. When it is prepared from lime and silica, there is formed as an intermediate stage either tobermorite, or badly crystallized material structurally related to tobermorite. The main object of the present work was to study the mechanism of the transformation of tobermorite into xonotlite, using single crystal methods, and to find out in particular whether the process is one in which order is preserved.

Materials and methods.

Dr. J. D. C. McConnell kindly provided the tobermorite. It was part of the specimen from Ballycraigy, N. Ireland, which has previously been described (McConnell, 1954). The identity of each crystal used was checked by single-crystal X-ray methods. Relatively large crystals (up to 500μ long) were needed, and all showed both disorder and angular spread in their X-ray reflections, but they approximated well enough to single crystals for the present purpose. All gave multiple basal reflections, the strong one of spacing 11·3 Å. being accompanied by weak or very weak ones of 14·0, 12·3, and about 9·7 Å., but examination of the X-ray patterns as a whole indicated that 11·3 Å. tobermorite was by far the most important constituent. All the crystals used were irregularly shaped laths with length *b* and cleavage (001).

After it had been checked, each crystal was placed in a specially designed hydrothermal bomb of about 1 ml. capacity (fig. 1). The construction is largely apparent from the figure. The crystal was placed in the silver cup, and a measured quantity of water in the cavity below; supercritical conditions were normally employed, and the pressure was calculated from Kennedy's data (1950). The bomb was placed in an electric furnace for a length of time that had been found sufficient to bring about partial conversion of the tobermorite into xonotlite at the temperature and pressure used. It was then cooled in an air-blast, and opened. Except in one case, mentioned later, the crystal was unchanged in general appearance, though semi-opaque, and was sometimes quite dry and sometimes slightly moist. It was removed and examined by X-ray oscillation, rotation, and Weissenberg photographs. In some cases, the crystal was heated at atmospheric humidity either before or after the hydrothermal treatment; X-ray single-crystal photographs were always taken after each stage in the treatment. Attempts to treat crystals with water or saturated steam below the critical temperature (374° C.) were not very successful, as considerable contamination by atmospheric CO_2 always occurred, giving randomly oriented crystals of calcite.

Results.

Table I lists the experiments performed and gives the phases produced. In all cases, the xonotlite showed strongly preferred orientation. Fig. 2 shows a typical X-ray photograph of a crystal after hydrothermal treatment. As the crystals were in general only partly converted into xonotlite, it was easy to determine the relative orientations of product and starting material; for this purpose, rotation photographs of crystals mounted about each of the three principal tobermorite axes, and equatorial Weissenbergs about the tobermorite *b*-axis, were especially useful. A single crystal of tobermorite was thus found to give an aggregate of xonotlite with two preferred orientations:

Tobermorite.	Xonotlite.		
	1st orientation.	2nd orientation.	
a 11·3 Å. ⟶	*a*	16·50 *kX*	$\bar{a}$
b 7·33 Å. ⟶	*b*	7·32 *kX*	*b*
c 22·6 Å. ⟶	*c*	7·03 *kX*	$\bar{c}$
$\alpha = \beta = \gamma = 90°$	$\alpha = \beta = \gamma = 90°$		

The unit-cell data quoted above are those obtained by Megaw and Kelsey (1956) for tobermorite, and by Mamedov and Belov (1956) for

xonotlite. Two orientations are possible for the xonotlite in spite of its orthogonal cell, because the symmetry is only monoclinic (Mamedov and Belov, 1956). Weissenberg photographs in the present case showed

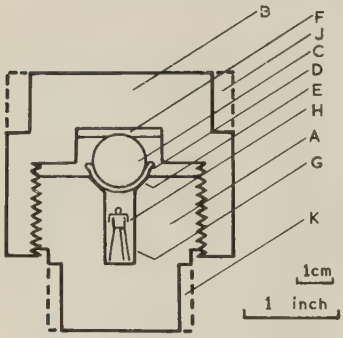

Fig. 1

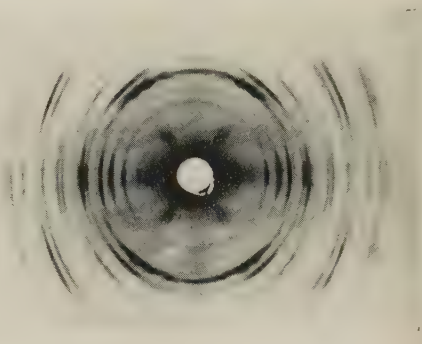

Fig. 2

Fig. 1. Bomb for hydrothermal treatment of single crystals. A, stainless steel body. B, stainless steel cap. C, steel ball. D, hardened silver gasket. E, conical surface tangential to steel ball. F, copper disk. G, cavity. H, silver cup for crystal, with lid and tripod of the same material. The body (A) and cap (B) are circular in section, with flats (J and K) to facilitate tightening and loosening.

Fig. 2. X-ray rotation photograph of crystal of 11·3 Å. tobermorite after hydrothermal treatment; rotation about the *b*-axis. Sharp reflections (slightly mis-set) are from residual tobermorite; preferred orientation streaks are from xonotlite.

no differences between the intensities of corresponding $h0l$ and $h0\bar{l}$ reflections. A weak, unoriented reflection of spacing 4·2 Å. was sometimes observed, and may have been due to silica.

Crystal A, which had been largely altered to xonotlite, was also examined optically. It was semi-opaque, with low birefringence and mean index about 1·53. Extinction was parallel to *b*, and the sign of elongation positive, in so far as measurements were possible. Crystal B was afterwards converted into β-$CaSiO_3$ (wollastonite or parawollastonite) by heating at 1000° C. The product was a preferred orientation aggregate with two principal orientations, as shown in fig. 3*a*. Crystal D, which had previously been heated at 300° C., was largely unchanged after hydrothermal treatment, but gave a few of the strongest reflections of xonotlite. The relative orientations of the 9·35 Å. tobermorite and the xonotlite seemed to be the same as with 11·3 Å. tobermorite, though this was not definitely established. Attempts to obtain a higher degree of oriented conversion of 9·35 Å. tobermorite into xonotlite (crystals E and F) were unsuccessful.

TABLE I. Hydrothermal treatments of tobermorite crystals

Crystal.	Preliminary treatment.	Principal basal spacing after preliminary treatment.	Hydrothermal treatment.	X-ray pattern after hydrothermal treatment.
A	None	11·3 Å.	380° C., 250 atm., 12 hours.	Strong, oriented pattern of xonotlite; weak pattern of residual 11·3 Å. tobermorite; powder ring 4·2 Å. (SiO_2?) No 9·35 Å. tobermorite.
B	Ditto	Ditto	Ditto	Ditto
			Crystal B afterwards heated at atmospheric humidity, 1000° C., 1 hr.	Oriented pattern of β-$CaSiO_3$.
C	Heated at 300° C. and atmospheric humidity for 3 hours.	9·35 Å.	As A	Unchanged 9·35 Å. tobermorite.
D	Ditto	Ditto	As A	Strong pattern of unchanged 9·35Å. tobermorite: weak oriented pattern of xonotlite.
E	Ditto	Ditto	420° C., 350 atm., 12 hrs.	Oriented pattern of β-$CaSiO_3$.
F	Ditto	Ditto	370–80° C., 250 atm., approx., 6 days.	Crystal disappeared: may have dissolved and recrystallized completely.

Discussion.

The results show that conversion of 11·3 Å. tobermorite (tobermorite *sensu stricto*) into xonotlite at 380° C. and 250 atmospheres pressure occurs without intermediate formation of 9·35 Å. tobermorite (riversideite of McConnell, 1954). Had the latter been formed, it would have been detected in the hydrothermally treated crystals A and B, unless

the subsequent change to xonotlite was fast. The results with crystals C and D, however, show that this change is slow under the conditions used.

A high degree of order is preserved during the transformation. In this, and some other respects, the latter resembles those of 11·3 Å. into 9·35 Å. tobermorite (McConnell, 1954; Taylor, 1958), 9·35 Å. tobermorite into β-$CaSiO_3$ (Taylor, 1958), and xonotlite into β-$CaSiO_3$ (Dent and Taylor, 1956). These related transformations are summarized below:

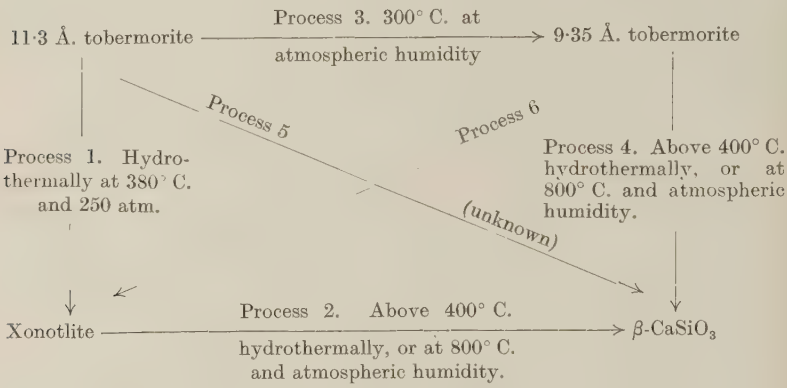
11·3 Å. tobermorite
Process 3. 300° C. at atmospheric humidity
9·35 Å. tobermorite
Process 5
Process 6
(unknown)
Process 1. Hydrothermally at 380° C. and 250 atm.
Process 4. Above 400° C. hydrothermally, or at 800° C. and atmospheric humidity.
Xonotlite
Process 2. Above 400° C. hydrothermally, or at 800° C. and atmospheric humidity.
β-CaSiO3

The results obtained on heating crystal B at 1000° C. after the hydrothermal treatment (table I and fig. 3*a*) confirm the orientation relationship previously found for the transformation of xonotlite into β-$CaSiO_3$ ($b \rightarrow b$, $c \rightarrow c$). Fig. 3 shows also that, when β-$CaSiO_3$ is formed from tobermorite, the type of twinning in the product depends on whether the process has occurred with intermediate formation of xonotlite (processes 1 and 2 above), or of 9·35 Å. tobermorite (processes 3 and 4).

Xonotlite is more easily formed from 11·3 Å. tobermorite (process 1) than from the 9·35 Å. form (process 6). In contrast, β-$CaSiO_3$ is easily obtained from 9·35 Å. tobermorite (process 4), but its direct formation from 11·3 Å. tobermorite (process 5) is not known to occur with normal specimens of tobermorite, although it apparently does happen with that from Loch Eynort, Scotland (Gard and Taylor, 1957). These facts could be explained if structural similarities existed between 11·3 Å. tobermorite and xonotlite on the one hand, and between 9·35 Å. tobermorite and β-$CaSiO_3$ on the other.

The existence of a close structural relationship in the case of 9·35 Å. tobermorite (riversideite) and β-$CaSiO_3$ has already been demonstrated,

and was shown to explain the observed orientation relationship for process 4 (Taylor, 1958). The two structures are very similar, especially as regards Ca–O packing. The structures of 11·3 Å. tobermorite and xonotlite appear to be less closely related. There is a relationship

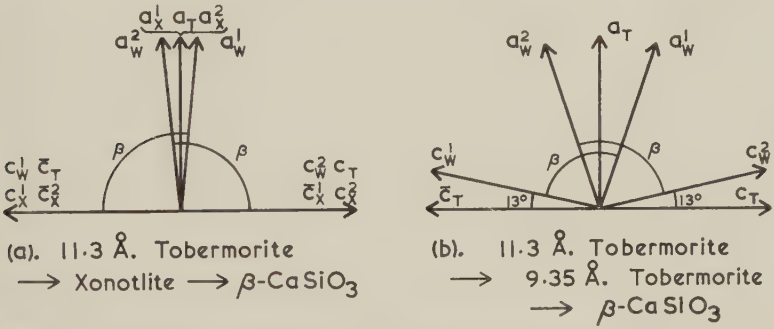

FIG. 3. Orientation relationships for transformations involving tobermorite, xonotlite, and β-$CaSiO_3$, viewed along the common *b*-direction. Suffixes: T = tobermorite (axial directions identical for 11·3 Å. and 9·35 Å. forms); X = xonotlite; W = β-$CaSiO_3$; 1, 2 = the two orientations for xonotlite and β-$CaSiO_3$. β-$CaSiO_3$ is referred to monoclinic axes (a = 15·417, b = 7·321, c = 7·066 Å., β = 95° 24′; Tolliday, 1958).

between the unit-cell dimensions, for (approximately) $3a_T = 2a_X$, $b_T = b_X$, and $c_T = 3c_X$, where suffixes T and X denote tobermorite and xonotlite respectively. Agreement in the *c*-direction would be somewhat worsened if the tobermorite was in the 9·35 Å. form. Beyond this, the similarity between the structures is not obvious; projections based on the results of Megaw and Kelsey (1956) for tobermorite and of Mamedov and Belov (1956) for xonotlite were compared in the correct relative orientations, but this did not reveal any striking resemblances. This may account for the fact that xonotlite can apparently only be formed hydrothermally, while β-$CaSiO_3$ can also be obtained by heating at atmospheric humidity, though at a much higher temperature; a more complicated rearrangement is needed to produce xonotlite, and this only occurs in the presence of high-pressure water or steam. Two complications in the change from tobermorite to xonotlite are the occurrence of twinning in the product, and the presumed segregation of silica; analogous problems have been discussed in connexion with the change from 9·35 Å. tobermorite to β-$CaSiO_3$ (Taylor, 1958). More detailed discussion of the change from tobermorite to xonotlite does not seem justified at present, especially in view of the fact that several important details

of the tobermorite structure are still uncertain. The experimental method used in the present work should be applicable to the study of other hydrothermal reactions occurring under comparable conditions, and such studies may help to elucidate the mechanism in the present case.

Acknowledgement. Dr. D. M. Roy very kindly read the typescript and made useful suggestions.

References.

Dent (L. S.) and Taylor (H. F. W.), 1956. Acta Cryst., vol. 9, p. 1002.

Gard (J. A.) and Taylor (H. F. W.), 1957. Min. Mag., vol. 31, p. 361.

Kennedy (G. C.), 1950. Amer. Journ. Sci., vol. 248, p. 540.

McConnell (J. D. C.), 1954. Min. Mag., vol. 30, p. 293.

[Mamedov (Kh. S.) and Belov (N. V.)] Мамедов (Х. С.) и Белов (Н. В.). 1956. Зап. Всесоюз. Мин. Общ., vol. 85, p. 13. Abstr. in Chem. Abstr. vol. 50, p. 16574*a*.

Megaw (H. D.) and Kelsey (C. H.), 1956. Nature, vol. 177, p. 390.

Taylor (H. F. W.), 1958. Proc. 6th Nat. Clay Conference (U.S.A.), Berkeley, 1957, p. 101.

Tolliday (J.), 1958. Nature, vol. 182, p. 1012.

A mineralogical application of X-ray absorption microspectroscopy: the hydration of larnite.

J. V. P. Long, M.A.
Cavendish Laboratory

and

J. D. C. McConnell, M.Sc., M.A., Ph.D.
Dept. of Mineralogy and Petrology

University of Cambridge.

[Read 6 November 1958.]

Summary. The technique of X-ray absorption microspectroscopy is described, with particular reference to the determination of calcium in a hydrogel formed in minute amounts in cavities in larnite. The method, which is applicable to other elements, enables chemical data to be obtained from selected small areas in a normal petrological thin section.

In many mineralogical problems it is desirable to obtain chemical information from extremely limited amounts of material. The technique now to be described is useful in this respect in that chemical data may be obtained from extremely small and precisely defined volumes within normal petrological thin sections. The advantage of studying chemical composition, at high resolution, within the fabric of a thin section will be apparent.

In the present paper the technique of X-ray absorption microspectroscopy is described and its usefulness illustrated in one particular case. This concerns the determination of the calcium content of a hydrogel formed in microscopic amount from the mineral larnite (β-Ca_2SiO_4) in small, sealed hydration cavities in larnite-bearing rocks where the cavities also contain calcium hydroxide (portlandite).

The present paper deals only with the determination of calcium. The technique can in practice be applied to the determination of other elements of higher atomic number.

Theory and method. The measurement of X-ray absorption at selected wavelengths provides an accurate method of determining the mass of an element present in a material of known thickness. A development of this method, using the fine focus X-ray tube devised by Cosslett and Nixon (1953), permits the analysis of small selected areas in a thin section without recourse to photographic recording (Long and Cosslett

1957; Long, 1958). In fig. 1 the transmission of an element is shown plotted against wavelength in the neighbourhood of an absorption edge. The abrupt change in transmission at the wavelength of the edge does

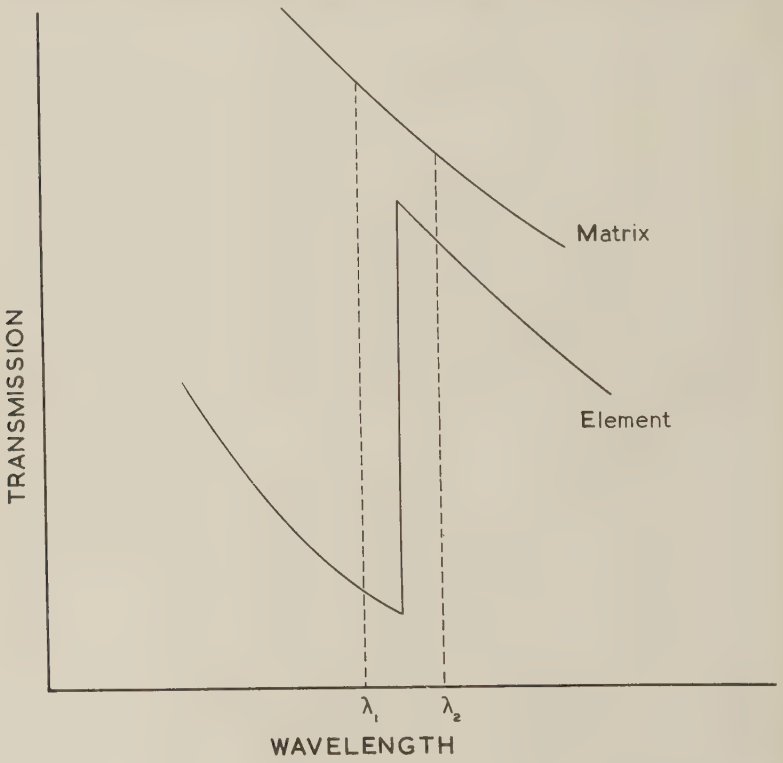

Fig. 1. Transmission of element and matrix in the neighbourhood of the absorption edge.

not occur in the corresponding transmission curve for other elements that may be present. Hence the ratio of the transmissions of the whole material at λ_1 and λ_2 immediately provides information on the mass of the element present, with only a small error due to the matrix, particularly if λ_1 and λ_2 lie close to the absorption edge.

In the present investigation the composition of the matrix could be estimated approximately, and the error due to its presence reduced to negligible proportions.

The transmission of any material is given by the equation:

$$I/I_0 = T = e^{-m\mu/\rho},$$

where μ/ρ is the mass absorption coefficient, m the mass per sq. cm. of the absorber. If this equation is written for the wavelengths λ_1 and λ_2 both for the element and the matrix the following relationship may be derived:

$$\frac{T_1}{T_2} = e^{-m[(\mu/\rho)_{\lambda 1}-(\mu/\rho)_{\lambda 2}]-m'[(\mu/\rho)'_{\lambda 1}-(\mu/\rho)'_{\lambda 2}]},$$

where T_1 and T_2 are the transmissions at wavelengths λ_1 and λ_2, m is the mass per sq. cm. of the element and m' the mass per sq. cm. of the matrix; $(\mu/\rho)_{\lambda 1}$ and $(\mu/\rho)_{\lambda 2}$ are the mass absorption coefficients of the element at λ_1 and λ_2 and $(\mu/\rho)'_{\lambda_1}$ and $(\mu/\rho)'_{\lambda_2}$ are the corresponding coefficients for the matrix material. In order to determine T_1/T_2 for areas only a few microns in diameter, Engström and others (Engström, 1946; Lindström, 1955) have made contact microradiographs on high resolution film of the Lippmann type, and have measured the density of small selected areas of the developed image with a microphotometer. In the present experiments a point projection method and direct electrical recording have been used.

The geometrical arrangement of the apparatus is shown in figs. 2 and 3. The X-ray tube consists of an electron gun and a magnetic lens, which focuses the electron beam to an area about one micron in diameter on a thin metal foil that forms both the target and the window of the X-ray tube. The X-ray source is thus about 1 μ in diameter, and, since the foil is only a few microns thick, the target to specimen distance t may be made very small in order that a high magnification may be obtained in the image recorded by a fluorescent screen or photographic plate placed a few centimetres from the target. The resolution in the image is equal to the source size, i.e. approximately 1 μ. If a circular aperture of diameter d is placed in a plane at distance D from the target, as indicated in fig. 3, it will pass radiation that has come through a circular area of diameter td/D in the specimen. In the arrangement used for the calcium determination, $d = 3$ mm., $t = 0{\cdot}5$ mm. and $D = 150$ mm. so that the area examined was 10 μ in diameter. The spectrometer crystal, placed above the aperture, selects the appropriate wavelengths from the continuous spectrum generated by the target, and their intensity is measured with a proportional counter.

In order to position the specimen so that the X-rays passing through a particular 10 μ area also pass through the aperture, a fluorescent screen is placed in a plane about 2·5 cm. above the target and accurately located in such a position that a marked point on its surface, the X-ray

source, and the centre of the aperture are in the same straight line. Since the X-ray contrast of many thin sections is insufficient to show detail on a fluorescent screen, an electron microscope grid is placed over the

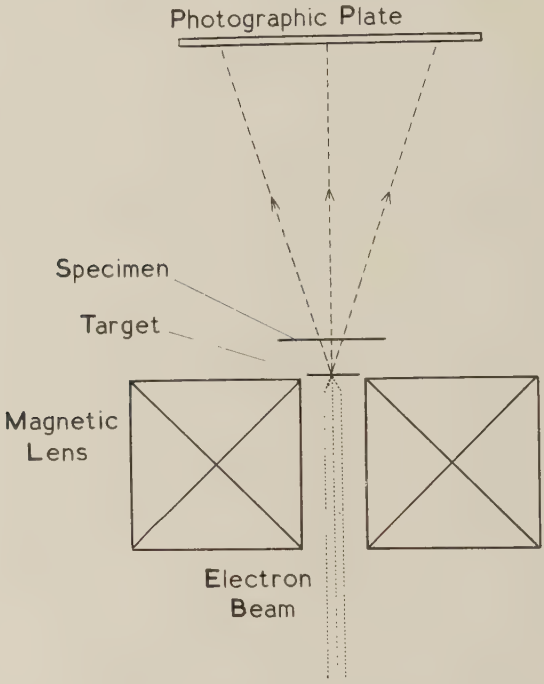

Fig. 2. The geometry of the X-ray projection microscope.

section. These grids have accurately formed squares of approximately 90 μ side, so that after locating an area in the specimen by means of an optical microscope, the same area may be identified on the fluorescent screen by reference to the easily visible X-ray image of the grid, which with the screen at a distance of 2·5 cm. from the target is seen at a magnification of 50 times. By moving the specimen stage the required area may be brought on to the marked point on the screen, so that, when the screen is removed, the X-rays passing through this area also pass into the aperture of the spectrometer.

The spectrometer crystal is arranged to alternate, eight times a minute, between two fixed angular positions corresponding to the wavelengths λ_1 and λ_2. A relay, operated synchronously with the solenoid controlling the position of the crystal, transmits the pulses from the

proportional counter, through an amplifier and pulse height analyser, to two separate scaling units. Thus at the end of a measurement, two

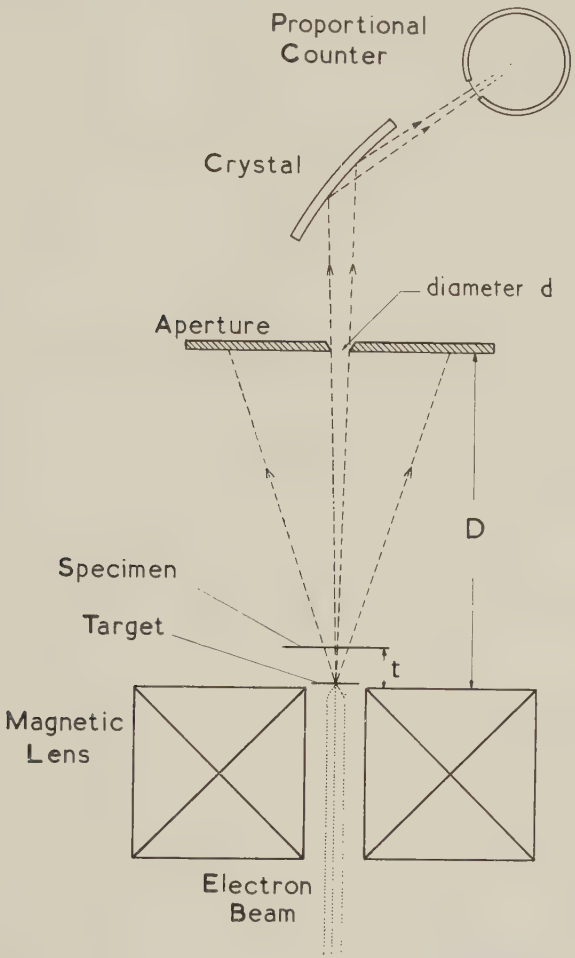

FIG. 3. Arrangement of point focus tube for microanalysis.

totals are obtained which represent the transmitted intensities at λ_1 and λ_2 respectively. In this way it is possible to measure the comparatively low count rates involved for periods of the order of half an hour without introducing errors due to drifts in the primary intensity from the X-ray tube. The ratio of the count rates at the two wavelengths

is also measured with no specimen in the beam in order to obtain the final ratio T_1/T_2 for the specimen. The ratio with no absorber present remains constant to about ± 1 %. It was always recorded for a short period before and after each measurement on a thin section.

For calcium the wavelength of the absorption edge is 3·07 Å., and 3·14 and 3·00 Å. were chosen for λ_1 and λ_2. In order to generate sufficient intensity in this part of the continuous spectrum, the X-ray tube was run at 25 kV with a target current of 10 microamps. For a 2 μ spot this gives a specific loading of 80 kW per sq. mm. Under these conditions the spectrum from the target (12 μ aluminium foil) contains a considerable intensity of continuous radiation whose wavelength is much shorter than 3 Å. It was found that the spectrometer crystal did not completely monochromatize the beam transmitted through the specimen. As a result of reflection of harmonics of the 3 Å. band, and of a small amount of Compton scattering that occurred at the monochromator, the measured calcium thickness was always slightly lower than the true value. The extent of the deficiency was determined by measuring the apparent thickness of calcium in the steps at the edge of a cleavage flake of gypsum, the true thickness of each step being measured subsequently on a polarizing microscope with the aid of a Berek compensator.

When monochromatization is incomplete the transmission ratio may be derived from an equation of the form:

$$(T_1/T_2)' = (T_{3\cdot14}+f.T_\lambda)/(T_{3\cdot00}+f.T_\lambda),$$

where $T_{3\cdot14}$ and $T_{3\cdot00}$ are the transmissions of a calcium compound at 3·14 and 3·00 Å. respectively. The intensity of the impurity radiation is expressed as f, the number of impurity quanta per 3 Å. quantum. Its effective wavelength is λ and T_λ is the transmission of the specimen for this wavelength. In the present experiments λ was found to be 1·56 Å. and f was 0·0139.

The values of T_1/T_2 calculated from the above equation were then found to agree with the measured values to within about ± 2 % for thicknesses of gypsum up to 50 μ. In the case of thick specimens of gypsum the effects of imperfect monochromatization are much greater than is the case for the thin sections of the natural calcium silicate minerals studied, since these contain a higher proportion of calcium, which in turn is associated with a matrix of lower absorption coefficient than the sulphate of the gypsum molecule.

The transmission ratio $(T_1/T_2)'$ may thus be calculated for any calcium compound and the curves for different compounds may be plotted

on the same graph if the thickness is expressed in terms of the mass of calcium per unit area. The calculated X-ray transmission relationships for the two minerals afwillite ($3CaO.2SiO_2.3H_2O$) and larnite are shown in fig. 4; this illustrates the very small effect of the matrix on the transmission ratio since the afwillite and larnite curves are almost coincident despite the very different calcium to silicon ratios. In practice the afwillite curve was used for the calcium silicate hydrogel studied. This is reasonable in view of the very small divergence of the larnite and afwillite curves.

Study of the natural hydrogel. The thin section was prepared for examination in the following manner: A suitable area was photographed and the areas to be analysed were carefully marked on the photograph. The coverslip was then removed and the section transferred from the slide to a thin aluminium disk provided with a central hole about 4 mm. in diameter, over which the area of interest was located. An electron microscope grid was then stuck over this area and the precise co-ordinates of the points to be examined determined with respect to the grid squares. It was necessary, at this stage, to refer back to the original photomicrograph. As already noted the positioning of the specimen in the X-ray beam was accomplished by observing the magnified image of the electron microscope grid on a fluorescent screen.

A photomicrograph of the hydration cavity studied in the present series of experiments is illustrated in fig. 5. The infilled cavity contains afwillite and portlandite and is surrounded by a narrow zone in which the larnite has been hydrated. The width of this narrow sheath is of the order of 150 μ. The determinations of the calcium content in the sheath of hydrogel and the larnite were carried out at specific points within the grid square whose position has been illustrated in the photomicrograph. Each single determination was carried out on an area of approximately one-hundredth of the figured grid square involving in the case of the hydrogel a mass of approximately 10^{-9} g. of calcium in the individual determinations.

Previous work has shown that the calcium oxide : silica ratio of calcium silicate hydrogels prepared in the laboratory at ordinary temperatures varies systematically with the calcium hydroxide content of the solutions involved. The effective limits of variation in the range where the hydrogels yield X-ray powder data indicating structural affinity with the calcium silicate hydrate mineral tobermorite are 0·8:1 and 1·5:1. The latter ratio is obtained in solutions saturated with calcium hydroxide.

In an earlier communication (McConnell, 1955) an account was presented of the hydration of natural β-Ca_2SiO_4 and the formation of a

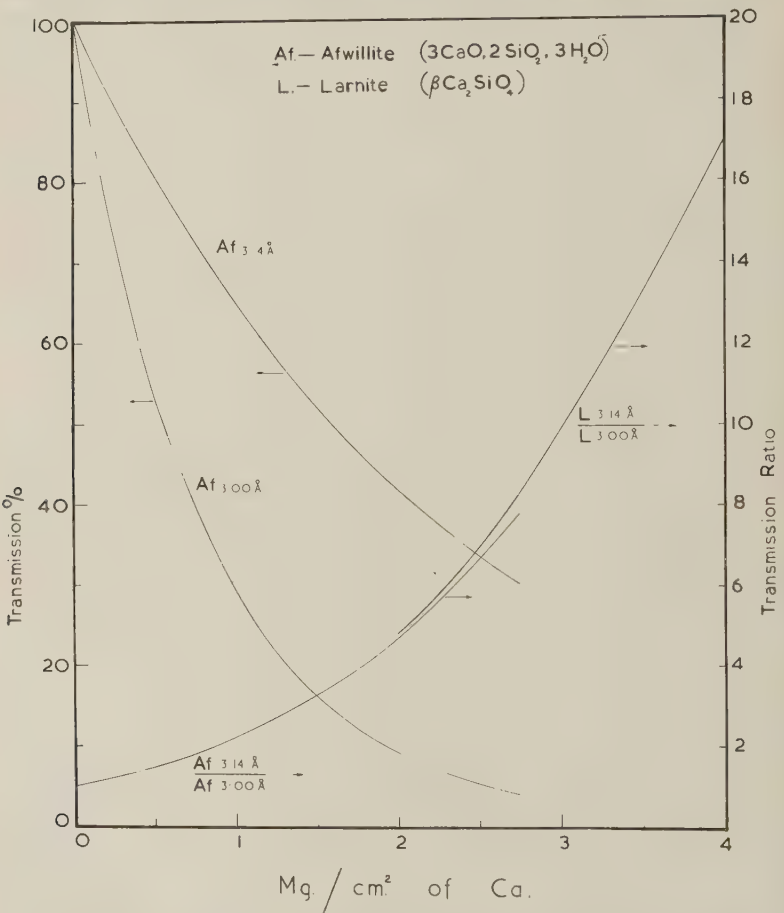

Fig. 4. X-ray transmission of afwillite and larnite as a function of thickness of calcium.

calcium silicate hydrogel corresponding in composition to the low-lime end of the above hydrogel series. The analysed specimens were taken from an environment in which the presence of circulating ground water of low pH was probable. An unpublished and more recent study of the microstructure of the low-lime hydrogel formed from bredigite, by the same author, involving low-angle scattering experiments, and a more detailed analysis of the adsorption isotherm of the low-lime hydrogel

indicated that the latter has a lamellar pore structure and comprises extremely imperfect crystalline sheets possibly one unit cell or less in thickness. These imperfect sheets are irregularly stacked but the preferred orientation (already noted, McConnell, 1955, p. 675) implies that they have developed by a process of topochemical reaction from the parent dicalcium silicate structure.

The pore structure observed in the low-lime hydrogel can only reasonably be explained in terms of the former production, at higher pH values, of a defect topochemical product of higher calcium content, the additional lime being present as calcium hydroxide intimately associated with the sheet silicate structure. In order to test this hypothesis it was necessary to determine the calcium content of the natural hydrogel where the latter had been produced and maintained in contact with solutions saturated with calcium hydroxide. This condition was considered to obtain in some of the smallest infilled hydration cavities in the larnite rocks at Ballycraigy, where, as illustrated in fig. 5, the centre of the cavity has been filled with portlandite and afwillite and the complete absence of carbonate implies that the cavity has, in effect, been sealed off from circulating ground water.

The equilibrium conditions illustrated by these cavities are of interest. The hydrogel formed by a process of topochemical reaction from larnite appears to represent a metastable equilibrium assemblage. The existence of afwillite and portlandite within the cavity represents crystallization of a stable equilibrium assemblage. It would appear that at the temperatures and pressure involved in the natural hydration process no dicalcium silicate hydrate phase is stable.

The results of the absorption microanalyses within the grid square outlined in fig. 5 are set out in table I. The values obtained for the larnite are consistent and provide immediate information on the thickness of the thin section. The last value for larnite was obtained at a point on the side of the cavity opposite that at which the other measurements were made. It indicates that although the section varies in thickness by about 10 % over the width of the cavity, any systematic change within the grid square will be negligible. The figures for the calcium content of the hydrogel present in the same grid square are based on the calculated ratio curve for afwillite illustrated in fig. 4.

A preliminary calculation indicated that the calcium content of the analysed low-lime hydrogel should be of the order of 0·9–1·0 mg./cm.^{2} in a section 20 μ thick. These limits were defined by the variable density of the low-lime hydrogels studied. Considerably higher values for the

calcium content were obtained for the hydrogel within the figured grid square as indicated in table I. These recorded values are consistent with a $CaO:SiO_2$ ratio for the gel of the order of 1·5. Table I illustrates one difficulty in the determination of the calcium content of the hydrogel.

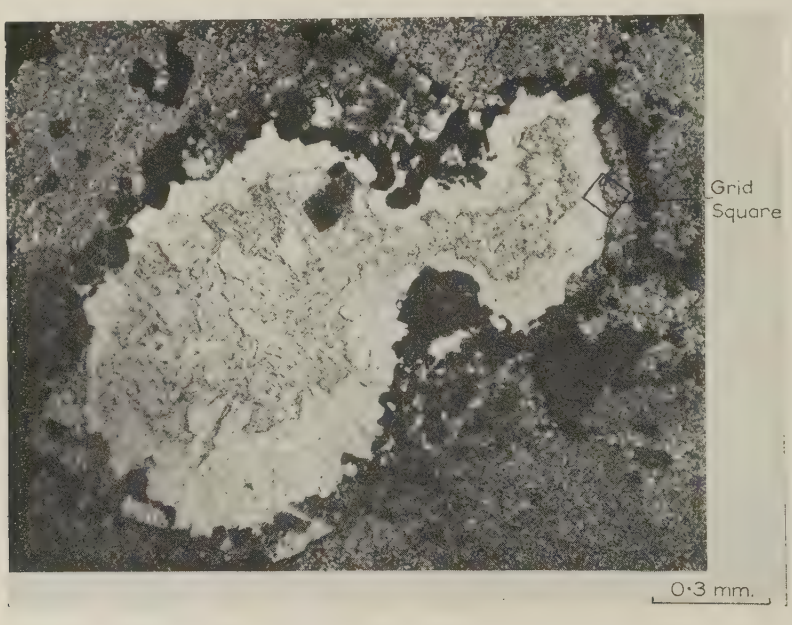

Fig. 5. A small infilled cavity in larnite spinel rock from Ballycraigy, Co. Antrim, showing calcium silicate hydrogel, afwillite, and portlandite.

Since the gel is extremely brittle, irregularities in its surfaces and the presence of cracks imply that the calcium contents determined must be regarded as minimum values. In table I the values of calcium content that are low have been marked with an asterisk. The corresponding areas were shown to correspond with the position of a crack in the thin section by taking a high resolution microradiograph of the area. This source of error is unlikely to be of importance in carefully ground thin sections of normal minerals.

The interest of the present determination lies in the recognition of a primary stage in the topochemical hydration reaction of natural β-Ca_2SiO_4 involving a defect phase of high lime content. Further study of the precise mechanism of this hydration reaction is of importance in that the mechanism can with reasonable certainty be applied to the

Table I.

	A.	B.	C.
Larnite . .	9·61	2·97	—
Larnite . .	9·43	2·94	—
Larnite . .	9·82	3·00	—
Larnite . .	9·53	2·96	—
Larnite . .	9·36	2·93	—
Hydrogel . .	3·57	1·62	1·66
Hydrogel . .	3·89	1·75	1·79
Hydrogel . .	3·31	1·46	1·50
Hydrogel . .	3·74	1·61	1·65
Hydrogel . .	3·17	1·41	1·47*
Hydrogel . .	2·10	0·90	0·92*
Larnite . .	10·60	3·12	—

A. Corrected ratio of transmissions.

B. Calcium content expressed as mg./cm.^{2} in the thin section studied.

C. Calcium content of the hydrogel stated in mg./cm.^{2} in a thin section of thickness 20μ. (The thickness of the section studied was found to be 19·6μ from the average of determinations made on the larnite present.)

* In these determinations the low values were correlated with the presence of a crack in the thin section.

hydration of cement clinker particles of β-Ca_2SiO_4. The extremely slow rate of hydration has so far prevented study of this process on grains of β-Ca_2SiO_4 in the laboratory. A more detailed account of the microstructure of the hydrogels formed and the mechanism of the topochemical hydration reaction will be presented elsewhere.

References.

Cosslett (V. E.) and Nixon (W. C.), 1953. Brit. Journ. Appl. Phys., vol. 24, p. 616.

Engström (A.), 1946. Acta Radiol., Suppl. 63.

Lindström (B.), 1955. Ibid., Suppl. 125.

Long (J. V. P.), 1958. Journ. Sci. Instr., vol. 35, p. 323.

—— and Cosslett, (V. E.), 1957. 'X-ray Microscopy and Microradiography', Academic Press, N.Y., p. 435.

McConnell (J. D. C.), 1955. Min. Mag., vol. 30, p. 672.

Mineralogy of the Silvermines district, County Tipperary, Eire.

(With Plates IV to VI.)

By H. N. Rhoden, Ph.D., D.I.C., A.R.S.M.
Redhill, Surrey.

[Communicated by Dr. A. P. Millman, taken as read 2 April 1959.]

Summary. The paragenesis of a suite of hydrothermal minerals (sulphides, baryte, rhombohedral carbonates, quartz, sericite, and chlorite) at four mines in this district is discussed. Of particular interest are the conversion of pyrrhotine to marcasite, which is shown to take place by loss of iron, the replacement of blende by chlorite, and the possible formation of primary goethite. The occurrence of gudmundite is recorded for the first time in the British Isles.

JUST over fifty years ago, Russell (1907) published in this journal 'Notes on the Mines and Minerals of the Silvermines District, County Tipperary'. A recent survey of various eighteenth- and nineteenth-century workings and one modern productive lead mine near Silvermines, coupled with microscopic examination of the ores, has revealed the presence of additional minerals and some unusual textural features.

A fuller description of the mines, local geology, and economic mineralization has been published elsewhere (Rhoden, 1958*a*, 1958*b*). Briefly, the ore deposits occur in Devonian and Carboniferous rocks bordering the Silvermines Fault, which is a complex system of major and tributary fractures that can be traced for over 25 miles across northern Tipperary and southern Clare.

Shallee and Gortnadyne mines.

At Shallee mine, ramifying veinlets of galena, baryte, and other minerals, listed in order of deposition in table I, are concentrated beneath gently dipping shale horizons in strongly fractured Devonian sandstones. At Gortnadyne mine the copper lode consists mainly of brecciated Devonian sandstone, re-cemented by quartz, sulphides, baryte, and carbonates.

Although dislocation of the beds preceded the onset of mineralization, structural dilation of the fractures continued throughout the sulphide phases, and finally ceased during the deposition of baryte, which filled

TABLE I. Epigenetic minerals at Shallee and Gortnadyne mines.

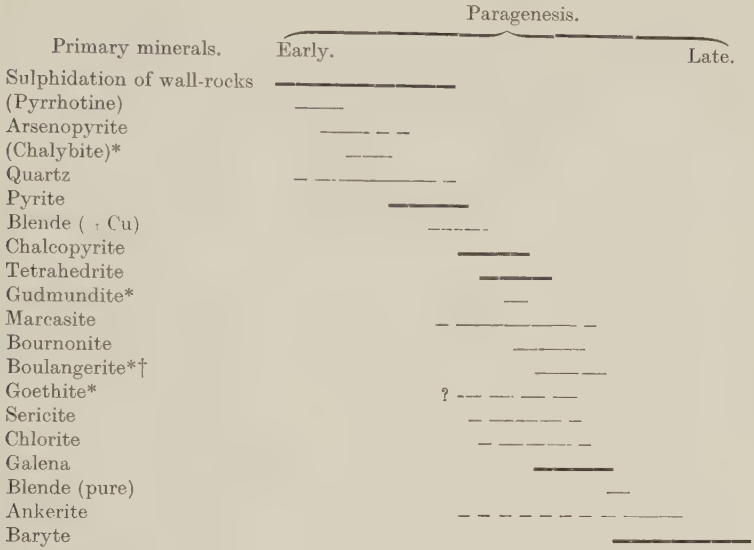

* Microscopic identification.
† Shallee only.
‡ Gortnadyne only.

the remaining space in the veins and breccias. During mineralization, the red and buff sandstones and shales were bleached to light grey and olive-green colours respectively, with redeposition of sedimentary hematite and goethite as pyrite; at the same time, ilmenite grains were replaced by clusters of rutile crystals set in translucent leucoxene and quartz.

The first epigenetic mineral of which traces still remain was *pyrrhotine*. Platy crystals, up to 1 inch square, grew parallel to the sandstone wall-rocks, giving the veins a streaky appearance. After slight fracturing, the pyrrhotine was often surrounded by euhedral crystals of *arsenopyrite*, and of a *rhombohedral carbonate* that was afterwards converted to ankerite and goethite (see p. 133), before being finally set in a matrix of *quartz* and later sulphides. During the subsequent deposition of copper, antimony, zinc, and lead minerals, all the pyrrhotine changed to marcasite and pyrite (see p. 131).

Of the principal minerals, *pyrite* was deposited earliest. Small pyrito-

hedra line the veinlets at Shallee mine, and are scattered throughout the sandstone and shale wall-rocks, having formed at the expense of sedimentary iron oxides. A few thin beds of dolomitic and sandy shale, however, contain abundant needles of arsenopyrite, to the exclusion of pyrite, indicating that arsenic may have been an original constituent of the rock (Goldschmidt and Peters, 1934).

Two forms of *blende* occur: one is dark brown, iron-rich, and often contains tiny inclusions of exsolved chalcopyrite; the other type is light yellow and free from inclusions. Deposition of the dark variety, which is more common at Gortnadyne than at Shallee, overlapped the formation of pyrite, producing alternate colloform banding. The purer blende was the last sulphide to crystallize, and is often associated with veinlets of ankerite. *Chalcopyrite*, followed closely and partly replaced by *tetrahedrite*, succeeded pyrite at both mines, but attained economic grade only at Gortnadyne.

The most abundant sulphide in the veins at Shallee mine, and probably also in the breccia at Gortnadyne, is *galena*; but if the 'ore' is assumed to include the inter-vein sandstone, galena may be exceeded by pyrite. Although galena slightly replaced all the earlier minerals, most of it was deposited in open fissures; but in places where the vein-walls had not been lined by pyrite or chalcopyrite, galena also replaced quartz and clay-mica minerals to give the marginal sandstone a distinct blue-grey coloration. Galena at Shallee mine contains 44 to 53 oz. of silver per long ton of lead metal (production data for 1949 to 1958), and at Gortnadyne, 20 to 25 oz. per long ton (Wynne, 1861).

A remarkable feature of the galena at Shallee mine is the multitude of inclusions of bournonite, boulangerite, and tetrahedrite. Some tetrahedrite grains are plainly relics left during the replacement of surrounding chalcopyrite; part of the bournonite may be a reaction 'front' between partly replaced copper minerals and galena; but most inclusions are remote from such replacement contacts, and the microscopic texture indicates that they have exsolved from the galena during cooling. Boulangerite occurs as a 'rash' of tiny untwinned laths up to 40 μ long, oriented along crystallographic planes within the galena. Bournonite inclusions, showing excellent parquet-like twinning, are larger and more rounded in shape, and tend to segregate at grain boundaries, leaving peripheral areas of the galena free from inclusions. Tetrahedrite is less common away from contacts with copper minerals, but occurs in the galena like bournonite. Inclusions of different minerals are never intermingled, but may occur in neighbouring grains of galena. Although

direct evidence is lacking, exsolution probably commenced with tetrahedrite, continued with bournonite, and ended with boulangerite; the type of inclusion produced in each grain of galena would depend on the concentration of copper and antimony, and on the original temperature of deposition. In direct contrast, galena at Gortnadyne mine rarely contains any exsolved minerals.

The growth of fibrous mats of *chlorite* and *sericite* in open veins at this stage of mineralization is described below (p. 134). Deposition of creamy-coloured *ankerite* (ω 1·712 to 1·720), containing a trace of manganese, probably started shortly after the pyritic stage, but reached a modest peak as sulphide mineralization ended with the crystallization of light yellow blende (see table I). The carbonate at Gortnadyne is contaminated by the presence of dolomite in parts of the breccia. Any remaining space in the veins or breccias was filled by pure white *baryte*, the last primary mineral deposited. The usual range of secondary minerals, listed in table I, developed during erosion.

Conversion of pyrrhotine to marcasite. The alteration of pyrrhotine to marcasite and pyrite is not a rare phenomenon in moderate to low temperature sulphide deposits,[1] having been first reported over fifty years ago (referred to by Allen, Crenshaw, Johnston, and Larsen, 1912). Some writers (summarized by Edwards, 1954) consider that the change occurred during the closing stages of mineralization, while others (Foslie, 1950) regard it as a supergene process. Although similar conversions of pyrrhotine to marcasite have been observed in ores from Abbeytown, Co. Sligo, Eire, and from Stari Trg, Trepča, Yugoslavia, the unique suite[2] of minerals from the Silvermines district establishes the exact point during the primary mineralization at which the alteration occurred.

As the first epigenetic mineral, pyrrhotine crystallized only in the 'strongest' veins at Shallee mine, and in the breccia at Gortnadyne. Single platy crystals with sharp edges, illustrated in pl. V, fig. 3, grew parallel to the vein wall, giving an appearance of 'flow texture' to the veins; pyrrhotine never occurs in the granular or rosette form commonly found at other deposits,[1] including Abbeytown and Trepča. After being lightly fractured, the pyrrhotine plates were partly covered by arsenopyrite (shown in pl. IV, fig. 1) or carbonate (possibly chalybite, see p. 133) crystals, before being finally set in quartz and later sulphides.

[1] Described by O'Malley and McGhie, 1939; Stillwell and Edwards, 1943, 1945, 1946; Stillwell, 1944; Carter, 1948.

[2] Type samples from Shallee and Gortnadyne mines are included in the reference collections of Economic Mineralogy at the Imperial College of Science and Technology, London.

Pyrrhotine remained stable throughout the pyritic stage of mineralization, but changed entirely to marcasite and pyrite during the subsequent deposition of copper, antimony, lead, and zinc minerals. Despite the simultaneous crystallization of iron-rich minerals, such as blende, chalcopyrite, and tetrahedrite, nearby and even within the pseudomorph, the pyrrhotine altered to disulphide by expelling roughly half its original iron content, and without consuming additional sulphur (see below). As the conversion progressed, tiny shrinkage cracks opened parallel to the basal parting of the pyrrhotine crystals, which otherwise retained their shape. The reduction in volume from pyrrhotine to disulphide can be measured microscopically, and is remarkably constant at 32 to 38 %.

Theoretically, the conversion of pyrrhotine to marcasite can take place in three ways (for convenience pyrrhotine is assumed to be FeS (troilite)): *constant volume*, in which sulphur must be added to the system and iron removed in the proportion expressed in the equation $4FeS + 2S = 3FeS_2 + Fe$; *constant iron*, in which sulphur is added ($FeS + S = FeS_2$), and the resulting marcasite occupies over 33 % more space than the original pyrrhotine; and *constant sulphur*, in which almost half the iron is expelled ($2FeS = FeS_2 + Fe$), leaving marcasite or pyrite to occupy only 66·8 % or 65·2 % of the pseudomorph respectively. Although natural pyrrhotine, which has a defect structure (Hägg and Sucksdorff, 1933), varies in composition between $Fe_{0.971}S$ and $Fe_{0.893}S$ with consequent change in density, its original composition should not change the ratio of atomic sulphur to molecular volume, nor affect the theoretical shrinkage to marcasite or pyrite in a constant sulphur system.

By comparing the theoretical reduction in volume by 33·2 % for marcasite or 34·8 % for pyrite with the measured 32 to 38 %, there can be no doubt that the pyrrhotine at Shallee and Gortnadyne mines changed to disulphide solely by the loss of iron. The same applies to the conversion of granular pyrrhotine at Abbeytown mine and Trepča, and to the typical 'bird's eye' textures observed in other ore deposits.

As the pyrrhotine decomposed, the shrinkage cracks were filled by the mineral being deposited in the vicinity. Most cracks contain chalcopyrite, tetrahedrite, iron-rich blende, galena, or quartz (see pl. IV, figs. 1 and 2), any single crack usually being filled with more than one mineral; less commonly, bournonite, boulangerite, gudmundite, a rhombohedral carbonate, and even later minerals, like iron-free blende and baryte, may be included. Although most of the pyrrhotine changed to marcasite, some idiomorphic pyrite developed near the edges of the

pseudomorphs, breaking the continuity of the tiny shrinkage cracks (see pl. IV, fig. 1). The marcasite occurs as minute lath-shaped crystals, oriented at right angles to the cracks and often separated from each other by almost sub-microscopic partings containing other minerals.

Gudmundite. Liberation of iron from the decomposing pyrrhotine produced some unusual results in the narrow shrinkage cracks and along the edges of the pseudomorphs. During an influx of tetrahedrite, a momentary excess of iron over copper would cause the deposition of gudmundite (FeSbS), and the remarkable angular texture illustrated in pl. IV, fig. 2; the tetrahedrite crystals shown in pl. V, fig. 4, were partly replaced by chalcopyrite, then covered by a thin, even layer of gudmundite, before remaining space in the centre of the crack was filled by quartz. Rarely, intergrowths of gudmundite and tetrahedrite occur separately from the pyrrhotine pseudomorphs.

Although the properties of gudmundite closely resemble those of arsenopyrite (Buerger, 1939), it can be readily identified in polished sections by its strong rose-coloured pleochroism. Ridland (1941) reported a Talmage hardness of F for gudmundite, similar to arsenopyrite; but most observers, including the writer, prefer a rating of D, closer to tetrahedrite. The apparent rarity of gudmundite may be due solely to the failure of many geologists to distinguish it from arsenopyrite.

Gudmundite, which is usually found in hypothermal deposits like the complex sulphide masses at Boliden (summarized by Sampson, 1941), or the gold–stibnite veins of Southern Rhodesia (Morgan, 1957), has not been previously reported from the British Isles, and may occur in other leptothermal deposits similar to those at Silvermines.

Replacement of carbonate mineral. The crystallization of a rhombohedral carbonate around pyrrhotine and on vein-walls before the deposition of pyrite was mentioned above (p. 129). Despite their characteristic outline, the rhombs are invariably filled with a granular aggregate of ankerite and goethite, which vary widely in relative proportion. Interlocking grains of ankerite are rarely in definite orientation either to one another or to the pseudomorph margins. In many pseudomorphs, like that illustrated in pl. V, fig. 5, galena appears to vein and partly to replace the aggregate along grain boundaries, or along the ankerite cleavage. In most samples, the galena seems to be related to the existing aggregate rather than to any 'ghost' structure of an original single carbonate crystal.

Theoretically, three interpretations of the texture are possible. Galena

may have veined and partly replaced either the original carbonate, the remainder of which changed to ankerite and goethite during supergene alteration; or an aggregate of ankerite or chalybite, only the goethite being formed later; or the present aggregate of ankerite and goethite, this being a primary replacement of an original chalybite crystal.

The third hypothesis accounts for the texture best, for goethite is always present in the pseudomorphs, while surrounding sulphides show no sign of supergene alteration. If the original carbonate was chalybite that had crystallized shortly after pyrrhotine, but before the complete sulphidation of iron oxides in the surrounding sandstones, it may have become unstable during the later phases of mineralization, when true ankerites were being deposited; as the chalybite changed to ankerite, some of the excess iron would remain in the pseudomorph as primary goethite. In a low-temperature deposit, like that at Shallee mine, such residual goethite might survive through the final stages of galena–baryte mineralization, for the decomposition temperature of goethite is about 150° C. in neutral or weakly alkaline hydrothermal solutions (Smith and Kidd, 1949). The formation of crystalline goethite in similar ores was reported by Edwards (1955).

Redeposition of pyrite. Crystallization of pyrite and blende overlapped at Gortnadyne mine, producing alternate colloform banding and mutual replacement. The dark brown iron-rich blende illustrated in pl. V, fig. 6, was lightly brecciated, then partly replaced by pyrite; subsequently, both minerals were replaced by galena. But the texture shown in this plate is unusual, for pyrite is moulded round typical galena crystals, and forms long, thin, broken veinlets along the cubic cleavage. This moulded form of pyrite is usually devoid of relics of blende.

The best explanation is that as galena replaced both minerals, some of the pyritic material remained almost *in situ*, and was redeposited around the growing crystals of galena, or along the cleavage; slight pressure would break these narrow veinlets shortly after formation. Zinc, however, would be removed from the site of replacement.

Chlorite and sericite in veins. Although extensive zones of alteration are not discernible in the wall-rocks at Shallee mine, the sericitic groundmass of sandstones and shales is often replaced by chlorite near some of the 'stronger' veins. During the later phases of mineralization (see table I), platy mats of chlorite and sericite lined the edges of freshly opened fissures, which were subsequently filled with galena, ankerite, or baryte. The feathery plates of sericite illustrated in pl. VI, fig. 9, curve and branch within galena without regard to the cubic cleavage; similarly,

in other samples, chlorite plates finger into baryte crystals without disturbing their optical continuity or utilizing their excellent cleavage.

In each instance, the microscopic texture indicates crystallization of galena and baryte around the chlorite or sericite plates, rather than development of the latter in fractures in, or replacing, the galena and baryte. Sometimes, rows of these plates lining a vein-wall are bent the same way, suggesting the flow direction of the solution depositing the encasing mineral. Growth of chlorite and sericite in veins, probably from material derived mainly from the wall-rocks, must be regarded as a distinct phase of mineralization, occurring just before the main deposition of galena and baryte.

Replacement of blende by chlorite. An unusual replacement phenomenon occurs at Shallee mine, in which isolated crystals of dark brown blende containing exsolved inclusions of chalcopyrite are marginally replaced by bright green chlorite. The original outline of a euhedral blende crystal, the margin of chlorite, and the unreplaced core, are illustrated in pl. VI, figs. 7 and 8. Irregular masses of light yellow blende, shown in pl. VI, fig. 8, have replaced clay-mica minerals in the rock groundmass surrounding the pseudomorph. Since the quantity of the light yellow form is comparable with the amount of replaced copper-rich blende, the inescapable conclusion is that blende replaced by chlorite was immediately redeposited nearby purged of its inclusions. Much of the uncommon, pure blende found at Shallee may have been derived from an earlier copper-rich variety (see paragenesis in table I).

According to Hey's (1954) optical data, both chlorites ($\omega = 1{\cdot}64$, $\epsilon - \omega = -0{\cdot}004$) mentioned above can be classed as brunsvigite.

Knockanroe and Ballygown South mines.

Along the northern side of the Silvermines fault at Knockanroe and Ballygown South mines, fractured dolomite near the base of the Carboniferous Limestone series contains disseminated pyrite, marcasite, blende, galena, and baryte. During prolonged pre-glacial erosion of the ore-zones, sulphides were oxidized and the products, with baryte and silica, became progressively concentrated with the removal of the host-rock. Less soluble minerals, such as anglesite, cerussite, unaltered galena, and baryte, accumulated on the surface with gossan. More soluble material, like zinc and some iron, migrated downwards in sulphate solution to replace fresh dolomite, forming smithsonite and chalybite respectively; these, in turn, changed to hemimorphite and goethite as the level of oxidation gradually deepened. The high-grade residual lead-silver

deposit, which gave rise to the name 'Silvermines', was exhausted during the seventeenth and eighteenth centuries; below it, the enriched zinc-iron ore-zone still remains, known as the 'Calamine Bed'. Primary minerals identified at these mines are listed in order of deposition in table II, and secondary minerals in order of depth zones in table III.

TABLE II. Primary minerals at Knockanroe and Ballygown South mines.

Primary minerals.	Paragenesis: Early.	Late.
Pyrite	– ——— –	
Marcasite	– ——— –	
Arsenopyrite	—	
Blende	– ——————— –	
(ex. pyrrhotine)*	—	
Galena	– ——— –	
Baryte	– ———	
Dolomite (recrystallized)	– – ———	

* Pyrrhotine exsolved from the earliest variety of blende, during cooling.

The first epigenetic minerals in the dolomite, or in the sandstone fault-breccia known as the 'Sulphur Lode', were *pyrite* and *marcasite*. Spherulites, up to 2 inches in diameter and composed mainly of radiating pyrite crystals, often contain wedges or segments of marcasite; the relic texture illustrated in pl. VI, fig. 10, indicates that clumps of marcasite crystals in the centres of spherulites may subsequently change to pyrite. Slight variations in pH caused by the dissolution of dolomite, rather than small changes in temperature, pressure, or concentration, would determine the mineral formed at the point of precipitation at each moment (Allen, Crenshaw, Johnston, and Larsen, 1912). As Tarr (1927) suggested, marcasite would crystallize during an influx of slightly acid solutions, but pyrite would be deposited as the quantity of dissolved lime increased and the temperature of the solutions decreased.

TABLE III. Secondary minerals at Knockanroe and Ballygown South mines.

Secondary minerals.	Depth zones: Surface.	Shallow.	Deep.
Goethite	——————————— –		
Cerussite	——— – – –		
Anglesite	——— – – –		
Hemimorphite	——— –		
Smithsonite	– ———		
Chalybite	– ———		

As in similar rocks at Shallee, abundant needles of *arsenopyrite*

developed in certain thin shaly beds within the dolomite, to the exclusion of pyrite or marcasite.

Deposition of *blende* overlapped that of pyrite and marcasite, causing alternate colloform banding round spherulites. The earliest blende was a dark brown variety, containing up to 4 % Fe, from which pyrrhotine subsequently exsolved; thereafter the blende became progressively purer, until clear, light yellow crystals were formed at the end of mineralization. The exsolution of pyrrhotine from blende at Knockanroe and Ballygown South mines, rather than chalcopyrite as at all other deposits in the Silvermines district, is noteworthy; it indicates that the total absence of copper minerals in the present superficial workings will probably continue in depth.

Deposition of *galena* started shortly after the earliest blende, but finished just before the final and purest variety of the latter. The high silver content of the lead ores made the locality famous in olden days; the figure of 80 oz. of silver per long ton of smelted lead quoted by Rutty (1772) and Wynne (1861) referred mainly to the oxidized ores, but Apjohn (1860) confirmed the same quantity in fresh galena. The last truly epigenetic mineral was *baryte*.

The hydrothermal minerals are closely associated with irregular veinlets of a light pink *dolomite* (ω 1·69) containing traces of iron and manganese, which has the same composition as the dark blue-grey host-rock. Redeposition of dolomite started during the later phases of sulphide mineralization, and continued afterwards until most fissure and solution cavities were sealed. At the western end of Knockanroe mine most veinlets were filled with baryte, which effectively restricted the recrystallization of dolomite.

The secondary ores at these mines resemble 'calamine' deposits elsewhere. In the residual lead-silver zone, cerussite and anglesite replace galena, often leaving a core of sulphide protected from oxidation. In the deeper 'calamine' zone, clear crystals of hemimorphite (first discovered by Capt. King (Wynne, 1860), and identified by Apjohn (1860)) occur in an ochreous mass of goethite, chalybite, smithsonite, unaltered primary minerals, and brown-stained dolomite.

References.

Allen (E. T.), Crenshaw (J. L.), Johnston (J.), and Larsen (E. S.), 1912. Amer. Journ. Sci., ser. iv, vol. 33, p. 169.

Apjohn (A.), 1860. Journ. Geol. Soc. Dublin, vol. 8, p. 157.

Buerger (M. J.), 1939. Zeits. Krist., vol. 101, p. 290 [M.A. **7**–387].

Carter (S. R.), 1948. 18th Int. Geol. Cong., London, pt. VII (1950), p. 195.

Edwards (A. B.), 1954. Textures of the ore minerals and their significance, 2nd edn. Australasian Inst. Min. Met., Melbourne.
—— 1955. Proc. Australasian Inst. Min. Met., new ser., no. 175, p. 55.
Foslie (S.), 1950. Norsk. Geol. Tidsskr., vol. 28, p. 144 [M.A. **11**–505].
Goldschmidt (V. M.) and Peters (C.), 1934. Nachr. Gesell. Wiss. Göttingen, vol. 1, p. 11.
Hägg (G.) and Sucksdorff (I.), 1933. Zeits. Physikal. Chem., Abt. B, vol. 22, p. 444 [M.A. **5**–466].
Hey (M. H.), 1954. Min. Mag., vol. 30, p. 277.
Morgan (D. A. O.), 1957. The Geology of the Sebakwe group of mines, Que Que, Southern Rhodesia, with special reference to the gold ore. Ph.D. thesis, University of London.
O'Malley (G. B.), and McGhie (R. R.), 1939. Proc. Australasian Inst. Min. Met., new ser., no. 116, p. 459.
Rhoden (H. N.), 1958*a*. The Geology and Mineralisation of the Silvermines Area, County Tipperary, Eire. Ph.D. thesis, University of London.
—— 1958*b*. Trans. Inst. Min. Met., vol. 68, p. 67.
Ridland (G. C.), 1941. Econ. Geol., vol. 36, p. 45 [M.A. **8**–247].
Russell (A.), 1907. Min. Mag., vol. 14, p. 350.
Rutty (J.), 1772. An essay towards a Natural History of the County of Dublin. 2 vols., Dublin.
Sampson (E.), 1941. Econ. Geol., vol. 36, p. 175 [M.A. **8**–275].
Smith (F. G.) and Kidd (D. J.), 1949. Amer. Min., vol. 34, p. 403 [M.A. **11**–90].
Stillwell (F. L.), 1944. Proc. Australasian Inst. Min. Met., new ser., no. 135, p. 1.
—— and Edwards (A. B.), 1943. Ibid., nos. 131–132, p. 173.
—— —— 1945. Ibid., no. 139, p. 149.
—— —— 1946. Ibid., no. 141, p. 31.
Tarr (W. A.), 1927. Amer. Min., vol. 12, p. 417 [M.A. **3**–453].
Wynne (A. B.), 1860. Journ. Geol. Soc. Dublin, vol. 8, p. 244.
—— 1861. Mem. Geol. Surv. Ireland, sheet 134.

Explanation of Plates IV to VI.

Plate IV.

Fig. 1. Edge view of pyrrhotine pseudomorph, composed chiefly of marcasite, and surrounded by euhedral arsenopyrite crystals, quartz, chalcopyrite, and tetrahedrite. In the pseudomorph, shrinkage cracks contain quartz (black), blende (dark grey), tetrahedrite (medium grey), chalcopyrite (light grey without relief), and galena (light grey with strong relief); areas of plain relief near margins are pyrite, which break the continuity of the cracks. Shallee mine, 320-ft. level, 9.6 W. stope; polished section ×170.

Fig. 2. Pyrrhotine pseudomorph containing marcasite (light grey) and quartz (black spots), with tetrahedrite (dark grey) in the shrinkage cracks. Angular lines are gudmundite, which covered the tetrahedrite crystals during a momentary pause in growth. Gortnadyne mine, breccia; polished section ×930.

Plate V.

Fig. 3. Side view of platy pyrrhotine crystals, showing sharp edges, surrounded by quartz (dark grey) and later sulphides (light grey shades). Pseudomorph filled

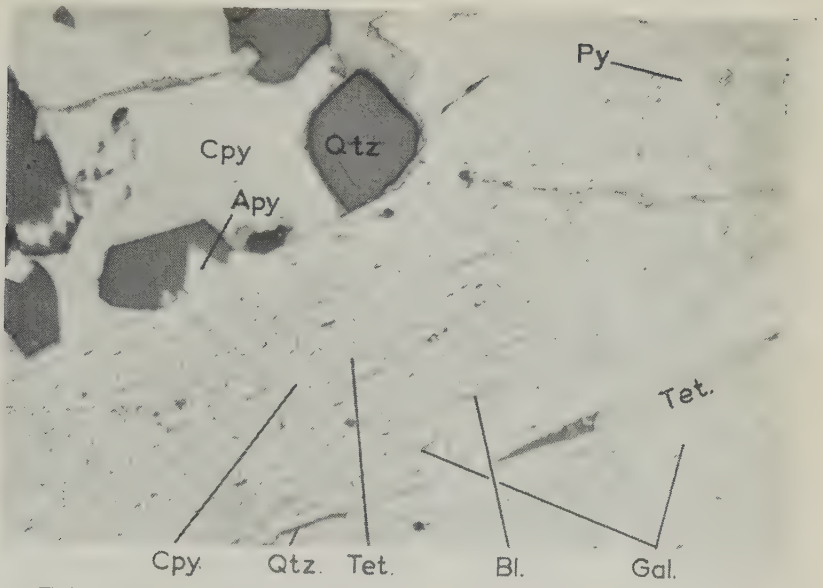

Fig. 1

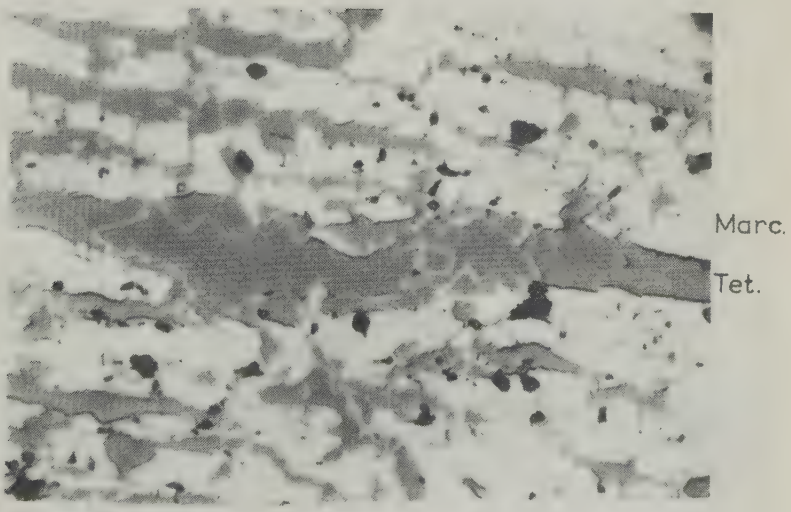

Fig. 2

Fig. 3

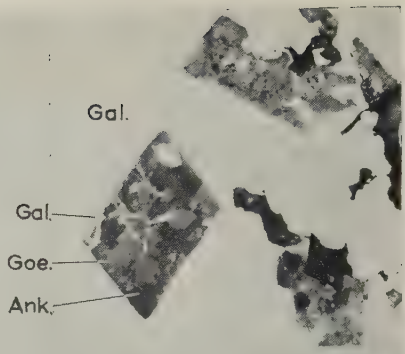

Fig. 5

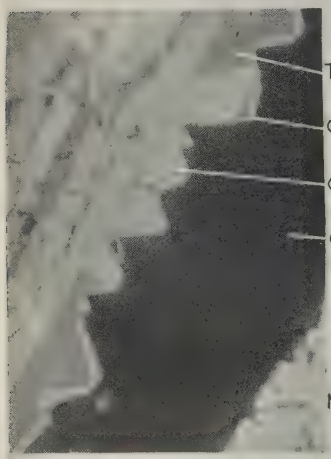

Fig. 4

Fig. 6

Fig. 7

Fig. 8

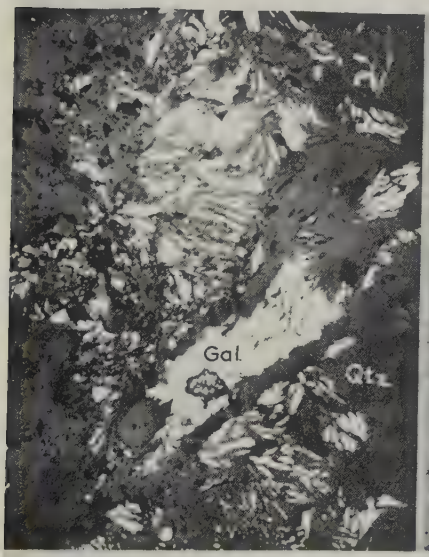

Fig. 9

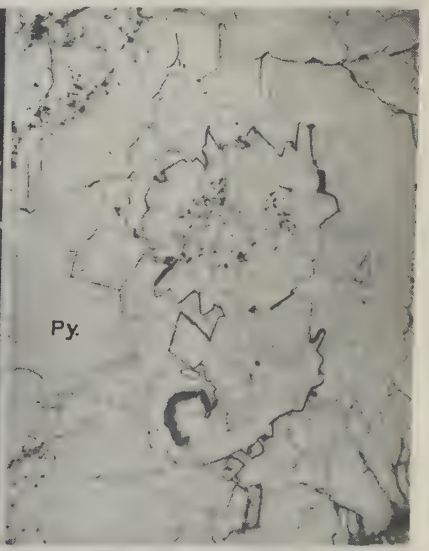

Fig. 10

with marcasite, with other sulphides in shrinkage cracks parallel to basal parting of original pyrrhotine. Shallee mine, 320-ft. level, 9·6 W. stope; polished section, ×41.

Fig. 4. Shrinkage cracks within pyrrhotine pseudomorph. Triangular-ended tetrahedrite crystals, which grew out from the marcasite edges, were partly replaced by chalcopyrite, then covered by a thin layer of gudmundite; remaining space in the crack was filled by quartz. Gortnadyne mine, breccia; polished section, ×1230.

Fig. 5. Pseudomorphs of early carbonate (chalybite?) crystals, filled with ankerite (darker grey shades) and goethite (lighter grey). Galena (white) embayed and veined the pseudomorph, partly replacing both minerals. Shallee mine, 320-ft. level; polished section, ×148.

Fig. 6. Brecciated iron-rich blende (dark grey), partly replaced by pyrite (white); both minerals were subsequently replaced by galena (light grey, deep relief). Some of the pyrite was redeposited around the developing crystals of galena, or in long, thin, broken veinlets along the cubic cleavage. Gortnadyne mine, breccia; polished section, ×90.

Plate VI.

Fig. 7. Pseudomorph of euhedral blende crystal (outlined in white), marginally replaced by chlorite; unreplaced core of blende (black) contains exsolved chalcopyrite. The surrounding rock is a shaly, dolomitic sandstone. Shallee mine, 260-ft. level, borehole 39 at 45 ft.; thin section with X-nicols, ×47.

Fig. 8. As for fig. 7. Unreplaced core of blende (white) surrounded by chlorite (medium grey). Irregular masses of light yellow blende (white) have replaced rock groundmass around pseudomorph. Copper-rich blende replaced by chlorite was redeposited nearby purged of inclusions. Shallee mine, 260-ft. level, borehole 39 at 45 ft.; polished section, ×47.

Fig. 9. Feathery plates of sericite (black) surrounded by galena (white) in a narrow vein, between sandstone wall-rocks. Shallee mine, borehole 2E at 12·5 ft.; polished section, ×67.

Fig. 10. Relic texture in centre of pyritic spherulite indicating former presence of clump of marcasite crystals. Knockanroe mine, 'Sulphur Lode'; polished section, ×51.

A differentiated boss of alkali dolerite from Cnoc Rhaonastil, Islay.

(With Plates VII and VIII.)

By

Frederick Walker, M.A., Ph.D., D.Sc.
Dept. of Geology, Queen's College, Dundee

and

E. M. Patterson, D.Sc., M.Sc., F.R.I.C.
West Kilbride, Ayrshire.

[Read 29 January 1959.]

Summary. An elongated boss of alkali dolerite is described having a NW. trend and measuring 800 m. by 250 m. Two main rock-types occur, an ophitic feldspar-rich analcime olivine dolerite or leucodolerite and a teschenite with subhedral pyroxene. The second type is intrusive into the first but the two are associated in vertical veins. Both show local banding and analcime nepheline–syenite forms a differentiate of both. Finer grained olivine-rich dolerite resembling the crinanites of Jura occurs at the NW. extremity of the boss and probably represents the original magma. All four types have been analysed and are thought to be the products of normal crystal fractionation with slight absolute iron enrichment. The boss was apparently headed not far above the existing exposures and is considered to be of Tertiary age. The pyroxene and olivine of the leucodolerite have been separated and analysed.

THE Tertiary NW. dykes of Islay and Jura form a well-marked swarm continuing across the Mull of Kintyre into Arran. They increase in number to the NW., and Richey (1939, p. 393) has suggested that their focus lies under the Atlantic in that direction. Petrographically they range between olivine-dolerite and crinanite *sensu stricto*, but the much broader boss of Cnoc Rhaonastil, 5 miles ENE. of Port Ellen, is an exception in its petrographic as well as in its physical characteristics. This was early recognized by Wilkinson (1907, p. 64) who drew attention to its striking appearance and abnormal mineralogy. Yet the present communication represents the first petrographic description. It was written by the first author, but the field work was shared and three of the main rock-types were analysed by the second author.

Field Characters.

Cnoc Rhaonastil is a conspicuous grassy hill only 300 feet high but standing out boldly from the rather featureless Dalradian landscape of southern Islay. It is composed almost entirely of alkali dolerite forming an elongated boss of NW. trend measuring 800 m. by 250 m. This

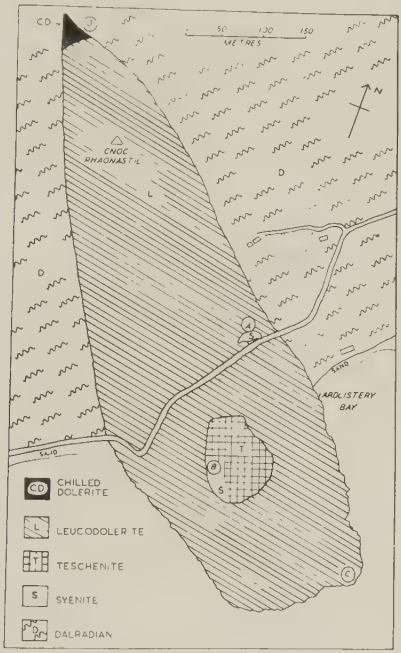

FIG. 1. Sketch map of the Cnoc Rhaonastil boss.

stretches down to the sea where it extends as a promontory separating Loch a' Chnuic from Ardlistery Bay. The National Grid reference of the summit is 434486.

Exposures along the shore section are almost continuous but the SW. side of the promontory is littered with large angular blocks which may have moved slightly from their source during severe storms. Apart from two abandoned quarries (A and B in fig. 1) exposures from shore to summit are scanty but behind the summit a series of rocky terraces falls abruptly to level arable ground where the boss wedges out rapidly to the NW. Air photographs suggest a similar submarine wedging to the SE. At no point is the contact exposed but the clear-cut terminations and moderate contact metamorphism of adjacent epidiorite sills indicate

its proximity. No chilling of the boss is seen except at the NW. where a small exposure of finer-grained olivine-rich dolerite is thought to represent the chill phase of the original magma (D in fig. 1).

The bulk of the intrusion consists of a fresh coarse-grained and highly ophitic olivine dolerite, light grey in colour and obviously very feldspathic. Irregular black clumps of pyroxene cause pustular weathering, especially round the summit, while green olivine is less prominent.

Very different material is seen in quarries A and B (fig. 1). In quarry A the ophitic dolerite is the main type but it has decomposed to light brown friable rubble from which knobs and veins of fresh rock project. Both knobs and veins consist partly of the ophitic dolerite and partly of two non-ophitic types. One is mafic and of troctolitic appearance, greasy grey in colour with well-defined dark spots of olivine and pyroxene. The second is a greyish-white coarse and drusy syenite of which the main constituent is alkali feldspar often showing sub-parallelism. Subordinate biotite and barkevikite in conspicuous black needles are visible in the hand specimen. The syenite is associated with the other two types in veins up to 60 cm. wide, generally vertical and showing marked banding (pl. VII, fig. 2), and in nests up to 2 m. in diameter.

Quarry B, now overgrown, is in a tree-clad knoll that forms a prominent physical feature probably representing a later intrusion. It consists almost entirely of the troctolite-looking rock but loose blocks show local gradation into syenite as well as rude banding into dark and light layers.

Similar banding is seen in the ophitic dolerite in places; near the summit it is rudimentary but at the end of the promontory (C in fig. 1) it becomes conspicuous. The bands are up to 5 cm. wide and have a seaward dip of 32°. At this point prominent platy jointing is developed parallel to the banding and to an 8 cm. felsic layer. Both here and NW. of the summit the disposition of banding and platy jointing indicate that the boss had a rounded head only a short distance above the existing exposures. A few thin ramifying veins of felsic material and some irregular patches of ophitic dolerite pegmatite occur below the banded dolerite at C.

Microscopic petrology.

Microscopic examination confirms that four principal rock-types[1] occur in the boss: ophitic analcime–olivine–dolerite or 'leucodolerite';

[1] In the remainder of this paper the names here in inverted commas will be used for brevity.

teschenite with troctolitic appearance or 'teschenite'; analcime-nepheline-syenite or 'syenite'; and fine-grained dolerite rich in Mg-olivine or 'chilled dolerite'. Some indication of the distribution of these types is shown in fig. 1 while tables I–IV and pl. VIII deal with their mineralogy, chemistry, and texture. Only diagnostic features are dealt with in the text below.

Leucodolerite. The main features of this unique dolerite are: abnormally high plagioclase content; poverty in pyroxene; extreme ophitic texture of pyroxene, 'nesophitic' of Walker (1957, p. 2); sub-ophitic to ophitic habit of Mg–Fe-olivine; and abundance of zeolites and widespread analcimization of plagioclase.

A variety of the leucodolerite with still less pyroxene but abundant ophitic olivine occurs on the shore section near the east end of the beach at the head of Loch a' Chnuic (4, table I).

Teschenite. This gabbroic rock is similar to some of the less ophitic teschenites of the Midland Valley (Walker, 1923) but differs from them in the following respects: absence of potash feldspar; presence of unaltered Mg–Fe-olivine; and very extensive development of zeolites and analcimization giving a greasy grey appearance megascopically.

Syenite. This drusy rock bears a marked resemblance to the greyish-white segregations of analcime-syenite of a sill in the Shiant Isles (Walker, 1930, p. 385), but shows the following minor differences: greater variation of mafic minerals, which in all cases bulk less than in the Shiant rock; slightly more abundant and better preserved nepheline; more complete zeolitization of feldspar; more calcic plagioclase (An_{20}); relative poverty in apatite.

Chilled dolerite. The rock is of smaller grain-size than the leucodolerite and closely resembles the type crinanite dykes of Jura in chemical composition, mineralogy and fabric with the following minor differences: curious habit of large Mg-olivines, which occur in elongated groups of welded grains up to 5 cm. in length and enclosing small plagioclase laths; and absence of vesicles.

Minor Types of restricted distribution are: Pegmatitic patches in leucodolerite at C (fig. 1), which contain much zeolitized labradorite, ophitic titanaugite in clumps up to 1 cm. across, and analcime as main constituents; ilmenite and soda-orthoclase are subordinate and olivine absent; a few pseudomorphs may represent nepheline. And anorthositic bands in leucodolerite, which occur sparingly at C; the constituent minerals are these of the leucodolerite but the mafic minerals are even scarcer.

TABLE I. Modes (volume %) of Cnoc Rhaonastil rocks compared with one from Jura. Also optical properties of the olivine and pyroxene.

	1.	2.	3.	4.	5.	6.	7.
Olivine	—	—	8·6	19·3	4·1	23·8	22·3
Pyroxene	2·4	1·2	9·3	6·6	25·2	19·9	14·9
Plagioclase }	71·0	78·6	70·4	67·6	54·1	46·2	54·6
K-feldspar }			—	—	—	—	—
Nepheline	5·2	2·8	—	—	—	-	—
Zeolites	13·1	12·2	7·5	3·1	6·7	1·9	3·6
Amphibole	5·4	0·8	—	—	1·2	—	—
Biotite	0·3	1·7	—	—	0·9	—	—
Iron ore	2·1	1·9	4·0	3·2	7·2	8·0	4·4
Apatite	0·5	0·8	0·2	0·2	0·6	0·2	0·2
Olivine:							
β	—	—	1·750	1·752	1·752	1·710	—
2V	—	—	75°	73°	73°	89°	—
Pyroxene:							
β	—	—	1·706	1·706	1·708	1·704	—
2V	—	—	50–54°	52°	50°	50°	—

1. Analcime nepheline syenite, nest in middle of quarry A (fig. 1), Cnoc Rhaonastil. Analysed rock, 1, table III.
2. Ditto from nest at SE. end of quarry A.
3. Leucodolerite from summit of Cnoc Rhaonastil. Analysed rock, 2, table IV.
4. Ditto with ophitic olivine, shore near N. end of Loch a' Chnuic.
5. Teschenite, S. end of quarry B (fig. 1), Cnoc Rhaonastil. Analysed rock, 3, table III.
6. Olivine-rich dolerite, NW. extremity of Cnoc Rhaonastil boss. Analysed rock, 4, table III.
7. Olivine-rich dolerite dyke, 300 m. N. of Faolin Ferry, Jura.

Mineralogy.

The properties of some of the chief minerals are given in table I. The olivine and pyroxene of the leucodolerite are of greater interest than the others for they represent the chief mafic constituents of an intermediate alkaline differentiate of unique character. They were therefore isolated and analysed. The pyroxene is a normal titanaugite lying slightly above Murray's curves for the pyroxene of the Garbh Eilean sill in the Shiant Isles (1954). The $100(Fe_2O_3+FeO)/(Fe_2O_3+FeO+MgO)$ ratios for the pyroxene (45), the rock (72), and the olivine (60) indicate a considerable degree of differentiation. It was not found possible to obtain the olivine completely free from feldspathic inclusions but when a slight correction for plagioclase and magnetite dust has been made the analysis (2, table II) yields a reasonable formula. The olivine and pyroxene of the teschenite have similar properties and compositions though the proportions are different. Zoning is not conspicuous in either but the specific

gravities and refractive indices indicate a limited range in composition. Refractive indices were determined by the immersion method (±0·003) and 2V measured by the Vincent stage (Vincent, 1954).

TABLE II. Analyses of olivine and pyroxene from leucodolerite, Cnoc Rhaonastil.

	Olivine. Weight %	Weight % corrected.		Atomic ratios to 4 oxygens.		*Pyroxene.* Weight %		Atomic ratios to 6 (O,OH)	
SiO_2	34·46	34·58	Si	0·978	SiO_2	49·14	Si	1·811	2·00
Al_2O_3	1·24	—			Al_2O_3	3·53	Al	0·153	
TiO_2	0·07	0·07	Ti	0·001	TiO_2	1·88	Ti	0·052 { 0·036 0·016	
Fe_2O_3	1·81	—			Fe_2O_3	2·27	Fe···	0·063	
FeO	35·84	37·76	Fe··	0·893	FeO	8·05	Fe··	0·248	
MnO	0·72	0·76	Mn	0·018	MnO	0·26	Mn	0·008	2·028
MgO	24·95	26·83	Mg	1·130	MgO	12·53	Mg	0·688	
CaO	0·53	—			CaO	21·54	Ca	0·850	
Na_2O	0·28	—			Na_2O	0·52	Na	0·037	
H_2O	0·15	—			H_2O	0·48	OH	0·118	
	100·05	100·00				100·20			

γ 1·767	$(Mg,Fe,Mn)_2SiO_4$	γ 1·722	$Ca_{48}Mg_{38}Fe_{14}$
β 1·750	$Fo_{56}Fa_{44}$	β 1·706	Violet-brown
α 1·725	Sp. gr. 3·69–3·87	α 1·698	Sp. gr. 3·39–3·47
γ–α 0·042	Pale brown 2V −75°	γ–α 0·024	2V +50 to 54°, +44°

Analyst: W. H. Herdsman

Chemistry.

The chemical analyses of the main basic types of the boss in table III bring out clearly its Thulean affinities with characteristically low potash:soda ratios. This is also a feature of the chilled dolerite which resembles closely in its chemistry the type crinanite of Jura (Guppy, 1931, p. 86). Olivine-rich crinanites and dolerites are very common in the Islay–Jura dyke swarm to which the boss belongs petrologically as well as petrographically.

The composition of the leucodolerite, though reflecting accurately its mineral content, is peculiar, for extremely high alumina is combined with low magnesia and iron. The only analogue is the analysis of a felsic vein in the crinanite sill of Clauchlands Point, Arran, which has however somewhat different mineralogy. Furthermore the host crinanite itself differs in chemical and mineralogical composition from any of the analysed types in the boss.

The teschenite analysis is unlike that of the only other Tertiary example, the calc-teschenite of Northern Trotternish (Walker, 1932, p. 249), which is considerably higher in lime and lower in alkalis. It is

TABLE III. New chemical analyses and norms of Cnoc Rhaonastil rocks.

	Chemical analyses.					*C.I.P.W. norms.*			
	1.	2.	3.	4.		1.	2.	3.	4.
SiO_2	55·18	49·28	47·85	44·68	or	25·6	3·3	3·9	3·9
Al_2O_3	20·66	21·07	15·48	15·99	ab	42·4	33·8	32·8	15·7
Fe_2O_3	2·21	1·80	2·90	2·88	ne	8·8	1·3	2·1	1·1
FeO	2·02	6·27	9·69	9·23	an	10·3	36·7	20·9	32·3
MgO	1·09	3·09	4·15	12·48	C	0·9	—	—	—
CaO	2·37	9·64	9·26	9·46	di wo	—	4·3	8·9	5·8
Na_2O	6·96	4·25	4·36	2·13	di en	—	2·1	4·0	3·8
K_2O	4·26	0·56	0·72	0·68	di fs	—	2·1	4·9	1·6
H_2O+	3·45	1·52	1·76	1·26	ol fo	1·9	3·9	4·5	19·2
H_2O-	1·12	1·09	1·14	0·09	ol fa	1·2	4·8	5·9	9·1
TiO_2	0·15	1·11	1·94	0·96	mt	3·3	2·6	4·2	4·2
P_2O_5	0·08	0·06	0·46	0·06	il	0·3	2·1	3·7	1·8
MnO	0·05	0·13	0·17	0·21	ap	0·3	0·3	1·3	0·3
CO_2	0·10	nil	tr.	nil	cc	0·2	—	—	—
	99·70	99·87	99·88	100·11	H_2O	4·6	2·6	2·9	1·4
Sp. gr.	2·50	2·75	2·81	3·07		99·8	99·9	100·0	100·2

1. Syenite nest in quarry A (fig. 1), Cnoc Rhaonastil. New analysis. Analyst: E. M. Patterson.
2. Leucodolerite, summit of Cnoc Rhaonastil. New analysis. Analyst: E. M. Patterson.
3. Teschenite, S. end of quarry B (fig. 1), Cnoc Rhaonastil. New analysis. Analyst: E. M. Patterson.
4. Olivine-rich dolerite. NW. extremity of Cnoc Rhaonastil boss. New analysis. Analyst: W. H. Herdsman.

much closer in composition to the Carbo-Permian teschenites of the Midland Valley though differing from them in its lower $K_2O/(Na_2O+K_2O)$ ratio, 0·14 against 0·29 for the average of six Survey analyses (Guppy, 1931, pp. 92–93).

The syenite analysis shows no really close resemblance to any other of this type, whether in the Hebridean Tertiary or Midland Valley Carbo-Permian. The $K_2O/(Na_2O+K_2O)$ ratio shows a marked rise to 0·38, potash evidently being concentrated in the late differentiates. The best match is with the syenite segregations of the Eilean Mhuire sill in the Shiant Isles (Walker, 1930, p. 387). The intrusion as a whole falls into the alkali-calcic division of Peacock (1931), the alkali index being 52.

Differentiation.

Initial magma. The olivine-rich dolerite at the NW. extremity of the boss seems to represent the initial undifferentiated magma. The mafic constituents and plagioclase are respectively more magnesian and more sodic than in the other varieties and the rock closely resembles the main

TABLE IV. Chemical analyses of Cnoc Rhaonastil rocks with others for comparison, calculated to 100 % water-free.

	1.	A.	2.	B.	3.	C.	4.	D.
SiO_2	57·9	60·0	50·6	48·3	49·3	50·4	45·2	45·0
Al_2O_3	21·7	16·3	21·7	24·1	15·9	15·5	16·2	14·5
Fe_2O_3	2·3	5·1	1·8	3·6	3·0	2·9	2·9	2·0
FeO	2·1	2·6	6·5	4·8	10·0	7·2	9·3	12·0
MgO	1·1	0·6	3·2	2·6	4·3	5·9	12·6	10·8
CaO	2·5	2·1	9·9	9·9	9·6	8·7	9·6	9·2
Na_2O	7·4	7·7	4·4	4·7	4·6	4·0	2·2	2·8
K_2O	4·5	4·4	0·6	0·4	0·7	2·4	0·7	0·3
TiO_2	0·2	0·5	1·1	1·3	2·0	2·2	1·0	2·6
etc.	0·3	0·7	0·2	0·3	0·6	0·8	0·3	0·8

1. Syenite nest in quarry A (fig. 1), Cnoc Rhaonastil. New analysis (table III, 1).
A. Syenite segregation in Eilean Mhuire sill, Shiant Isles. Analyst: E. G. Radley (Walker, 1930, p. 355).
2. Leucodolerite, summit of Cnoc Rhaonastil. New analysis (table III, 2).
B. Segregation vein in crinanite sill, Clauchland's Point, Arran. Analyst: W. H. Herdsman (Tyrrell, 1928, p. 121).
3. Teschenite, S. end of quarry B (fig. 1), Cnoc Rhaonastil. New analysis (table III, 3).
C. Teschenite, below Craigens sill complex, Ayrshire. Analyst: E. G. Radley (Guppy, 1931, p. 92).
4. Olivine-rich dolerite, NW. extremity of Cnoc Rhaonastil boss. New analysis (table III, 4).
D. Crinanite dyke. Inver Lodge, Jura. Analyst: E. G. Radley (Guppy, p. 86).

type of the Jura–Islay dyke swarm in which the boss is situated. Of medium grain, the rock is chilled only in the sense that the cooling process at the wedge-shaped termination was too rapid to permit significant differentiation. Its richness in Mg-olivine points to a magma intermediate in character between the Mull plateau type and the picritic liquids postulated by Drever (1952). Similar magnesia-rich lavas occur in Antrim (Patterson, 1952).

Gravitational differentiation. The leucodolerite on the other hand is a strongly differentiated type. Its relationship to the previous type is not seen but the iron-rich nature of its mafic minerals indicates that it is far advanced in the crystallization series. Furthermore, it is a highly felsic rock containing no less than 78 % of plagioclase and zeolites. The former evidence favours crystal fractionation and the latter gravitational settling of magnesian olivine and possibly, at a later stage, large ophitic aggregates of pyroxene and plagioclase or olivine and plagioclase (4, table I), which would sink by virtue of their bulk.

A subtraction diagram shows that the most basic material that can be subtracted from the chilled dolerite to produce the leucodolerite has

a normative composition including 27 % anorthite, 15 % pyroxene, and 47 % Mg-olivine. Both the nature and proportions of these minerals are in keeping with the hypothesis of gravitational differentiation suggested above. Complementary to the settling process there would be a concentration of the later residues in the upper part of the magma chamber and this again is in keeping with the high zeolite content of the leucodolerite. Lastly the observations of the first author on ophitic texture (Walker, 1957) agree with the suggested differentiation process.

The *teschenite* intrusive probably represents the result of crystallization differentiation at depth without the thorough gravitational cleansing shown by the leucodolerite, for its mafic content is considerably higher. It is closely associated with both leucodolerite and syenite elsewhere and cannot be far removed in time from the main intrusive episode, though the mechanism of injection remains in doubt through lack of exposures.

Syenite occurs as thin partings in vertical veins of alkali-dolerite, as rounded patches or nests in the leucodolerite (A, fig. 1), and as schlieren in loose blocks of the teschenite (B, fig. 1). It is of variable mineralogy which may point to diversity of origin. There is, however, little doubt that the rounded masses so conspicuous in quarry A arose in the same way as the analcime-syenites of Ayrshire described by Tyrrell (1928), that is through enclosure by or injection into a hot crystal framework of aqueous and alkaline residual magma. Certainly they have no stratiform tendency but this may be explained by the difference in form between the Ayrshire sills and the Islay intrusion, which seems to represent the rounded head of an elongated boss. The local sub-parallelism of the alkali feldspar indicates that the syenite is a magmatic residue rather than a replacement deposit but the varied mineralogy and extensive zeolitization point to its highly aqueous and mobile nature.

The syenite bands and schlieren in the loose teschenite blocks of quarry B are too scanty to yield information as to their origin and the thin partings of the banded vertical veins of quarry A are dealt with below.

Dolerite pegmatite at C has a patchy habit like that of the same rock-type developed in tholeiitic intrusions described by the first author (Walker, 1953) and there is no need to postulate a different origin. Like those of syenitic nature they are thought to represent residual magma trapped in a growing crystal framework.

Banding. The rudimentary banding seen at a number of localities, notably behind the summit and at C (fig. 1), shows an inclination more or less in conformity with the surface topography and platy joint system. In sheet or dyke injections similar banding and jointing have been

recorded near and parallel to the margin and it is thought that the banded outcrops of the boss are not far from the upper contact now removed by erosion. If this is so the boss must have had a rounded upward termination.

The bands fail to show the more perfect segregation of light and dark minerals displayed by the great layered intrusions, nor is there any preferred orientation. The dark bands are thinner than the light and show more clearly on a weathered surface than in a large thin section. At C where the banding shows its most regular development individual layers do not exceed 8 cm. in thickness (pl. VII, fig. 4).

Somewhat similar banding has been observed by the first author in the Palisade sill, New Jersey, by Mr. H. G. Wright (priv. comm.) in a Skye sill, and by Mr. P. L. C. Grubb (priv. comm.) in dolerite sills in Bechuanaland. It appears to be a phenomenon of rhythmic crystallization rather than of convectional sorting and sedimentation. The mechanism proposed by Coats (1937) may possibly be applicable. Its investigation continues.

The thick vertical veins of quarry A show much more clear-cut banding but again there is no preferred orientation of any of the constituent minerals. On the other hand the thin syenite partings, less than 5 mm. wide (pl. VII, fig. 2), show a well-marked co-planar arrangement, parallel to the contacts, of long needles of alkali amphibole. The other elements of the bands consist of leucodolerite and teschenite with transitional types but containing the same minerals as occur in the massive rock.

These veins give proof of the contemporaneity of leucodolerite, teschenite, and syenite. They probably represent material filling and dilating rifts in a hot crystal framework near the upper contact. The infilling seems to have taken place in the order leucodolerite, teschenite, syenite. It is possible that the syenite partings are the result of replacement.

The four analysed rocks represent the liquid line of descent of an alkaline basaltic magma rich in olivine. The trend of differentiation is well shown on the MgO, $(FeO+Fe_2O_3)$, (Na_2O+K_2O) diagram of fig. 2. The suite exhibits absolute as well as relative iron enrichment, though the peak of the curve is much less high and sharp than in many tholeiitic provinces such as the Palisades (Walker, 1953, p. 53).

Comparison with other British Tertiary bosses. Bosses and plugs of dolerite are common in the British Tertiary province but with few exceptions are confined to the lava regions, notably the Antrim plateau

(Patterson and Swaine, 1957). They consist mainly of undifferentiated rock and doubtless acted as feeders of flows now removed by erosion. Being conduits they have occasionally produced striking metamorphic

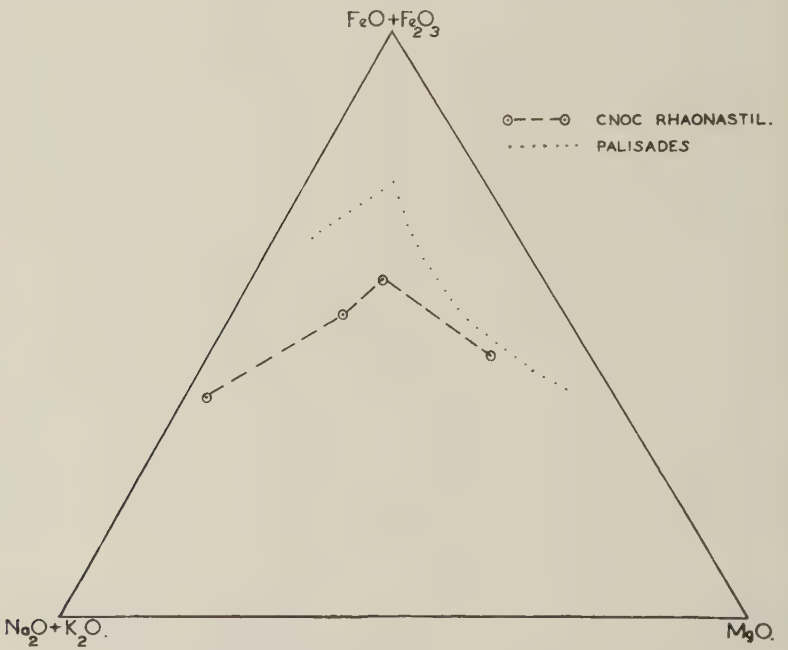

Fig. 2. Differentiation trends of the Cnoc Rhaonastil and Palisades (New Jersey) dolerites.

effects on the country rock (e.g. at Scawt Hill, Tilley and Harwood, 1931, and at Tievebulliagh, Agrell and Langley, 1958). In the latter case inclination of the plug has resulted in accumulation of olivine on the foot wall to form a local development of picrodolerite.

The boss of Cnoc Rhaonastil is very different. The main rock-type is a highly differentiated leucodolerite and the contact metamorphism of the adjacent epidiorite sills is only slight. This is in keeping with a headed boss of static magma but not with a constantly replenished conduit. Furthermore, the outcrop of Cnoc Rhaonastil is lens-shaped with the major diameter parallel to the trend of the associated dyke-swarm and not circular or elliptical as in the pipes referred to.

The only Scottish intrusion at all comparable to Cnoc Rhaonastil is the elongated boss of Maiden Island near Oban (Walker, 1939), but

apart from a local marginal development of picrite and some residual veins and patches the latter is an undifferentiated olivine-dolerite; it lies just within the Mull dyke swarm, to which its trend is parallel, and only six miles from the nearest lavas of that island. Cnoc Rhaonastil on the other hand has no apparent connexion with any volcanic area and is unique in its high degree of differentiation.

Acknowledgements. The authors are grateful to Mr. H. C. G. Vincent of Cape Town University for separating the olivine and pyroxene of the leucodolerite and to Messrs. P. L. C. Grubb and H. G. Wright for assistance on the field. They also desire to express their indebtedness to the Council of the University of Cape Town for financial aid towards travel and chemical analysis.

References.

Agrell (S. O.) and Langley (J. M.), 1958. Proc. Roy. Irish Acad., vol. 59, p. 93.
Coats (R. R.), 1937. Journ. Geol., Chicago, vol. 44, p. 407.
Drever (H. I.), 1952. Medd. Dansk Geol. For., vol. 12, p. 227.
Guppy (E. M.), 1931. Chemical analyses of igneous and metamorphic rocks and minerals. Mem. Geol. Surv.
Murray (R. J.), 1954. Geol. Mag., vol. 91, p. 17.
Patterson (E. M.), 1952. Geochimica Acta, vol. 2, p. 283.
—— and Swaine (D. J.), 1957. Trans. Roy. Soc. Edin., vol. 63, p. 317.
Peacock (M. A.), 1931. Journ. Geol., Chicago, vol. 39, p. 54.
Richey (J. E.), 1939. Trans. Edin. Geol. Soc., vol. 13, p. 393.
Tilley (C. E.) and Harwood (H. F.), 1931. Min. Mag., vol. 22, p. 439.
Tyrrell (G. W.), 1928. Quart. Journ. Geol. Soc., vol. 84, p. 540.
Vincent (H. C. G.), 1954. Min. Mag., vol. 30, p. 513.
Walker (F.), 1923. Geol. Mag., vol. 60, p. 242.
—— 1930. Quart. Journ. Geol. Soc., vol. 86, p. 355.
—— 1932. Trans. Roy. Soc. Edin., vol. 57, p. 241.
—— 1939. Trans. Edin. Geol. Soc., vol. 13, p. 475.
—— 1953. Amer. Journ. Sci., vol. 251, p. 41.
—— 1957. Journ. Geol., Chicago, vol. 65, p. 1.
Wilkinson (S. B.), 1907. The geology of Islay, Mem. Geol. Surv.

Explanation of Plates VII and VIII.

Alkali dolerite from Cnoc Rhaonastil, Islay.

Plate VII.

Fig. 1. Quarry A showing 30 cm. vertical banded vein (left) and syenite nest (right) projecting from friable, weathered leucodolerite.

Fig. 2. 30 cm. vertical vein in quarry A seen from side and showing banding and syenite parting with planar arrangement of barkevikite needles.

Fig. 3. Pustular weathering and slab like jointing of leucodolerite at summit.

Fig. 4. Banding and jointing of leucodolerite at C (fig. 1).

Plate VIII.

Fig. 1. Leucodolerite. Ordinary light. Showing sparse ophitic titanaugite and sub-ophitic olivine intergrown with abundant plagioclase An_{60}. Titanomagnetite and analcime are subordinate. ×8.

Fig. 2. Teschenite. Ordinary light. Euhedral to sub-ophitic titanaugite and pale brown olivine are embedded in plagioclase An_{60}. Subordinate analcime occurs in interspaces and replaces plagioclase. Titanomagnetite is prominent and sparse marginal growths of biotite and barkevikite are accessory. ×8.

Fig. 3. Syenite. Ordinary light. Large analcimized tables of anorthoclase and oligoclase are prominent while analcime and other zeolites fill interspaces. A dark prism of barkevikite is conspicuous near top and ægirine-augite is accessory. A rectangular pseudomorph after nepheline occurs near centre. ×8.

Fig. 4. Chilled dolerite. Ordinary light. Abundant Mg-olivine in large elongated aggregates of grains enclosing small plagioclases. Matrix consists of ophitic purple titanaugite and plagioclase An_{65} with subordinate iron-ore and analcime. ×8.

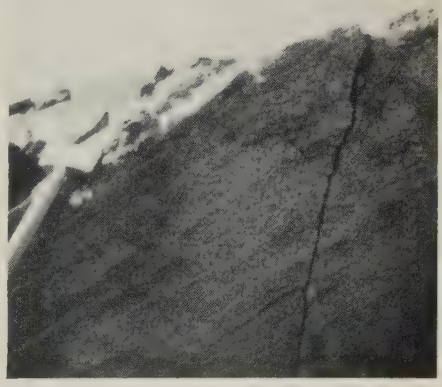

F. WALKER AND E. M. PATTERSON: ALKALI DOLERITE FROM ISLAY

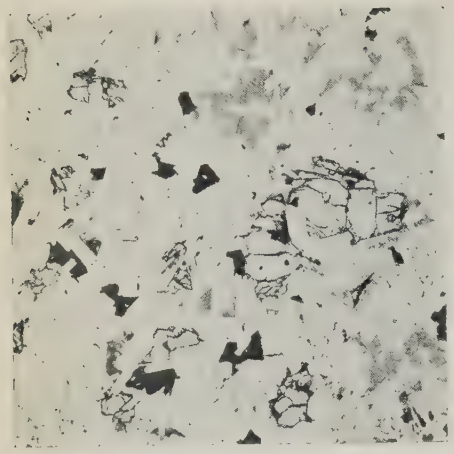

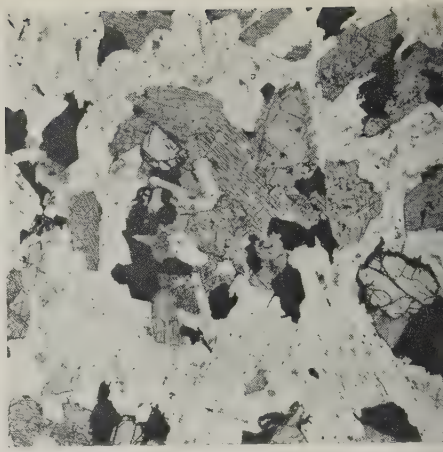

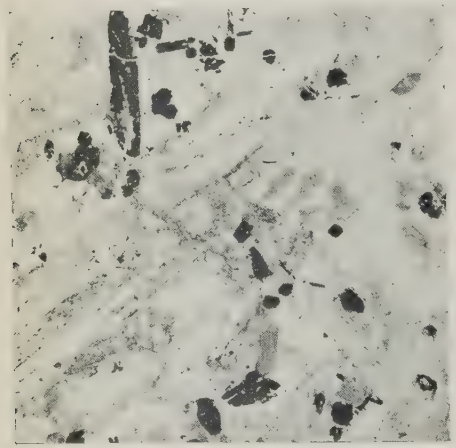

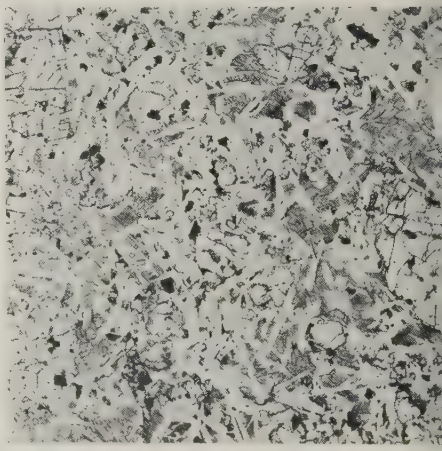

F. Walker and E. M. Patterson: Alkali Dolerite from Islay

The ageing of sesquioxide gels. I. Iron oxide gels.

By Robert C. Mackenzie, D.Sc., Ph.D., F.R.I.C.
The Macaulay Institute for Soil Research, Craigiebuckler, Aberdeen, Scotland,

and Robert Meldau, Prof. Dr.-Ing.
Laboratorium für Staubtechnik, Harsewinkel, Westfalen, Germany.

[Read 2 April 1959]

Summary. The gels prepared by adding ammonium hydroxide rapidly to ferric chloride solutions to various pH values are shown to consist of amorphous material and crystalline goethite; no other iron oxide was definitely identified in the present experiments, although this does not preclude other oxides being present in gels prepared under slightly different conditions. The goethite grows as acicular crystals on ageing at all pH values, but the rate of growth is greater at higher pH values. The exothermic peaks appearing on differential thermograms of such gels are apparently due to coalescence of extremely minute hematite particles to give larger particles, the sharpness of the peak indicating to some extent the size of the original hematite particles. These observations are related to data for other iron oxides, and the morphology of ferric oxide polymorphs under the electron microscope is considered.

THE brown iron oxide gel is of considerable interest in pedology because of its occurrence in some soils (Mackenzie, 1949), as well as in bog-iron ores (Kurnakov and Rode, 1928). It is known to be present only in systems in dynamic equilibrium (Kurnakov and Rode, 1928), but it may, because of its reactivity and large surface area, have a disproportionate influence on soil properties. The conditions for its formation and stability have been previously examined (Mackenzie, 1952*a*, 1957), but there is still much contradictory evidence upon certain factors, such as the mineralogical constitution of the gel. The electron diffraction studies of Weiser and Milligan (1940) and Milligan (1952) suggest that the ions are arranged in approximately the same configuration as in hematite, but the electron diffraction pattern quoted by Mackenzie (1952*a*) bears a closer resemblance to the X-ray diffraction pattern of β-$Fe_2O_3.H_2O$. On ageing, Weiser (1935) and Milligan (1952) found the washed gels to go to hematite, while Gheith (1952) obtained goethite. Mackenzie (1957) found mixtures of goethite and hematite on ageing in the mother-liquor, the rate of ageing being more rapid at higher pH values.

In view of these discrepancies it may be that the preparative conditions, &c., are critical for these gels; consequently, the characteristics of one carefully prepared and well-characterized gel are of some interest.

Experimental.

Materials. Two ferric oxide gels were prepared by adding a 9 N ammonium hydroxide solution dropwise to solutions of 5g. anhydrous ferric chloride in 250 ml. water until the pH, as measured by a glass electrode, reached in one instance pH 5, and in the other pH 10. A.R. chemicals were used throughout. The gels were allowed to settle for two hours, filtered off on Buchner funnels and washed free from Cl^- with distilled water. The bulk of each gel was then re-suspended in distilled water and brought to its initial pH value (pH 5 or 10) with NH_4OH or HCl, the remainder being divided into two parts, one of which was re-suspended in distilled water in a polythene container and retained for electron-optical study while the other was dried at 105° C. and ground to −100-mesh for differential thermal, X-ray, and infra-red examination. The suspensions at pH 5 and pH 10 were allowed to stand at room temperature at these pH values for 60 days, when they were again washed free from salts on the Buchner funnel and divided up into three portions, the bulk of the material being re-suspended at the original pH value. This final portion was washed free from salts after 155 days, part retained for electron-optical examination, and part dried and ground as previously. This gave in all six samples of material: (1) gel brought to pH 5 unaged; (2) gel aged at pH 5 for 60 days; (3) gel aged at pH 5 for 155 days; (4) gel brought to pH 10 unaged; (5) gel aged at pH 10 for 60 days; (6) gel aged at pH 10 for 155 days.

Methods. A Siemens electron microscope was used for the electron-optical studies, the suspension being dried out on the carrier after ultrasonic dispersion. X-ray examination of selected samples was carried out on a Hilger HRX unit, using Co-$K\alpha$ radiation. The apparatus used for differential thermal analysis has been previously described (Mackenzie, 1952*b*). Infra-red absorption spectra were obtained on a Grubb Parsons double-beam spectrometer.

Results.

The gels change in colour somewhat on ageing. The colours of the samples used for differential thermal analysis were checked against a Munsell Soil Colour Chart, and it was found that all the aged gels were yellowish red (5 YR: 4/6) while the unaged gels were dark reddish

brown, the pH 5 gel being somewhat denser in colour (5 YR: 3/4) than the pH 10 gel (5 YR: 3/3).

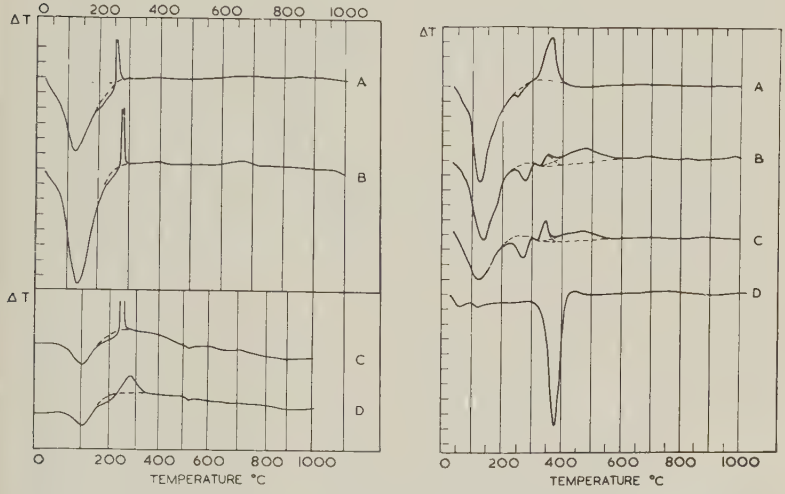

Fig. 1. Differential thermal curves for: *A*, pH 5 gel, unaged (250 mg. sample); *B*, pH 5 gel, aged for 60 days (250 mg. sample); *C*, pH 5 gel, unaged (15 mg. sample on sensitive apparatus); *D*, pH 5 gel, aged for 155 days (15 mg. sample on sensitive apparatus).

Fig. 2. Differential thermal curves for: *A*, pH 10 gel, unaged (250 mg. sample); *B*, pH 10 gel, aged for 60 days (250 mg. sample); *C*, pH 10 gel, aged for 155 days (200 mg. sample); *D*, goethite, Příbram, Czechoslovakia (350 mg. sample).

The differential thermal curves show the trends previously noted (Mackenzie, 1957). Thus, the unaged pH 5 gel shows a large endothermic peak at 125° C., which increases in size on ageing for 60 days, a shoulder at about 200° C., and a very strong exothermic peak at 257° C., which broadens and moves to a higher temperature on ageing (curves *A* and *B*, fig. 1). Insufficient of the 155-day aged sample was available for determination of a conventional differential thermal curve. However, on a very sensitive apparatus using only 15 mg., curve *D* (fig. 1) was obtained, indicating a continuation of the trend of movement and broadening for the exothermic peak; the endothermic peaks cannot be compared since the samples were evacuated before the determination, thus upsetting the water régime. Curve *C* (fig. 1) for the unaged pH 5 gel obtained on this same apparatus has been inserted for comparison purposes.

The relationships for the pH 10 gel are rather more complex. The unaged gel shows a large endothermic peak at 125° C., followed by a very small peak at about 250° C., suggesting the presence of goethite, and a strong exothermic peak at 365° C. (curve *A*, fig. 2). On ageing, the initial large endothermic peak decreases markedly in size (as would be expected if crystallization, with a reduction in surface area, were taking place), the goethite peak increases in size and moves to a slightly higher temperature, and the exothermic peak for the unaltered gel decreases in size and moves to a higher temperature (480° C.) (curves *B* and *C*, fig. 2). In addition, however, a sharp exothermic peak develops at about 350° C. and, in parallel with the goethite peak, increases in size with time of ageing.

The curves for all these gels indicate that they contain small amounts of goethite, the broken lines in figs. 1 and 2 indicating the approximate base-lines. The full interpretation of the curve will be considered later in the light of other evidence.

X-ray examination indicated that the original gels were amorphous. On ageing the goethite pattern appeared, this being strongest for the 155-day aged pH 10 gel. The latter specimen on heating to 300° C. in the differential thermal apparatus gave a pattern indicative of fine-grained hematite in addition to a broad band at about 4 Å.; heating to 385° C. and 600° C. caused the disappearance of this band and induced progressively better crystallization of the hematite.

The infra-red absorption spectra indicated that both the unaged gels (pH 5 and pH 10) were amorphous and showed strong bands due to sorbed water. The pH 5 gel after ageing for 60 days showed incipient goethite formation, but the material was still largely amorphous; the 60-day aged pH 10 gel, on the other hand, gave well-defined bands of goethite at 11·23 μ and 12·60 μ, but still showed the presence of amorphous material and sorbed water (band at 5·13 μ). Both the unaged and aged pH 10 gels had unassigned bands near 6·6 μ and 7·5 μ, which might be associated with sorbed NH_4^+ or CO_3^{2-}.

The electron-optical study revealed that the unaged pH 5 gel consisted largely of a 'pepper' of very fine particles (fig. 3*a*). The size of these particles is difficult to determine at all accurately, but they appear to be less than 40 Å. across and to fall within a remarkably small size range. In addition to this fine pepper there are also some small black specks, of irregular outline, up to about 0·04 μ across; most of these are undoubtedly clumps of the finer particles, but whether some represent minute crystals it is difficult to determine. Close examination also

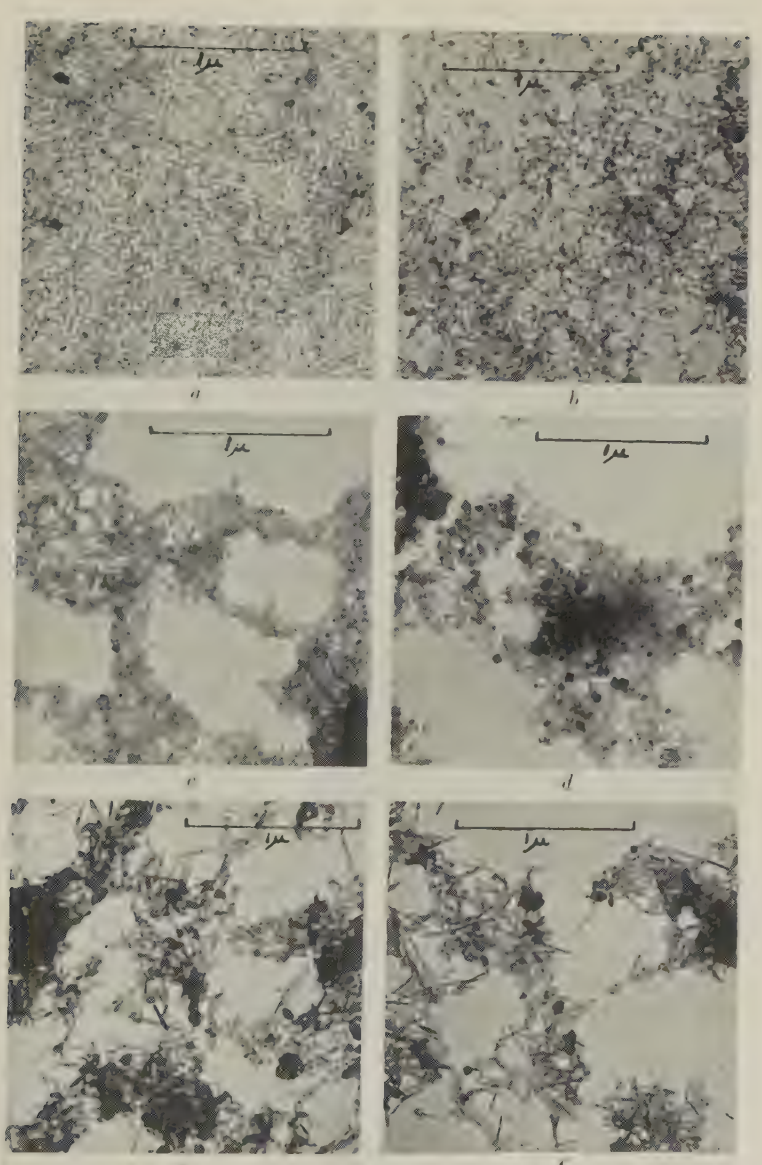

FIG. 3. Electron micrographs of precipitated ferric oxides: *a*, pH 5, unaged; *b*, pH 5, aged for 60 days; *c*, pH 5, aged for 155 days; *d*, pH 10, unaged; *e*, pH 10, aged for 60 days; *f*, pH 10, aged for 155 days.

reveals a tendency to the formation of extremely fine needles of the order of 0·06 μ long by about 40 Å. (i.e. single particle cross-section) wide. The electron diffraction pattern for this particular sample is very diffuse, in agreement with the small particle size, but bands appear in the regions associated with goethite.

The same gel aged for 60 days shows a much more pronounced tendency for the particles to clump together into aggregates of quite variable size, up to about 0·2 μ across (fig. 3*b*). Individual particles seem larger than in the unaged gel, being up to about 80 Å. across. There is no incontrovertible evidence of plates, but needles are much more apparent, their size being up to about 0·12 μ long by about 80 Å. across. They are still, therefore, very small. The electron diffraction pattern is very sharp and is essentially that of goethite, but the presence of some hematite cannot be entirely excluded.

On ageing for 155 days, clumping of the particles is particularly observable; needles are rather more clearly visible, but do not seem to be very much larger than at 60 days (fig. 3*c*). Individual particles are difficult to identify, but seem to be 80–100 Å. across. The electron diffraction pattern, although again essentially that of goethite, is rather diffuse—which may be accounted for by rather more gel material being in the field chosen.

The unaged pH 10 gel resembles the pH 5 gel aged for 155 days in that the particles tend to clump closely together (fig. 3*d*). The individual particles seem to be rather similar to, or only slightly larger than, those in the unaged pH 5 gel (i.e. 40–60 Å.). The dense black 'particles' (about 0·04–0·08 μ across), which often have a roughly hexagonal outline, appear usually to be but a collection of the primary particles closely packed together; again, it is difficult to decide whether or not some are true crystals of, for example, hematite. The usual acicular crystals, about 0·08 μ long by about 40 Å. across, are obvious throughout the gel, and the electron diffraction pattern, as before, indicates largely goethite. The diffuseness of the pattern indicates the very fine nature of the material: the pattern is, if anything, clearer than that for the unaged pH 5 gel.

After ageing for 60 days the material is largely composed of long acicular crystals of about 0·25 μ in length and up to 0·02 μ in thickness (fig. 3*e*). The length is remarkably uniform, but the thickness varies somewhat. A fair amount of residual gel is still visible, but the number of dense black aggregates has decreased considerably. Again, the electron diffraction pattern indicates essentially goethite, in agreement with X-ray data.

The needles in the 155-day aged pH 10 gel are even larger than previously, being up to about 0·4 μ in length and generally about 0·02 μ in thickness (fig. 3*f*). There are still considerable patches of unaltered gel, but the clumping is particularly noticeable. The electron diffraction pattern indicated goethite, the lines being quite spotty owing to the large crystal size. This gel was also examined under the electron

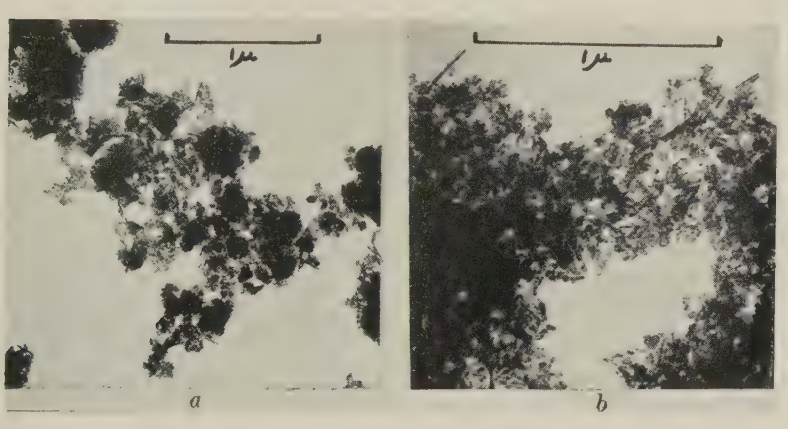

FIG. 4. Electron micrographs of 155-day aged pH 10 gel heated to: *a*, 300° C.; *b*, 600° C.

microscope after heating to 220° C., 300° C., 385° C., and 600° C. in the differential thermal analysis apparatus, these temperatures being chosen from the characteristics of the differential thermal curve (*C*, fig. 2). The electron micrograph of the material heated to 220° C. was very similar to fig. 3*f*, but there appeared to be rather fewer needles and a greater number of dense clumps—probably because of the drying and grinding procedure undergone by this sample. Small particles about 50–100 Å. across, but of indefinite shape, could also be detected. The samples heated to 300° C. (fig. 4*a*) and 385° C. showed a progressive decrease in the number and size of needles and a progressive breakdown of the clumps into particles of 50–100 Å. across. In the 385° C. material only a few needles were observable, and these were about 0·07 μ long by about 50 Å. thick. Needles are very much more numerous again in the material heated to 600° C. (fig. 4*b*) and, on close examination, are seen to be non-uniform along their length. Length and thickness vary, maximum length being about 0·20 μ and thickness about 0·015 μ. The original solid aggregates are now completely broken down into a network

of these needles and small particles of about 50–200 Å. across. Some of the larger of these particles tend to show a hexagonal outline. The electron diffraction patterns of these samples show the presence of goethite along with hematite at 220° C., but only hematite at temperatures above this: the dense background also disappears above 220° C., indicating that the amorphous material has apparently crystallized to hematite by 300° C.

Apart from the unaged pH 5 gel where the particles are smaller, all the needle sizes quoted above are within the size range observed by Fricke and Weitbrecht (1943) for goethite prepared from gel at 100° C. in 2 N KOH (Glemser, 1937)—namely, 0·096–0·470 μ long by 82–165 Å. wide. Parallel orientation of the needles as observed by Fricke and Weitbrecht (1943) is nowhere observable; on the contrary the needles in the above-described gels are oriented in all directions and at times tend to form a criss-cross mat (see fig. 3*f*). The conditions of formation must, therefore, have some influence upon this factor.

Discussion.

The data presented above indicate the predominance of goethite as a crystalline component in all phases of this gel. In the early stages there *may* be small amounts of hematite, which would account for the black specks noted particularly in the unaged pH 10 gel, but this is doubtful, and later these are not observable. Ageing causes the primary particles to come together to form needles, which in the early stages may be seen to consist of primary particles cemented together in a row rather than true crystals (fig. 3*a*—this may not show up clearly in reproduction). Longer ageing leads to true acicular crystals. Ageing is more rapid at high pH values, but also occurs quite measurably even at pH 5 at room temperature. The acicular crystals are undoubtedly goethite and presumably the elongation is [001], since growth in this direction is apparently continuous and it is in this direction that macroscopic fibres of goethite are elongated. In view of the similarity of primary particle cross-section and needle width, growth originally would appear to occur by accretion of gel material on the (001) face, a similar situation to that observed by Méring and Oberlin (1957) for $Mg(OH)_2$ precipitates (cf. the observations of Bagno, Longuet-Escard, and Mathieu-Sicaud (1951) for $Ni(OH)_2$). The particles of $Mg(OH)_2$ observed by Méring and Oberlin (1957) differ from those of goethite in being platy and not acicular; on the other hand, the $Mg(OH)_2$ particles forming in the hydration hulls round partially decomposed dolomite particles are clearly acicular

(Meldau and Robertson, 1953), but there is no information as to direction of elongation or direction of growth.

In view of the fact that all samples described above contain goethite, the thermal reactions are of considerable interest. It is impossible to state definitely what is the constitution of the primary particles of the gel: that they are largely amorphous even to electrons is evidenced by the heavy background on most of the electron diffraction patterns. Nevertheless, since they tend to coalesce into needles very rapidly, it seems likely that their structure (which must necessarily be very rudimentary) is closely akin to that of goethite. The exothermic peak on the differential thermal curves for these gels is thus rather surprising since the goethite→hematite change is an oriented transformation with no intermediate stable amorphous phase and no heat evolution would be expected. Some goethite is observable on all the curves (figs. 1 and 2), as indicated by the dotted lines, but these small peaks obviously do not represent the dehydration of all the gel and can be accounted for by the amount of acicular crystals in each sample. In addition, hematite was observed by electron diffraction at 220° C. (i.e. before the goethite peak) for the 155-day aged pH 10 gel. One must therefore conclude that the very small primary particles lose their water entirely during the period of the low-temperature endothermic peak giving minute particles of hematite, which later coalesce with evolution of heat to give particles of sufficient size to diffract X-rays (for previous explanations of the exothermic effect see Fricke and Hüttig, 1937, and Mackenzie, 1957).

For the 155-day aged pH 10 gel, X-ray examination indicated that the particles of hematite at 300° C. were very small, but were progressively larger at 385° C. and at 600° C. (fig. 4). The growth of hematite needles and of somewhat larger particles in the sample between 385° C. and 600° C. would account for the result for the material heated to 600° C. and for the somewhat broad exothermic peak on the differential thermal curve at about 480° C.; there seems to be little on the electron micrographs which would account for the apparent growth of the particles between 300° C. and 385° C. The basic particles in the 385° C. sample seem slightly larger, but there is not as much difference as one might expect. On the other hand, there are many needles at 300° C. (fig. 4*a*), but virtually none at 385° C. It may be, therefore, that the needles at 300° C. are actually aggregates of extremely minute hematite particles pseudomorphous after goethite (goethite is known to be absent at this temperature) and that these coalesce into hematite crystals of about the same size as the ground-mass between 300° C. and 385° C. This

would accord with the obvious relationship between the size of the goethite peak and the sharp exothermic peak at about 350° C. (fig. 2). The particles involved in this recrystallization are clearly very much smaller than those involved in the recrystallization between 385° C. and 600° C.—a fact which would explain both the position and the shape of the 480° C. peak. The shift in exothermic peak temperature and increase in breadth of the exothermic peak on ageing support this interpretation, since under such conditions the particles tend to be larger and to cover a wider range of particle size.

It is interesting to consider whether this interpretation can apply to the β-$Fe_2O_3.H_2O$ differential thermal curve, which shows a strong exothermic peak at 450° C. (Mackenzie, 1957). Electron micrographs of this material (fig. 5*a*) show beautiful crystals shaped rather like wheat grains, which on heating to 250° C. retain their outline but consist only of an extremely thin honeycombed skeleton, rather like a sponge (fig. 5*b*).[1] From X-ray evidence (Mackenzie, 1957) this skeleton must be largely hematite (although small amounts of residual β and of γ-Fe_2O_3 may also be present). The exothermic peak could then be accounted for as in the above gels by the coalescence of the extremely minute particles in the β-$Fe_2O_3.H_2O$ pseudomorph into discrete crystals of hematite. With such a mechanism it is clearly incorrect to conclude that all samples giving exothermic peaks belong to the same family, as was previously suggested (Mackenzie, 1952).

The increase in the size of the low-temperature endothermic peak on ageing of the pH 5 gel for 60 days remains to be explained. Close examination of the shape of this peak on curves *A* and *B*, fig. 1, indicates that on curve *A* the exothermic reaction for the coalescence of the fine particles (i.e. the exothermic peak) commences before all the water is removed, the endothermic peak thus being truncated by the superposition of the commencement of the exothermic peak. In curve *B*, on the other hand, the first peak is symmetrical, indicating complete dehydration before recrystallization. This is in accordance with what would be expected from the primary particle size of the gels.

The fact that the crystalline portion of the gels here studied consists largely of goethite is no indication that all brown gels are necessarily

[1] Decompositions leaving a mosaic have previously been observed—e.g. the dehydration of gypsum and some other sulphates and the decarbonation of zinc carbonate may be cited as examples (Meldau, 1956); on the other hand, many minerals, such as chrysotile, dehydrate without passing through this phase (R.H.S. Robertson, private communication).

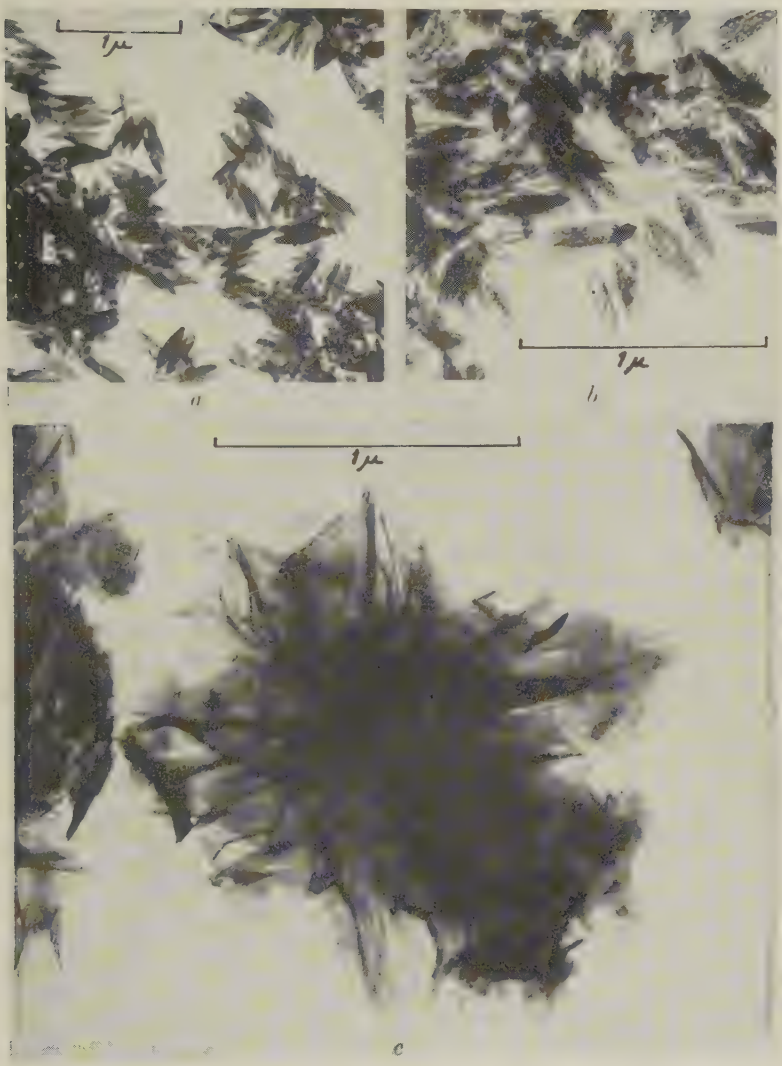

FIG. 5. Electron micrographs of: *a*, β-$Fe_2O_3.H_2O$; *b*, β-$Fe_2O_3.H_2O$ heated to 250° C.; *c*, γ-FeOOH.

of this constitution. Thus, there is no similarity between the electron diffraction pattern of this gel and that of β-$Fe_2O_3.H_2O$, as was observed for a previous gel. The preparative conditions may, therefore, easily

determine the rudimentary structure of the primary particles and the explanation for the exothermic peak given above would be in accord with the fact that all such gels give similar exothermic effects irrespective of the constitution of their primary particles.

The morphology of the goethite crystals noted above is in conformity with its habit in macroscopic form and also with the acicular crystals previously observed in synthetic goethite by Fricke and Weitbrecht (1943) and in a mixture of lepidocrocite and goethite by Meldau (1957).[1] The electron diffraction pattern for the latter sample (fig. 2*f* in Meldau, 1957) is anomalous, as crystals of both goethite and lepidocrocite can be clearly observed on the electron micrograph (fig. 1*f* in Meldau, 1957), and may have been due to the field chosen for diffraction containing much uncrystallized gel.

The crystal morphology of most members of the hydrated ferric oxide series would thus appear to be clear. Thus, goethite (α-FeOOH) forms acicular crystals (fig. 3*f* is typical); β-$Fe_2O_3.H_2O$ occurs as very regular crystals, which look rather like wheat grains (fig. 5*a*), and which on heating to 250° C. retain their outline but appear to consist of a skeletal mosaic (fig. 5*b*); very thin and very flexible plates that show pronounced crumpling (fig. 5*c*) normally characterize lepidocrocite (γ-FeOOH), but Fricke and Weitbrecht (1943) claim that it may also occur in acicular form.[2] The shape of 'δ-$Fe_2O_3.H_2O$' cannot at present be determined: the sample examined by Meldau (1957) had dehydrated into hematite (as evidenced by the electron diffraction pattern) under the conditions inside the electron microscope.

The morphology of the anhydrous forms is not yet known with any certainty. Watson and Freeman (1956) associate maghemite (γ-Fe_2O_3) with a platelet structure. An unidentified iron oxide of hexagonal outline has been reported by the same authors, and a chain-forming iron oxide of very small particle size has been observed by von Ardenne

[1] The crystals of yellow hydrated iron oxide used as a paint pigment are of the same shape (Anon., 1956), and are also presumably goethite. In contrast, the particles of goethite observed by Robertson (1958) in electron-micrographs of a clay from Kenya are not acicular but are of the type noted in the ground-mass of the gels described above, the particle size being about 60–150Å. across. The differential thermal curve for this goethite is consistent with such a small particle size, the endothermic peak occurring at about 200° C. (Mackenzie, 1958), but no reason can currently be suggested as to why this material has not aged to give acicular crystals.

[2] This observation of Fricke and Weitbrecht might be explicable on the basis of contamination of the lepidocrocite sample with some goethite. Their photographs of lepidocrocite are somewhat reminiscent of those obtained by Meldau (1957, fig. 1*f*) for a sample containing both minerals.

(1940). Hematite (α-Fe_2O_3) has been shown above to grow from a pepper of small particles to small needles. The growth of hematite crystals and the morphology of authentic samples of maghemite and magnetite (Fe_3O_4) therefore deserve further study.

Acknowledgements. The authors desire to express their thanks to Fraulein Widuch of the Westfälisches Institut für Übermikroskopie for her assistance with the electron-optical studies, and to Mr. W. A. Mitchell and Dr. V. C. Farmer of the Macaulay Institute for Soil Research for performing the X-ray and infra-red examinations, respectively.

References.

Anon., 1956. Pigment Particles. Their Character and Behaviour in Paint. Paint Research Station, Teddington, Middlesex.

Ardenne (M. von), 1940. Naturwiss., vol. 28, p. 113.

Bagno (O.), Longuet-Escard (J.), and Mathieu-Sicaud (A.), 1951. Compt. Rend. Acad. Sci. Paris, vol. 232, p. 1350.

Fricke (R.), and Hüttig (G. F.), 1937. Hydroxyde and Oxydhydrate, in Handbuch der allgemeinen Chemie, Band IX. Akademische Verlagsgesellschaft, Leipzig.

—— and Weitbrecht (G.), 1943. Zeits. anorg. Chem., vol. 251, p. 424.

Gheith (M. A.), 1952. Amer. Journ. Sci., vol. 250, p. 677.

Glemser (O.), 1937. Ber. deut. chem. Ges., vol. 70, p. 2117.

Kurnakov (N. S.) and Rode (E. J.), 1928. Zeits. anorg. Chem., vol. 169, p. 57.

Mackenzie (R. C.), 1949. Nature, vol. 164, p. 244.

—— 1952*a*. Problems of Clay and Laterite Genesis (W. O. Milligan, editor). A.I.M.E., New York, p. 65.

—— 1952*b*. An. Edafol. Fisiol. veg., vol. 11, p. 159.

—— 1957. The Differential Thermal Investigation of Clays (R. C. Mackenzie, editor). Mineralogical Society, London, p. 299.

—— 1958. Proc. Inst. Civil Engrs., vol. 11, p. 345.

Meldau (R.), 1956. Handbuch der Staubtechnik. V.D.I. Verlag, Düsseldorf, vol. 1, p. 55 and fig. 44.

—— 1957. Arch. Eisenhüttenw., vol. 28, p. 615.

—— and Robertson (R. H. S.), 1953. Nature, vol. 172, p. 998.

Méring (J.) and Oberlin (A.), 1957. Bull. Soc. franç. Min. Crist., vol. 80, p. 158.

Milligan (W. O.), 1952. Problems of Clay and Laterite Genesis (W. O. Milligan, editor). A.I.M.E., New York, p. 232.

Robertson (R. H. S.), 1958. Proc. Inst. Civil Engrs., vol. 9, p. 389.

Watson (J. H. L.) and Freeman (M. W.), 1956. Kolloidzeits., vol. 148, p. 127.

Weiser (H. B.), 1935. Inorganic Colloid Chemistry. Wiley and Sons, New York, vol. 2.

—— and Milligan (W. O.), 1940. Journ. physical Chem., vol. 44, p. 1081.

Note added in proof. It is possible that the rearrangement of Fe^{3+} in the oxygen-hydroxyl lattice, believed by Francombe and Rooksby (*Clay Min. Bull.*, in press) to occur during the dehydration of goethite to hematite, may contribute to the exothermic peak. The extent of the contribution of this factor is, however, uncertain, since the largest exothermic peaks occur with the gels of the smallest particle size where crystal growth would be expected to be predominant.

X-ray study of psilomelane and cryptomelane.

By Bibhuti Mukherjee, M.Sc., D.Phil.

Geological Survey of India, Calcutta.

[Communicated by the Editor; taken as read 2 April 1959.]

Summary. Psilomelane has been shown to be orthorhombic with a 8·254, b 13·40, c 2·864 Å. by the application of Lipson's method. The indexing of powder photographs of psilomelane ($R''_2\,Mn^{iv}_8\,O_{16}(OH)_4$, where R'' includes the bivalent metals Mn, Ba, Ca, Mg, Co) indicates the space-group $P2_12_12$ (D^3_2) with one molecule per unit cell. Indexing of powder photographs of psilomelane is not satisfactory with Vaux's axes. Fermor's 'psilomelane' is cryptomelane, which is tetragonal with a 9·822, c 2·858 Å. Cryptomelane (KR_8O_{16}, where R stands for Mn in different valency states, partly replaced by other cations) is body-centred tetragonal with one molecule per unit cell. Fermor's stalactitic 'psilomelane' has an inner dull core of cryptomelane and an outer fine-grained crust of pyrolusite in each needle-shaped body.

Psilomelane.

PSILOMELANE, a botryoidal material from Schneeberg, Saxony, was first described by Haidinger (1831). The chemical and X-ray study by Vaux (1937) of the original psilomelane from Schneeberg indicates that the name belongs to an orthorhombic species with the composition $H_4BaMnMn_8O_{20}$ having 10 to 17 % BaO. Vaux reported the cell-dimensions of psilomelane, a — 9·1 Å., b — 13·7 Å., c — 2·86 Å. as new data without detailed information on the method of derivation. Fleischer and Richmond (1943) gave X-ray powder spacing data of psilomelane for a sample from Vaux's collection. Wadsley (1953) studied a minute platy crystal (0·1 × 0·06 × 0·02 mm.) separated from the outer crust of the botryoidal core of a psilomelane from Vaux's collection and showed that the crystals have monoclinic symmetry with the dimensions, a = 9·56 Å., b = 2·88 Å., c = 13·85 Å., β = 92° 30′, Z = 2 for $(Ba,H_2O)_2Mn_5O_{10}$ and the space-group $A2/m$. The b-axial length was determined from a single setting of the crystal about the b-axis and a, c, and β from a zero-level Weissenberg photograph. Fermor (1909) described psilomelane from manganese ores of Indian deposits and named manganites with 5 to 15 % BaO from Tekrasai, Singhbhum, and Kajlidongri, Jhabua, 'baryta-psilomelane'.

Orthorhombic psilomelane (massive) containing 10 to 15 % BaO has been detected in manganese ores from the Jhabua and Ratanpur deposits

(Bilaspur, Madhya Pradesh) by X-ray powder diffraction methods. The powder spacing data of this psilomelane are in good agreement with those reported by Fleischer *et al.* for Vaux's psilomelane. Lipson's method (1949) for orthorhombic systems has been successfully applied to index the powder data of psilomelane. For orthorhombic crystals,

$$q_{hkl} = \sin^2\theta_{hkl} = h^2A + k^2B + l^2C,$$

where $A = \lambda^2/4a^2$, $B = \lambda^2/4b^2$, $C = \lambda^2/4c^2$. Lipson's method is to examine systematically the differences between the observed values of q in order to get relationship such as $q_{0kl} - q_{1kl} = A$ &c.; A occurs as differences between q values, where h values differ by unity and the kl values for the two lines are the same. Such differences are found in the powder spacing data of psilomelane by the diagrammatic method of Lipson. The possible values deduced from difference diagram are: $A = 0{\cdot}01375$, $B = 0{\cdot}00522$, $C = 0{\cdot}1142$; Fe-$K\alpha$-radiation was used for the powder photograph. The cell-dimensions are: $a = 8{\cdot}254$ Å., $b = 13{\cdot}40$ Å., $c = 2{\cdot}864$ Å.; $a:b:c = 0{\cdot}616:1:0{\cdot}214$. After indexing of all the powder lines (table I), it is found that the only systematic absences are the odd orders of $h00$ and $0k0$ indicating the space-group $P2_12_12$ (D_2^3).

Vaux's values for the cell-dimensions give $A = 0{\cdot}01132$, $B = 0{\cdot}00499$, $C = 0{\cdot}1145$, according to the above calculation. Indexing of all the powder lines of psilomelane (Fleischer's data) is not satisfactory with these values; the error of q_{hkl} values for some of the intense lines is quite high. It is, however, possible to index the powder photograph on the basis of Wadsley's (loc. cit.) monoclinic cell; but the space group suggested by the powder lines so indexed differs from that ($A2/m$) proposed by Wadsley. On the other hand, the agreement in indexing on the basis of an orthorhombic cell is better than that obtained on the assumption of monoclinic symmetry. The present specimen studied is, therefore, distinctly different from that described by Wadsley.

The chemical analyses of a number of psilomelanes by Vaux and Fermor show that the number of atoms in the unit cell per 20 oxygen atoms comes out at $Mn^{iv} \approx 7{\cdot}6$ to $7{\cdot}9$, $Mn'' \approx 0{\cdot}9$ to $1{\cdot}0$, $Ba \approx 0{\cdot}8$ to $1{\cdot}1$, $Ca+Mg+Co \approx 0{\cdot}2$ to $0{\cdot}3$, and $H \approx 4$. The ideal formula is

$$R''Mn_8O_{16}(OH)_4,$$

where R'' includes the bivalent metals Mn, Ba, Ca, Mg, Co, &c. The molecular weight is calculated with the atomic weight of R'' as the weighted mean value of the atomic weights of all the bivalent metals

TABLE I. X-ray powder data for psilomelane from Jhabua (VV-S 17/1, contains 11 % BaO; specimen collected by Mr. V. Venkatesh of the Geological Survey of India) and from Ratanpur (BNS-9(X), contains 13 % BaO; specimen collected by Dr. B. N. Sinha of the Geological Survey of India). *B*, broad and diffuse.

d.	I/I_0.	$\sin^2\theta$ (obs.).	*hkl*.	$\sin^2\theta$ (calc.).	*d*.	I/I_0.	$\sin^2\theta$ (obs.).	*hkl*.	$\sin^2\theta$ (calc.).
6·95 Å.	20	0·0194	110	0·0190	1·925	10	0·2529	241	0·2527
4·14	10	0·0547	200	0·0550	1·865	10	0·2695	170	0·2695
3·93 *B*	10	0·0606	210	0·0602	1·815	50	0·2845	331	0·2849
			130	0·0607	1·735	15	0·3113	360	0·3117
3·49	80	0·0769	220	0·0759				270	0·3108
3·33 *B*	20	0·0844	040	0·0835	1·71	20	0·3205	341	0·3215
3·11	20	0·0968	140	0·0973	1·675	5	0·3339	080	0·3341
3·02 *B*	15	0·1026	230	0·1020	1·64	25	0·3483	180	0·3478
2·86 *B*	15	0·1145	001	0·1142				510	0·3490
2·81	10	0·1187	011	0·1194	1·563	40	0·3835	171	0·3837
2·66	20	0·1326	111	0·1332	1·515	10	0·4082	460	0·4079
2·63	5	0·1355	021	0·1351	1·483	5	0·4259	271	0·4250
2·405	100	0·1620	031	0·1612				361	0·4259
2·36	20	0·1683	201	0·1692	1·425	40	0·4615	012	0·4620
2·315	5	0·1747	131	0·1749				181	0·4620
			211	0·1744					
2·25	15	0·1851	250	0·1855	1·403	25	0·4759	112	0·4758
2·24	40	0·1869	060	0·1879				470	0·4758
2·215	10	0·1909	221	0·1901	1·375	5	0·4955	600	0·4950
2·18	100	0·1971	041	0·1977	1·363	5	0·5044	032	0·5038
2·15	30	0·2026	160	0·2017				531	0·5049
2·13	5	0·2065	340	0·2073	1·353	10	0·5119	202	0·5118
2·065	10	0·2197	400	0·2200	1·340	5	0·5218	0.10.0	0·5220
2·035	15	0·2262	410	0·2252				461	0·5221

Mn, Ba, Ca, Mg, and Co in the proportions stated above, when with the above values of axial lengths and a density 4·6±0·1 g./cm.^{3} for psilomelane, the number of molecules per unit-cell comes out to be $Z \approx 1$.

A spectrum analysis of psilomelane (VV-S 17/1) shows Mn and Ba as major constituents, Mg, Al, Fe, Si, Ca, K, Na, Co, Ni, Cu as minor, and V, Ag, Pb, W, As, Ti, Ge, Ga, Sn, Sb, Li as traces. Spectrum analysis was carried out using a Hilger 'Large Quartz Spectrograph' with a direct current arc between 'Spec-pure' carbon rods at 9 amps, 220 volts.

Cryptomelane.

Fermor (1909) described psilomelane as a manganite containing potassium, barium, and sodium in different proportions. Richmond and Fleischer (1942) first proposed the name cryptomelane for the commonest variety of crystalline 'psilomelane', which is a distinct mineral species characterized by the presence of potassium, with little or no barium. Ramsdell (1942) determined the cell-dimensions of cryptomelane as $a = 9{\cdot}82$ Å., $c = 2{\cdot}86$ Å. (body-centred tetragonal).

The X-ray study of a number of specimens of Fermor's 'psilomelane' (registered collection in the Indian Museum) shows that the powder pattern corresponds exactly with that of Ramsdell's cryptomelane. Fermor's psilomelane (A. 680) from Chikhli, Satara, Bombay, containing about 2 % potassium with small amounts of barium and sodium, is considered as an ideal cryptomelane (table II). The cell-dimensions

TABLE II. X-ray powder data for cryptomelane from Chikhli, Satara, Bombay, India (Fermor's No. A. 680).

d.	I/I_0.	$\sin^2\theta$ (obs.).	hkl.	$\sin^2\theta$ (calc.).	d.	I/I_0.	$\sin^2\theta$ (obs.).	hkl.	$\sin^2\theta$ (calc.).
6·94	70	0·0195	110	0·0194	1·830	30	0·2797	141	0·2799
4·91	60	0·0388	200	0·0388	1·638	10	0·3493	600	0·3496
3·475	20	0·0776	220	0·0777	1·538	50	0·3962	251	0·3964
3·108	100	0·0970	130	0·0971	1·428	20	0·4594	002	0·4592
2·455	10	0·1555	400	0·1554	1·352	20	0·5127	451	0·5130
2·395	70	0·1633	121	0·1633	1·290	10	0·5632	370	0·5633
2·198	20	0·1939	240	0·1942	1·235	5	0·6144	402	0·6146
2·153	50	0·2022	301	0·2022	1·216	5	0·6338	332	0·6340
					1·148	5	0·7111	152	0·7117

determined after indexing of all the powder lines by Hesse's method (1948), are $a = 9{\cdot}822$ Å., $c = 2{\cdot}858$ Å. ($\pm 0{\cdot}003$ Å.), and the axial ratio c/a 0·291. The conditions limiting possible reflections are: hkl only with $h+k+l = 2n$, $00l$ only with $l = 2n$, $h00$ only with $h = 2n$. These conditions indicate one of the space-groups $I4/mmm$, $I\bar{4}2m$, $I\bar{4}m2$, $I4mm$, $I422$, $I4/m$, $I\bar{4}$, or $I4$, in agreement with Ramsdell. The recorded chemical analyses of a number of cryptomelanes by Fleischer and Fermor indicate that the ideal formula is KR_8O_{16}, where R stands for Mn in different valency states (predominantly Mn^{iv}), partly replaced by other cations. With the above values of axial lengths and density $4{\cdot}4 \pm 0{\cdot}1$ g./cm.^{3} for cryptomelane the number of formula units per unit-cell comes out to be $Z \approx 1$. The spectrum analysis of cryptomelane (A. 680) shows Mn as the major constituent, K, Mg, Al, Fe, Si, Ca, Na, Ba, Co, Ni, Cu, Ti, Li as minor, and V, Ag, Pb, Sn, As, Mo, W, Ga, Ge, Zn, Zr, Pt, Sb as traces.

Fermor's 'baryta-psilomelane' from Tekrasai, Singhbhum (A. 380), containing 15 % BaO was not available. Two specimens of psilomelane of Fermor (A. 377 and A. 385) from Tekrasai containing small amounts of barium, potassium, and sodium give similar powder patterns to that of cryptomelane. Fermor's stalactitic psilomelane (A. 268) from Garbham, Vizagapatam, reveals an interesting example of the pseudomorphous changes that occur in manganites. The outer fine-grained crust,

scraped from one of the constituent needle-shaped bodies, gives a powder pattern of pyrolusite (MnO_2, tetragonal, $a = 4{\cdot}382$ Å., $c = 2{\cdot}855$ Å.) whereas the inner dull core gives a powder pattern of cryptomelane. The deposition of pyrolusite on cryptomelane suggests that the alkali ions which are loosely bound to the cryptomelane structure along the a-direction are displaced from the lattice as a result of which an outer crust of pyrolusite is formed, the c-axial length remaining the same for both minerals. The nature of the transformation seems to imply that pyrolusite was formed by a shifting and re-stacking of the structure already existing in cryptomelane, due to the displacement of alkalis, and not by *de novo* recrystallization of the oxide (Bernal *et al.*, 1957).

Mathieson and Wadsley (1950) studied a crystalline specimen of 'hollandite' (No. 4199, Geological Survey of India collection) from Sitapar, Chhindwara, India, and found it to be 'monoclinic cryptomelane' with cell-dimensions, $a = 9{\cdot}79$ Å., $b = 2{\cdot}88$ Å., $c = 9{\cdot}94$ Å., and $\beta = 90° 37'$. Byström and Byström (1950) observed that Weissenberg photographs of the prismatic crystals of 'hollandite' showed tetragonal Laue symmetry C_{4h} with $a \approx 9{\cdot}9$ Å. In order to index the powder pattern of hollandite, a small monoclinic deformation with the tetragonal c-axis as b-axis in the monoclinic cell was assumed with the dimensions, $a = 9{\cdot}91$ Å., $b = 2{\cdot}87$ Å., $c = 9{\cdot}75$ Å., and $\beta = 90{\cdot}6°$, but the structure was derived on the tetragonal basis. An X-ray study of a hollandite crystal with well-developed crystal faces from Fermor's original collection has been made in this laboratory. The zero-layer and equi-inclination Weissenberg photographs about the a and b crystallographic axes of hollandite showed the monoclinic symmetry of the crystal, and the results will be published shortly.

Acknowledgements. The author wishes to thank the Director of the Geological Survey of India for kind permission to publish these results and to Professor H. Lipson of the University of Manchester for kindly going through the paper and offering valuable suggestions. Thanks are also expressed to Professor B. S. Basak of the Presidency College, Calcutta, for helpful discussion and to Dr. A. N. Chowdhury, Chemist, Geological Survey of India, for the determination of barium and potassium.

References.

Bernal (J. D.), Das Gupta (D. R.), and Mackay (A. L.), 1957. Nature, vol. 180, p. 645.

Byström (A.) and Byström (A. M.), 1950. Acta Cryst., vol. 3, p. 147 [M.A. **11**–238].

Fermor (L. L.), 1909. Mem. Geol. Surv. India, vol. 37, p. 105.

Fleischer (M.) and Richmond (W. E.), 1943. Econ. Geol., vol. 38, p. 269 [M.A. **9**–4].

Haidinger (W.), 1831. Trans. Roy. Soc. Edinburgh, vol. 2, p. 129.

Hesse (R.), 1948. Acta Cryst., vol. 1, p. 200 [M.A. **10**–527].
Lipson (H.), 1949. Ibid., vol. 2, p. 43 [M.A. **11**-96].
Mathieson (A. M.) and Wadsley (A. D.), 1950. Amer. Min., vol. 35, p. 99 [M.A. **11**–99].
Ramsdell (L. S.), 1942. Ibid., vol. 27, p. 611 [M.A. **8**–310].
Richmond (W. E.) and Fleischer (M.), 1942. Ibid., p. 607 [M.A. **8**–310].
Vaux (G.), 1937. Min. Mag., vol. 24, p. 521.
Wadsley (A. D.), 1953. Acta Cryst., vol. 6, p. 433 [M.A. **12**–93, **12**–328].

Recent secondary minerals in the Billingham anhydrite mine.

By L. R. Raymond, B.Sc.

Research Dept., Imperial Chemical Industries Ltd.,
Billingham-on-Tees, Durham.

[Taken as read, 2 April 1959.]

Summary. A number of secondary minerals have grown in recent years in a part of the Billingham anhydrite mine, by evaporation of water from the Upper Magnesian Limestone, and include some unusual species, the most interesting of which is thought to be *ilsemannite*.

THIS mine is located beneath Imperial Chemical Industries' factory site at Billingham, about 3 miles NE. of Stockton-on-Tees. The workings are in the Main Anhydrite, between 500 and 900 feet below sea-level. The anhydrite, which immediately overlies the Upper Magnesian Limestone, has been disturbed only slightly on a regional scale but locally strong disturbances have broken the gentle regional south-easterly dip. Some of these disturbances are in the form of asymmetrical synclines with one vertical limb. These synclines may cover an elliptical area over 300 yards long and 60 yards wide. Part of the steep limb of one such syncline was mined (see fig. 1) but was abandoned because the anhydrite became attenuated and water from the Upper Magnesian Limestone flooded the working. About two years after the working was abandoned, it was found that multicoloured efflorescences had grown in irregular scattered patches on part of the exposed limestone and anhydrite forming the walls and floor of the working. The efflorescences on the walls were mainly in the form of crusts or tufts of acicular growth, those on the floor coral-like and often very beautiful. The colours of the growths included light blue, vivid dark blue, green, yellow, orange, brown, white, and colourless. Specimens of each type were collected and examined microscopically, but with great difficulty as the crystals were usually only a few microns across. In view of this, X-ray and spectrographic examinations were also carried out on most of the material.

Dark blue efflorescence. This consisted of a hygroscopic crust of crystals which, when dried in a desiccator, gave a yellow powder with a green-

blue surface layer. The latter contained halite, anisotropic crystals too small to identify, and blue material that picked up water too quickly for microscopical examination to be effective. X-ray examination indicated halite, epsomite, and an unidentified phase. The yellow powder contained a trace of normal halite with n 1·544 and some isotropic

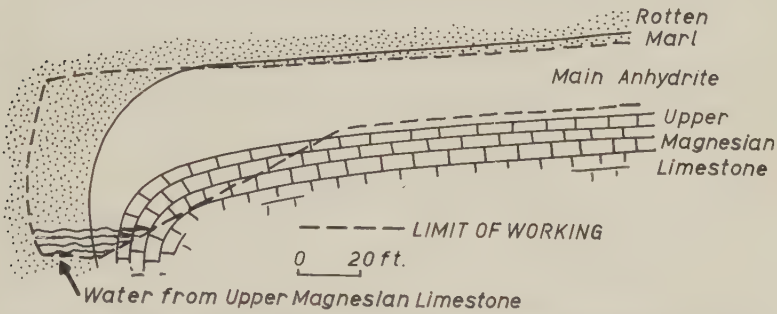

Fig. 1. Cross-section of part of a syncline, anhydrite mine, Billingham, Durham.

crystals with n 1·539 ± 0·002. The latter phase was also identified as halite by X-ray examination. It should be noted here that several of the efflorescences contained isotropic crystals identified as halite by X-rays but with n persistently 1·539. The yellow powder also contained aggregates of exceedingly fine-grained anisotropic crystals that could not be identified, and rectangular prismatic crystals thought to be aphthitalite.

The above examinations did not explain the strong blue colour of the unaltered efflorescence, so it was decided to resort to chemical analysis. A sample was leached with water, and the resulting solution gently evaporated to dryness and analysed with the following result: MoO_3 6·4, SO_3 23·4, Na_2O 22·4, K_2O 0·2, CaO 0·5, MgO 1·4, $(Fe,Al)_2O_3$ 9·6, Cl′ 22·8, loss at 400° C. 18·6 %, total (less O Cl 5·1) 100·2 %. The loss at 105° C. was only 4·3 %. The amount of molybdenum was remarkable and was clearly responsible for the bright blue colour. It remained in solution until evaporation was carried almost to complete dryness and was therefore exceedingly soluble.

The efflorescence was undoubtedly precipitated out of Upper Magnesian Limestone water which crept up and evaporated from the walls of the working. However, an analysis of the water revealed no molybdenum, neither did spectrographic examinations of the surrounding rocks. The water analysis suggested the following combinations: $CaCO_3$

100 p.p.m., $MgSO_4$ 2580 p.p.m., $CaCl_2$ 14740 p.p.m., $MgCl_2$ 6650 p.p.m., and NaCl 84240 p.p.m. For comparison, Sunderland Town water which is also obtained from the Magnesian Limestone contains the following suggested combinations: $CaCO_3$ 201 p.p.m., $MgSO_4$ 57 p.p.m., $CaCl_2$ 17 p.p.m., NaCl 38 p.p.m., and $MgCO_3$ 89 p.p.m.

Examination of the water-insoluble residue of the blue efflorescence revealed gypsum, talc, sulphur, abundant pyrite crystals (anhedral, botryoidal, cubes, octahedra, and rare pyritohedra), together with possible small amounts of arsenopyrite and molybdenite. Spectrographic examination of this material indicated Fe, Ca, S, Si, Mo, K, As, Zn, and Al.

Pale yellow efflorescence. This was all water-soluble and consisted mainly of halite (X-ray) with n 1·539±0·002. A small amount of a rectangular prismatic phase, with extinction inclined up to 40° and exhibiting lamellar twinning, was tentatively identified as tamarugite. A little tachhydrite was also thought to be present (the sample contained some hygroscopic phase).

White efflorescence. The major phase was isotropic and was identified by X-rays as halite, but with n = 1·539. Some gypsum and a little sylvine were present. Spectrographic examination indicated traces of Cu, Al, Bi, and Sr, but no minerals containing any of these elements were identified. Some colourless to white curved bladed crystals about 1 cm. in length proved to be thenardite. When removed from the mine they broke down to a white powder, but still consisted of thenardite.

Brown efflorescence. This mainly consisted of gypsum, with a coating of rusty brown material identified as lepidocrocite. A little halite was also present.

Orange efflorescence. The major phase was halite in well-formed cubes, in needles, or as granules. A little gypsum was also present, and an unidentified extremely fine-grained yellow material. The spectrograph indicated Cl as a major element and Fe, Ca, and Na as minor elements. It seemed, therefore, that the yellow material was largely iron chloride.

Yellow efflorescence. Most of the material was present as laths and acicular crystals with indices between 1·602 and 1·698, and was almost certainly an iron sulphate of some kind (the spectrograph indicated strong Fe and S but X-ray analysis could not identify it). A little halite was also present.

An interesting efflorescence of trona is widespread on the rise side of the mine. It occurs as colourless needles and plates, growing on rusty rails, bolts, &c., but can never be found on wood or stone.

Conclusions.

Briefly, the mineralogy of the efflorescences was as follows: Proved present, halite, thenardite, gypsum, epsomite, talc, sylvine, pyrite, sulphur, lepidocrocite. Probably present, ilsemannite, tamarugite, tachhydrite, a ferric sulphate, ferric chloride. Possible or doubtful, aphthitalite, arsenopyrite, molybdenite. There was clearly no doubt that the efflorescences were very recent secondary growths that had been precipitated from Upper Magnesian Limestone water that had crept up the walls of the working and evaporated.

The most interesting feature of the investigation was the discovery of molybdenum. It was thought to be in the form of ilsemannite or molybdenum blue and was undoubtedly responsible for the blue coloration of the first efflorescence described, which, like the other efflorescences, was precipitated largely from limestone water. However, waters rich in calcium, such as the limestone water, should precipitate any molybdenum in the form of insoluble salts. If it is assumed that the ratio between molybdenum and the other dissolved substances in the limestone water should roughly correspond to the ratio of molybdenum to the other solids in the efflorescences, then approximately 0·7 % of molybdenum should have been present in the limestone water, but, in fact, none was detected ($<$ 1 p.p.m.). It seemed impossible therefore that evaporation of this water could yield an efflorescence containing such a large amount of molybdenum. The wall rock behind the blue efflorescence was examined but it contained no molybdenum (it was thought that limestone water generally containing no molybdenum might have leached molybdenum out of localized areas of the wall rock as it seeped upwards).

Chrome molybdenum steel drilling bits are used in the mine and it was thought that a fragment of this material might have been the source of the molybdenum. However, this also appears to be unlikely in view of the distribution of the blue efflorescence and also the fact that no chromium was detected.

Such conflicting evidence obviously precludes the possibility of explaining how the ilsemannite was formed and the origin of the molybdenum can only be the subject of speculation.

Acknowledgements. Professor K. C. Dunham very kindly read the manuscript and his suggestions and encouragement are gratefully acknowledged. The assistance of my colleagues Dr. J. M. Skinner and Dr. T. T. Harding, who carried out respectively the chemical and X-ray analyses connected with this work, is also gratefully acknowledged.

SHORT COMMUNICATIONS

A simple spectroscope eye-piece for testing monazite under the microscope.

A MICROMETER eye-piece may be converted into a spectroscope eye-piece by putting a suitable stop (fig. 1) in place of the micrometer disc and a liquid prism (stippled in figs. 2 and 3) over the upper lens. The

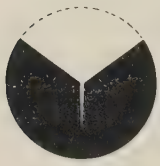

FIG. 1

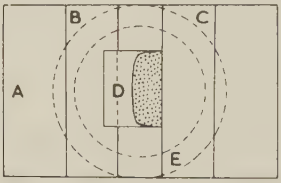

FIG. 2

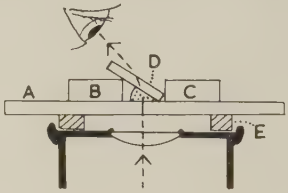

FIG. 3

stop, which may be made of Bristol board darkened with Indian ink, provides a viewing area and a tapering slit, the latter being made by a single cut with a razor blade and forced open slightly at the free end. The holder for the liquid prism is a piece of microscope slide (A in figs. 2 and 3) with two strips of glass, B and C, glued to it to support a loose piece of glass, D. A cardboard ring E, fixed to the undersurface of A, serves to keep the device in position. A few drops of some liquid with high dispersion (e.g. α-bromonaphthalene or nitrobenzene) are placed between A and D, and after use can be washed away by means of benzene.

The spectrum is seen by viewing obliquely (fig. 3). It is brighter than that given by more elaborate instruments but the red and violet are less widely separated. In testing monazite grains it is found that the absorption band in the yellow is sharply defined, particularly if the slit is carefully focused and the grain is moved to correspond to the narrow part of it.

The instrument has been successfully used in the identification of monazite in heavy residues from soils.

School of Agriculture,
University College of North Wales,
Bangor.

F. SMITHSON

A note on 'bleached hornblende'.

The presence of 'bleached hornblende' was noted by Dunn and Dey (1942) in dioritic rocks of Singhbhum, Bihar. Saha (1954) described the colourless amphibole from the granodiorites of Mayurbhanj; the loss of colour was thought to be due to replacement of iron by alkalis.

The phenomenon of bleaching actually entails some mineralogical transformation. As compared with the bleaching of biotite, in the case of hornblende not only does the mineral lose its characteristic absorption colours but there are distinct changes in optical characters.

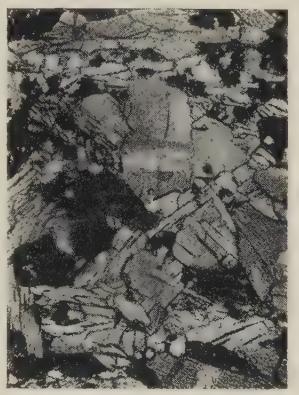

Fig. 1. Bleached hornblende invading coloured hornblende. ×12½.

Near the village Kadakora (22° 6′ N., 85° 39′ E.), Singhbhum, Bihar, a lenticular amphibolite body has been invaded by gneissic granite and is exposed in a few isolated patches within the basic body. The basic metamorphites under the microscope reveal the presence of 'bleached' amphibole; the dominant coloured amphibole approaches common hornblende in its optical characters (Winchell, 1951). Bleaching takes place along cleavages and edges of the mineral but preferentially along the trace of (001) plane (see fig. 1). The boundary between the two types is often very sharp and usually straight, and the two can be distinguished easily even between crossed nicols because of the contrast in interference colours. The optical characters of the colourless amphibole may be compared with those of the parent coloured amphibole (which has α pale green, β green, γ darker green in thin section) and with those of the colourless amphibole described by Saha:

Colourless . . .	α 1·626	γ 1·655	$2V_\alpha$ 68° ± 2°	$\gamma : c$ 22°
Coloured . . .	1·624	1·651	—	21°
Colourless (Saha) . .	1·623	1·649	67°	19°

The volumetric proportion of the bleached amphibole is found to increase towards the granite, together with an increase in the amount of biotite. The two phenomena (bleaching and biotitization of amphibole) could be correlated with an influx of alkalis hydrothermal solutions from the granite. Bleaching of amphibole has also been noticed in this locality in the calcgneissic rock along a zone of hydrothermal

activity and in basic inclusions near the periphery of the granite body (Bose, 1957).

A parallel example has also been observed associated with an amphibolite band in contact with granite gneiss near Bhagwa (23° 43′ N., 86° 21′ E.), Bihar (Bose, 1955). Here thin sections of the systematic samples at an interval of 3 yards (towards the granite) revealed the stages and mode of transformation of the coloured amphibole into the 'bleached' type. The initiation of alteration is marked by the appearance of fine colourless striations (parallel to the trace of (001)), which gradually widen to narrow stripes and finally appear as bands and then encroach along the cleavage direction in prismatic grains and ultimately replace a major part of the hornblende, leaving some islands of coloured rectangular blocks (with major axis parallel to the trace of (001)). The coloured amphibole in this stage often shows twin lamination in prismatic sections, which in rare cases are parallel to (001). Micrometric analyses of thin sections not only show an absolute increase of the bleached type but also increase in the ratio of colourless to total amphibole towards the granite boundary.

The increasing amount of bleaching towards the granite and the regular pattern in the bleaching suggest the phenomena to be an instance of intralattice metasomatism produced by hydrothermal solutions from the granite.

Geological Laboratory,
Presidency College,
Calcutta.

Mihir Kumar Bose

M. K. Bose, Proc. 42nd session Indian Sci. Congr., 1955; ibid., 44th session, 1957.
J. A. Dunn and A. Dey, Mem. Geol. Surv. India, 1942, vol. 69, pt. 2.
A. K. Saha, Journ. Geol. Min. Met. Soc. India, 1954, vol. 26, no. 2.
A. N. Winchell and H. Winchell, Optical Mineralogy, 1951, 4th edn., pt. 2.

A preliminary note on chromian mica in an ankerite–quartz–pyrite rock from southern Ross-shire, Scotland.

Published records of British examples of chromium-bearing muscovites are, to my knowledge, restricted to two occurrences of 'fuchsite' noted by Heddle[1] from Argyllshire, and by Clough[2] from Glenelg, Inverness-shire. It is, therefore, of considerable interest to record a new occurrence of a chromian mica from southern Ross-shire, Scotland.

The mica forms 10–12 % of an ankerite–quartz–pyrite rock associated with an ESE.–WNW. trending fault-zone in the upper reaches of An Leth Allt, a stream which drains into Loch Duich from the northern slopes of Sgùrr an Airgid. The actual fault-line averages 7 feet in width, but the cataclastic effects and accompanying carbonatization, kaolinization, and chloritization extend over a zone approximately 15–20 feet wide. Within this zone the metamorphic textures of the country-rock gneisses, mainly of Moine Series age, are broken down and the rocks are partially replaced by ankerite and calcite. The mica–ankerite–quartz–pyrite rock is one of the products of this replacement and forms four main outcrops, the largest of which is some 40 square feet in area.

The chromian mica is bright green in colour and imparts an irregular foliation to the rock. Chemical analysis has shown that the mica contains more than 2·0 % of Cr_2O_3 and approximately 25 % of Al_2O_3. Under the microscope it is pale green in colour and exhibits the characteristic optical properties of muscovite. X-ray powder-studies show that it possesses a single-layer monoclinic (1M) muscovite structure. The properties of the mica define it as a relative of the chromian muscovite *fuchsite*.

Because of its bright green colour the mica appears to dominate the mineralogy of the rock. In fact, however, ankerite constitutes more than 50 % of the rock by weight, and its oxidation results in a rusty ferruginous crust on weathered outcrops. Under the microscope the ankerite shows a random crystallographic orientation interpreted as depositional. The remaining 30–40 % of the rock is made up of lenticular aggregates of elongated quartz crystals disposed in vug-like array. Pyrite, chalcopyrite, and sphene are the most important accessory minerals. The chemical composition of the rock is: SiO_2 39·43, TiO_2 0·14, Al_2O_3 2·91, Fe_2O_3 0·72, Cr_2O_3 0·33, FeO 3·55, MnO 0·18, MgO 9·03, CaO 17·27, Na_2O 0·25, K_2O 0·83, H_2O+ 0·65, H_2O- 0·33, CO_2 24·58, total 100·20 % (Analyst: Erna Padget).

In its mineralogy and association with a fault-zone, this rock is closely similar to the fuchsite–carbonate–quartz–sulphide rocks which are characteristic of the gold deposits of the Larder Lake district of Canada,[3] and the Kalgoorlie district of Australia.[4] Similar carbonate rocks, containing the chromian muscovite *mariposite*, have also been described from the gold-mining area of the Mother Lode of California, U.S.A.[5] To date, however, no trace of gold has been found in specimens from southern Ross-shire.

The An Leth Allt fault-zone is but a minor representative of a whole

plexus of similar faults to which the Strathconon Fault is the master fracture.[6] Furthermore, throughout the Scottish Highlands there are a number of similar post-Moinian fault systems, which are related to the Strathconon Fault.[7] Viewed in this light, this preliminary description of the chromian-mica–ankerite–quartz–pyrite rock from southern Ross-shire is intended to draw attention to the possibility of similar lithological types, perhaps of economic significance, elsewhere in the metamorphic area of the Northern and Grampian Highlands of Scotland. A fuller description of the mica, and of the rock and its associations and origin, awaits further laboratory and field work.

Dept. of Geology,
The University,
Leeds.

T. N. Clifford

[1] M. F. Heddle, The Mineralogy of Scotland, 1924, vol. 2, p. 115.

[2] C. T. Clough (*in* Peach *et al.*), The geology of Glenelg, Lochalsh and south-east part of Skye, Mem. Geol. Surv. Scotland, 1910, p. 35.

[3] H. C. Cooke, Geol. Surv. Canada, 1922, Mem. 131, p. 48.

[4] F. R. Feldtmann, Geol. Surv. Western Australia, 1916, Bull. 69, p. 36.

[5] A. Knopf, U.S. Geol. Surv., 1929, Prof. Paper, 157, p. 38.

[6] B. N. Peach *et al.*, The geology of central Ross-shire, Mem. Geol. Surv. Scotland, 1913, p. 81; T. N. Clifford, Quart. Journ. Geol. Soc. London, 1957, vol. 113, p. 59.

[7] E. M. Anderson, The Dynamics of Faulting, 2nd edn., 1951, p. 93.

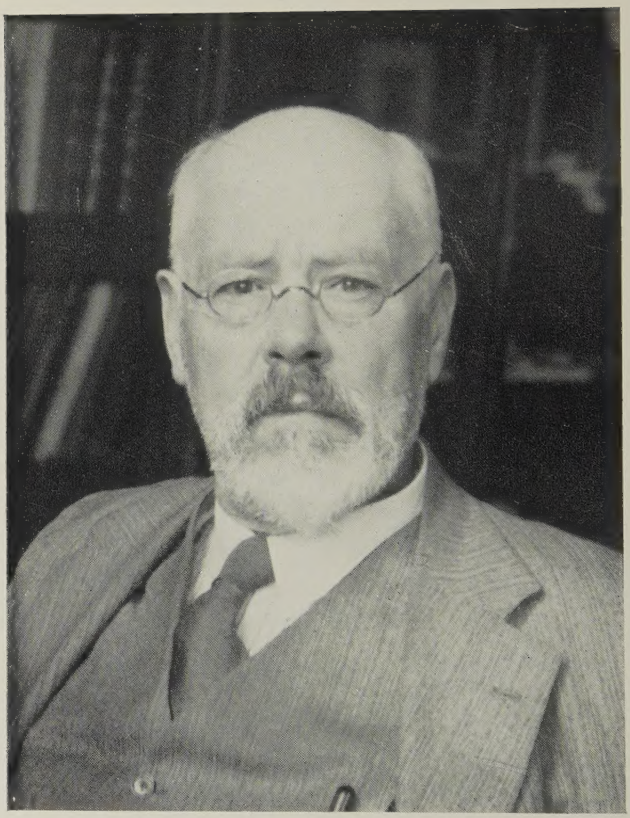

Leonard James Spencer (1870–1959)